Biogeochemical processes governing microplastic transport in freshwater reservoirs

Rico Leiser

Dissertation (kumulativ)
zur Erlangung des akademischen Grades
„doctor rerum naturalium" (Dr. rer. nat.)
in der Wissenschaftsdisziplin „Mikrobiologie"

eingereicht an der Mathematisch-Naturwissenschaftlichen Fakultät
Institut für Biochemie und Biologie (IBB)
der Universität Potsdam

und am

Helmholtz-Zentrum für Umweltforschung (UFZ) Magdeburg
Department Seenforschung

Ort und Tag der Disputation: Potsdam,
Hauptbetreuerin: PD Dr. Katrin Wendt-Potthoff, Universität Potsdam
1. Gutachter: Prof. Dr. Hans-Peter Grossart, Universität Potsdam
2. Gutachter: Prof. Dr. Werner Manz, Universität Koblenz-Landau

Published online on the
Publication Server of the University of Potsdam:
https://doi.org/10.25932/publishup-52024
https://nbn-resolving.org/urn:nbn:de:kobv:517-opus4-520240

Contents

List of Figures

List of Tables

Abbreviations

CLSM Confocal Laser Scanning Microscopy

DOC Dissolved Organic Carbon

EDS Equivalent Spherical Diameter

EDTA Ethylenediaminetetraacetic Acid

EPS Extracellular Polymeric Substances

EX-PS Expanded Polystyrene

MP Microplastics

OD Optical Density

OTU Operative Taxonomic Unit

PE Polyethylene

PET Polyethylene terephthalate

POM Particulate Organic Matter

PP Polypropylene

PMMA Polymethylmethacrylat

PUR Polyurethane

PS Polystyrene

PVC Polyvinyl chloride

Q-Q plot Quantile-Quantile plot

TEP Transparent Exopolymeric Particles

TRIS Tris(hydroxymethyl)aminomethane

XRD X-ray Diffraction

Summary

The presented study investigated the influence of microbial and biogeochemical processes on the physical transport related properties and the fate of microplastics in freshwater reservoirs. The overarching goal was to elucidate the mechanisms leading to sedimentation and deposition of microplastics in such environments. This is of importance, as large amounts of initially buoyant microplastics are found in reservoir sediments worldwide. However, the transport processes which lead to microplastics accumulation in sediments, were up to now understudied.

The impact of biofilm formation on the density and subsequent sedimentation of microplastics was investigated in the eutrophic Bautzen reservoirs **(Chapter 2)**. Biofilms are complex microbial communities fixed to submerged surfaces through a slimy organic film. The mineral calcite was detected in the biofilms, which led to the sinking of the overgrown microplastic particles. The calcite was of biogenic origin, most likely precipitated by sessile cyanobacteria within the biofilms.

Biofilm formation was also studied in the mesotrophic Malter reservoir. Unlike in Bautzen reservoir, biofilm formation did not govern the sedimentation of different microplastics in Malter reservoir **(Chapter 3)**. Instead autumnal lake mixing led to the formation of sinking aggregates of microplastics and iron colloids. Such colloids form when anoxic, iron-rich water from the hypolimnion mixes with the oxygenated epilimnetic waters. The colloids bind organic material from the lake water, which leads to the formation of large and sinking iron-organo flocs.

Hence, iron-organo floc formation and their influence on the buoyancy or burial of microplastics into sediments of Bautzen reservoir was studied in laboratory experiments **(Chapter 4)**. Microplastics of different shapes (fiber, fragment, sphere) and sizes were readily incorporated into sinking iron-organo flocs. By this initially buoyant polyethylene microplastics were transported on top of sediments from Bautzen reservoir. Shortly after deposition, the microplastic bearing flocs started to subside and transported the pollutants into deeper sediment layers. The microplastics were not released from the sediments within two months of laboratory incubation.

The stability of floc microplastic deposition was further investigated employing experiments with the iron reducing model organism *Shewanella oneidensis* **(Chapter 5)**. It was shown, that reduction or re-mineralization of the iron minerals did not affect the integrity of the iron-organo flocs. The organic matrix was stable under iron reducing conditions. Hence, no incorporated microplastics were released from the flocs. As similar processes are likely to take place in natural sediments, this might explain the previous described low microplastic release from the sediments.
This thesis introduced different mechanisms leading to the sedimentation of initially buoyant microplastics and to their subsequent deposition in freshwater reservoirs. Novel processes such as the aggregation with iron-organo flocs were identified and the understudied issue of biofilm densification through biogenic mineral formation was further investigated. The findings might have implications for the fate of microplastics within the river-reservoir system and outline the role of freshwater reservoirs as important accumulation zone for microplastics. Microplastics deposited in the sediments of reservoirs might not be transported further by through flowing river. Hence the study might contribute to better risk assessment and transport balances of these anthropogenic contaminants.

Zusammenfassung

Die vorliegende Arbeit befasst sich mit dem Einfluss mikrobiologischer und biogeochemischer Prozesse auf die physikalischen Transporteigenschaften und den Verbleib von Mikroplastik in Stauseen. Ein Schwerpunkt lag auf der Untersuchung von Mechanismen, welche die Sedimentation von Mikroplastik einleiten. Dies ist von hoher Relevanz, da große Mengen eigentlich schwimmfähigen Mikroplastiks in Stauseesedimenten gefunden werden, aber die Transportprozesse vom Wasser in das Sediment bislang unbekannt waren.
In der eutrophen Talsperre Bautzen wurde der Einfluss der Biofilmbildung auf die Dichte und Sedimentation von Mikroplastik untersucht **(Kapitel 2)**. Biofilme sind komplexe mikrobielle Lebensgemeinschaften, welche sich in Form schleimiger Filme auf im Wasser befindlichen Oberflächen bilden. Es konnte ein Zusammenhang zwischen der starken Dichtezunahme beziehungsweise dem Absinken der bewachsenen Partikel und dem Vorhandensein des Minerals Calcit innerhalb des aufwachsenden Biofilms festgestellt werden. Das Calcit war biogenen Ursprungs und wurde infolge der Photosynthese sessiler Cyanobakterien gebildet.

In der mesotrophen Talsperre Malter wurde ebenfalls die Biofilmbildung auf Mikroplastik untersucht **(Kapitel 3)**. Dort veränderte die Bildung von mikrobiellen Biofilmen das Sedimentationsverhalten von verschiedenen Mikroplastik-Polymeren nicht. Stattdessen wurde beobachtet, dass die Herbstzirkulation des Sees zur Bildung von Aggregaten aus Mikroplastik und mineralischen Eisenkolloiden führte. Diese Eisenkolloide bilden sich durch die Mischung von eisenreichen, sauerstofffreien Tiefenwasser mit sauerstoffhaltigem Oberflächenwasser. Die Kolloide verbinden sich mit organischem Material aus dem See und formen dadurch größere Flocken.
Da die Bildung von eisenhaltigen Flocken ein für geschichtete Stauseen wichtiger Prozess ist, wurde ihr Einfluss auf die Schwimmfähigkeit von Mikroplastik und den darauffolgenden Einbau in die Sedimente untersucht **(Kapitel 4)**. In Laborversuchen konnten verschiedene Formen (Fasern, Fragmente, Kugeln) und Größenklassen von Mikroplastik in die Flocken eingebaut werden. Da die Flocken im Wasser

absinken, können sie zuvor schwimmfähiges Polyethylen-Mikroplastik zur Sedimentoberfläche transportieren. Dort angekommen, beginnen die Flocken zusammen mit dem Mikroplastik langsam in das Sediment einzusinken und transportieren es dadurch in tiefere Sedimentschichten. Im Labor konnte innerhalb von zwei Monaten keine signifikante Freisetzung des so transportierten Mikroplastiks aus den Sedimenten beobachtet werden.

Die Transformation der Flocken und welchen Einfluss dies auf die Freisetzung von Mikroplastik hat, wurde in Versuchen mit dem eisenreduzierenden Modelorganismus *Shewanella oneidensis* untersucht **(Kapitel 5)**. Hierbei zeigte sich, dass die Auflösung oder Umwandlung des Eisens beziehungsweise der Eisenminerale innerhalb der Flocken, nicht zur Zerstörung der Flocken führte. Die organische Matrix der Flocken blieb unverändert stabil und umschloss auch weiterhin das eingebaute Mikroplastik. Da im Sediment ähnliche Abbauprozesse ablaufen, gibt dies einen möglichen Hinweis darauf, warum abgelagertes Mikroplastik nicht mehr aus Sedimenten freigesetzt wird.

Im Rahmen dieser Arbeit konnte gezeigt werden, dass in Talsperren unterschiedliche Prozesse zum Absinken und zur Deposition von Mikroplastik führen. Es wurden neuartige Prozesse wie die Aggregation mit eisenhaltigen Flocken identifiziert und ungewöhnliche Aspekte wie die biogene Mineralbildung näher beleuchtet. Dadurch können wichtige Implikationen hinsichtlich des Transports von Mikroplastik in Fluss-Stausee-Systemen abgeleitet werden. Aufgrund der beschriebenen Sedimentationsprozesse sind Stauseen wichtige Akkumulationszonen für Mikroplastik. Im Stausee sedimentierendes Mikroplastik wird potentiell nicht vom aufgestauten Fluss weitertransportiert. Daher könnten die hier beschriebenen Prozesse zu einer Verbesserung von Risikoabschätzungen und Transportbilanzen dieser anthropogenen Belastung führen.

Chapter 1

Introduction

1.1 Background and motivation

Microplastics (MP, plastic particles smaller than 5 mm), are globally distributed contaminants found in earths biosphere (Hermsen et al., 2018), hydrosphere (Van Sebille et al., 2020), lithosphere (Dioses-Salinas et al., 2020), atmosphere (Dris et al., 2017) and cryosphere (Kanhai et al., 2020), which raised concerns in both science (see Figure 1) and society (e.g. #plasticfree, 3.7 million uses on Instagram, 28.04.2021) over the past decade. The entry paths of intentionally manufactured (primary) or fragmented (secondary) MP into the environment are diffuse, ranging from waste water treatment effluents over sewage sludge application to washouts from landfills and general littering (reviewed in Waldschläger et al., 2020).

Lotic and lentic systems are widely recognized to facilitate the transport of MP produced on land to the oceans (Schmidt et al., 2020), which are considered as terminal sinks for these contaminants (Woodall et al., 2014). Models hypothesized, that rivers convey 0.8 - 12.7 million tons plastics a^{-1} to the worlds oceans (Jambeck et al., 2015; Meijer et al., 2021). However, only a minor fraction (~1 %) of this "hypothetical" environmental plastic pollution can be found in water and sediment samples from the oceans (Koelmans et al., 2017). The reasons for this might be the still inadequate, non-harmonized sampling and analyzing procedures used for MP detection (Primpke et al., 2020). But also the lacking knowledge on environmental transport behaviour might result in poor MP finding rates and model estimates. It is likely that MP accumulate in environmental compartments usually overlooked by sampling campaigns and transport models.

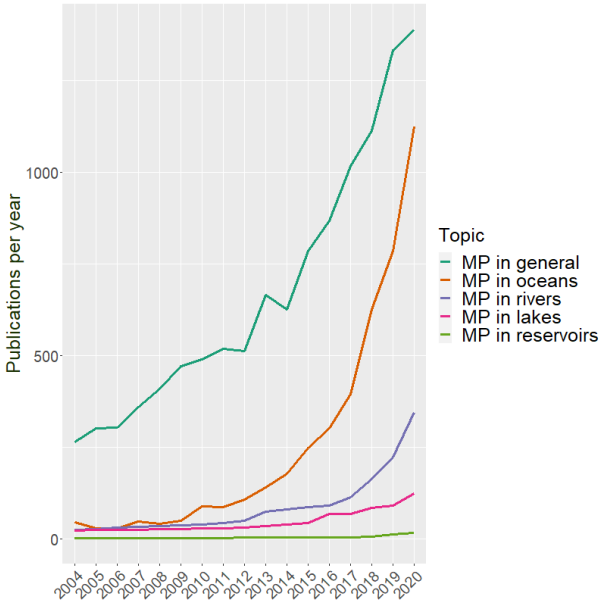

Figure 1: Annual number of peer reviewed publications on plastics in different environmental systems per year since 2004 until 2020. Search words, MP in general: "micro" AND "plastic*", Oceans: "marine" AND "*plastic*", Rivers: "river*" AND "*plastic*", Lakes: "lake*" AND "*plastic*", Reservoirs: "*reservoirs*" AND "freshwater" AND "*plastic*", from Web of Science (search on 26.04.2020).

Impoundments, dams and reservoirs are such accumulation points for riverine transported plastics, as they reduce flow velocity, which leads to enhanced settling rates of particulate matter. Hence, these man made structures have a high impact on the MP loads of rivers flowing through them (Hübner et al., 2020; Watkins et al., 2019), and may ultimately even act as permanent sinks for these particles (Turner et al., 2019). In comparison to other freshwater environments, such as lakes and rivers, reservoirs are understudied (see Figure 1). The few data on MP distribution in water and sediments of reservoirs (summarized in Table 1 and citations therein) indicate their high potential to accumulate and store MP.

Table 1: MP in the surface waters and bottom sediments of freshwater reservoirs. Size refers to lower and upper border of the used sampling devices. MP concentrations are biased by the used sampling device, with increasing lower border size resulting in decreasing particle numbers. Studies employing manta trawling, providing area related MP concentrations were intentionally excluded. In addition, studies on plastics in beach sediments were also excluded from this list.

Surface water

Location	Size [mm]		Concentration				Most common		Source
	min	max	min	max	mean	Unit	Shape	Polymer	
China, Danjiangkou Reservoir	0.048	5	467	15017	2594	MP m^{-3}	Fiber	PP	(Di et al., 2019)
China, Danjiangkou Reservoir	0.075	5	530	24798	7205	MP m^{-3}	-	PA	(Lin et al., 2021)
China, Qing River (dam)	0.01	5	0.07	0.45	0.17	MP l^{-1}	Fragment	-	(Wang et al., 2020)
China, Shuikou Reservoir	0.3	5	-	-	0.42	MP l^{-1}	Fiber	-	(Huang et al., 2020)
China, Three Gorges Reservoir	0.048	5	1597	12611	4703	MP m^{-3}	Fiber	PE	(Di and Wang, 2018)
Turkey, Sureyyabey dam lake	0.1	5	4.09	5.25	-	MP m^{-3}	Fiber	-	(Tavşanoğlu et al., 2020)

Sediment

Location	Size [mm]		Concentration				Most common		Source
	min	max	min	max	mean	Unit	Shape	Polymer	
China, Danjiangkou Reservoir	-	5	15	40	24	MP kg^{-1}	Fiber	PP	(Di et al., 2019)
China, Danjiangkou Reservoir	-	5	708	3237	1818	MP kg^{-1}	Fiber	PP	(Lin et al., 2021)
China, Huangjinxia reservoir	<0.1	5	233	870	558	MP kg^{-1}	Fiber	PE	(Li et al., 2020)
China,Three Gorges Reservoir	0.045	5	25	300	82	MP kg^{-1}	Fiber	PS	(Di and Wang, 2018)
Serbia, Iron gate I	0.02	5	-	-	150	MP kg^{-1}	Fiber	-	(Pojar et al., 2021)
South Africa, Nandoni Reservoir	0.063	5	5	6417	77.5	MP kg^{-1}	-	PE	(Mbedzi et al., 2020)

With MP concentrations in sediments exceeding the particle concentrations in water roughly 208 times (comparing means), reservoir sediments can be seen as important sinks of riverine MP. In Germany alone, 311 large reservoirs (after criteria of the International Commission on Large Dams) are listed, which impound most of the larger German rivers (Danube, Elbe, Oder, Rhine, Saale and Spree)(Köngeter, 2013). This exemplifies the widespread importance of reservoirs for the retention of riverine transported MP.

Interestingly polyethylene (**PE**) is among the most commonly found polymer type in reservoir sediments (Table 1). This is surprising, as PE is expected to float in water, given by its low density (Table 2). Mechanisms facilitating the sinking and burial of initially buoyant MP in freshwater reservoirs were previously not studied. Therefore the main goal of the presented work was to elucidate how initially buoyant MP end up in the sediments of German freshwater reservoirs. Emphasis was

given to biogeochemical processes which influence particle properties and govern the sedimentation of MP.

In the next section, it will be reported how MP particle properties influence their environmental transport. This is followed by sections on how biogeochemical processes in reservoirs may alter these properties and by this affect the environmental transport of MP.

Table 2: European usage of different plastic polymer types in the year 2019. 1: PlasticsEurope, 2020, 2: Duis and Coors, 2016.

Polymer	Abbreviation	Demand in Europe [Mt a^{-1}][1]	Density range [g cm^{-3}][2]
Low density polyethylene	LD-PE	8.5 (17.40 %)	0.89-0.93
High density polyethylene	HD-PE	6.2 (12.40 %)	0.94-0.98
Polypropylene	PP	9.9 (19.40 %)	0.83-0.92
Polystyrene	PS	1.5 (3.05 %)	1.04-1.1
Expanded polystyrene	EX-PS	1.55 (3.15 %)	0.01-0.05
Polyvinylchlorid	PVC	5.0 (10.00 %)	1.16-1.58
Polyethylene terephthalate	PET	3.9 (7.90 %)	0.96-1.45
Polyurethane	PUR	4.00 (7.9 %)	1.2

1.2 Microplastic properties and their relation to transport behaviour

MP are particles with complex properties, which exacerbates the investigation of their transport behaviour in aquatic systems. Density, shape and size have been identified as the most important parameters to describe MP movement in water (Khatmullina and Chubarenko, 2019).

Density is mainly influenced by plastic type (Andrady, 2017) and the amount of additive or fillers (Ateia et al., 2020) added to the polymer matrix. Typical densities range from 0.01 g cm^{-3} for expanded polystyrene (Duis and Coors, 2016) to 2.3 g cm^{-3} for polytetrafluoroethylene (Khatmullina and Chubarenko, 2019). Accordingly MP can be divided into polymers which initially float ($\rho < 1$ g cm^{-3}) such as PE, PP and EX-PS or polymers which sink in water ($\rho > 1$ g cm^{-3}) including PET, PS and PMMA (Linders et al., 2018). In 2019 around 52 % of all produced plastics

was made up of low density polymers PE, PP and EX-PS, while negatively buoyant PET, PS and PUR made up 28 % (Table 2). Initially buoyant polymer types might to be transported over wide distances in the water phase (Van Sebille et al., 2020), while dense polymer types are expected to accumulate in the sediments (Daily and Hoffman, 2020) or to be transported as bed loads (Waldschläger and Schüttrumpf, 2019b).

The size of plastic particles do not only influence their behaviour in water, but is also the only parameter which defines them as MP (Khatmullina and Chubarenko, 2019). No universal or exact size limits are defined, but in the past decade most researchers agreed on 5 mm as the upper border for particles referred to as MP (Andrady, 2017). Recently the opinion to define particles 1000 - 5000 µm as mesoplastics or large MP and 10 - 1000 µm as MP became increasingly popular (Hartmann et al., 2019). Assuming uniform density and shape, the settling or rising velocity of particles increase with their size (Dietrich, 1982). Hence, large and negatively buoyant MP ($>$ 500 µm) are assumed to settle quite fast (10 - 100 m d^{-1}), while small particles ($<$ 5 µm) might not sink at all (Linders et al., 2018). This is expressed in equations 1.1 & 1.2 where the settling velocity W_s [m s^{-1}] of a particle in semi-turbulent flow (Re $<$ 2 x 10^5) is mainly influenced by its diameter D [m] (Zhiyao et al., 2008). Further W_s is depending on the kinematic viscosity ν [m^2 s^{-1}] and the density gradient between particle ρ_0 [kg m^{-3}] and water ρ_w [kg m^{-3}] (Chubarenko et al., 2016). Still the settling velocity is mostly affected by the diameter of the particle (Chubarenko et al., 2016).

$$d_* = \left(\frac{\frac{(\rho_0 - \rho_w)}{\rho_w} * g}{\nu^2} \right)^{\frac{1}{3}} * D \tag{1.1}$$

$$W_s = \frac{\nu}{D} * d_*^3 \left[38.1 + 0.93 d_*^{\frac{12}{7}} \right]^{-\frac{7}{8}} \tag{1.2}$$

MP come in quite different shapes, roughly divided and generalized as quasi one-dimensional fibers or lines, quasi two-dimensional films or sheets, and three-dimensional fragments, beads or spheres (Khatmullina and Chubarenko, 2019). Fibers are usually the most abundant shape of MP found in freshwater (González-Pleiter et al., 2020), but also fragments, spheres or films are frequently detected (Kooi and Koelmans, 2019). The shape influences the drag coefficient of the MP particles, by this changing rising or settling velocity (Kowalski et al., 2016). Fur-

ther irregular shaped particles (fragments, fibers) (Waldschläger and Schüttrumpf, 2019a) tend to secondary movements, such as tumbling, rotating or oscillating (Kowalski et al., 2016), thereby influencing settling velocity and direction of movement (Khatmullina and Isachenko, 2017).

The presented insights on how density, size and shape of MP change their rising and settling behaviour are the fundamentals to understand the environmental transport of these particles. However, all presented results were deducted from laboratory studies excluding important biogeochemically mediated processes possibly altering the MP properties in nature. For example the relation between size and settling velocity might not be as straightforward, as indicated by the equations 1.1 & 1.2. Experimental studies indicated that with decreasing size, the collision frequency between the MP particles and other natural particles (Quik et al., 2014) increases, which lead to the formation of heteroaggregates. These heteroaggregates are larger in size and increase the settling velocity of the incorporated MP particles (Besseling et al., 2017). Under natural conditions MP particles < 10 µm will rapidly form aggregates, leading to high settling velocities, regardless of their initial small size (Besseling et al., 2017). Hence, secondary processes possible altering the three basic parameters density, shape and size need to be quantified in order to holistically approach MP transport in the environment. Furthermore this topic is currently under debate and other, yet not investigated, particle properties (e.g. surface hydrophobic), might also be relevant for MP transport in the environment.

In the upcoming section relevant biogeochemical processes influencing the settling and deposition of MP in aquatic environments with emphasis on freshwater reservoirs, will be discussed.

1.3 Aggregation based transport of microplastics

The term aggregation summarizes a variety of different processes leading to the formation of larger particles from smaller particles by merging together through collision or intermolecular forces (Wang et al., 2021). Aggregation of particles relies on various parameters, involving particle surface chemistry (hydrophobicity, roughness) (Zhang et al., 2019), water chemistry (ionic strength, pH, organic matter) (Li et al.,

2018) and physical processes (Brownian motion, turbulent or laminar water flow) (Sun et al., 2021). The fundamental aspects of nanoplastics and MP aggregation in aqueous solutions have been studied and reviewed extensively (Alimi et al., 2018; Wang et al., 2021; Yan et al., 2021). Working with highly artificial systems, such as water with low ionic strength (Shams et al., 2020), non-mixed ions (Cai et al., 2018), no organic matter or organisms, small particles sizes ($<$ 10 µm) (Sun et al., 2021) and high particle concentrations (Li et al., 2019b), these studies revealed novel insights towards the factors driving homoaggregation of nanoplastics/MP. However, these findings cannot be transferred to "real" freshwater systems, where water chemistry, biological parameters, particles properties and abundance differ vastly from the conditions applied in these laboratory experiments.

Therefore, this section will rather summarize the implications of MP heteroaggregation with naturally occurring particles for their environmental transport. In freshwater reservoirs a large variety of natural particles which govern the potential to aggregate MP can be encountered. Potential relevant particles are transparent expolymeric particles (TEP), cells (bacteria, phyto-, and zooplankton), organic macromolecules, inorganic particles (carbonates, clay, hydroxides, oxides, quartz) or macroscopic flocs (lake snow, iron snow) typically ranging from 10^{-9} to 10^{-2} m in size (Grossart et al., 1997; Linders et al., 2018; Reiche et al., 2011). MP can be expected to coagulate with such particles by laminar or turbulent shear, differential settling or through biogenic aggregation processes (McCave, 1984). Differential settling and laminar or turbulent flow will physically cause particle collision. Depending on their properties, particles have a certain chance of sticking together each time they collide, by this forming larger aggregates (Linders et al., 2018). Due to their stickiness, particles of organic origin, such as algae cells (Lagarde et al., 2016) or TEP (Drago et al., 2020) are expected to aggregate more readily with MP than inorganics such as iron oxides (Li et al., 2019a).

Biogenic aggregation processes involve the active uptake of MP by macroorganisms, followed by excretion and incorporation into (pseudo)feces and fecal pellets. This displays an important mechanisms and is observed for different marine organisms such as copepods (Cole et al., 2016), crabs (Watts et al., 2014), sea cucumbers (Bulleri et al., 2021) or mussels (Moreschi et al., 2020).

MP incorporation into aggregates is seldom reported from real environmental samples, as sampling procedures often destroy the embedding organic matrix (Wang et al., 2021). Still, MP have been observed in sinking aggregates from the pacific ocean (Zhao et al., 2017; Zhao et al., 2018) and the Mediterranean sea (de Haan et al., 2019). MP was found in 73 % of all macroaggregates (marine snow, mean size: ~500 µm) with buoyant PP as the most abundant polymer type in samples from the Pacific ocean (Zhao et al., 2018). Further aggregation seems to be size selective, favoring the incorporation of small particles into marine aggregates (de Haan et al., 2019; Zhao et al., 2018).

MP in freshwater aggregates have not been reported, yet. Still their presence in freshwater systems and especially in reservoirs seems to be likely, as comparable aggregate types (lake snow) can be found in most larger lakes or freshwater reservoirs (Grossart and Simon, 1993; Grossart et al., 1997).

Several laboratory studies showed the aggregation of small and intermediate MP of variable shapes (fibers, fragments, beads) into sinking aggregates reassembling marine snow (see Table 3).

Table 3: Summary of laboratory experiments describing MP forming sinking hetero-aggregates with natural particles. Studies with plastic particles < 1 µm or focusing on homo-aggregation of MP were excluded from this summary.

Polymer	Particle size [µm]	Shape	Particle concentration	Aggregation partner	Source
PVC	63 - 125	Fragment	1 - 10 mg l^{-1}	Sediment	(Andersen et al., 2021)
PMMA PS	106-250	Fragment	12.5 -125 mg l^{-1}	Phytoplankton	(Cunha et al., 2019)
PS	1 - 6	Sphere	10^6 - 10^{10} particles l^{-1}	TEP	(Drago et al., 2020)
PS	10	Sphere	5 g l^{-1}	Phytoplankton	(De Oliveira et al., 2020)
PP HDPE	400 -1000	Fragment	1 g l^{-1}	Phytoplankton	(Lagarde et al., 2016)
PS	2	Sphere	10^{-4} particles l^{-1}	Phytoplankton	(Long et al., 2015)
PS	2	Sphere	3.96 g l^{-1}	Phytoplankton	(Long et al., 2017)
PS	1	Sphere	100 mg l^{-1}	Phytoplankton	(Liu et al., 2021)
PS	1	Sphere	100 mg l^{-1}	Phytoplankton	(Mao et al., 2018)
PS	700 - 900	Sphere	50 particles l^{-1}	TEP	(Michels et al., 2018)
PA	10 x 50	Fiber	50 particles l^{-1}	Marine snow	(Porter et al., 2018)
PS	7 - 30	Sphere			
PE	9 - 11	Sphere			
PVC	115 - 156	Fragment			
PA	6 - 30	Fragment			
PP	23 x 3000	Fiber			
PS	0.5 - 1	Sphere	5 µg l^{-1}	Marine snow	(Summers et al., 2018)

Further also freshwater microalgae (e.g. *Chlamydomonas reinhardii*) form large (several mm) and sinking colonies (ρ: 1.2 g cm^{-1}) with large HDPE and PP fragments ($>$ 400 µm) (Table 3, Lagarde et al., 2016).

Given the large spectrum of different aggregates found to incorporate MP, it is likely that aggregation will influence MP transport in freshwater systems. However, appropriate laboratory or even field studies to elucidate the role of aggregation for MP transport in freshwater reservoirs are still lacking.

1.4 Biofilms and biofouling on microplastics

Shortly after submerging in water, the surfaces of MP particles will become colonized by various kinds of different micro-, (Amaral-Zettler et al., 2020) and macroorganisms (Kaiser et al., 2017). This greatly impacts density, size and surface properties (stickiness, roughness, hydrophobicity) of the colonized particles. Therefore colonization or biofouling (Rosenhahn et al., 2010) is considered as key process governing MP transport in freshwaters.

Bacteria are usually the first colonizer, adhering to the polymer surface by forming slimy films comprised of sticky proteins (Flemming et al., 2007), polysaccharides (Neu et al., 2001), lipids or nucleic acids (Flemming and Wingender, 2010) summarized under the term extracellular polymeric substances (EPS). This slimy film matures into a complex three-dimensional, structured biofilm, which provides different ecological niches (Battin et al., 2016) and protection for bacterial cells (Romaní, 2010) or other microbial biofilm members such as cyanobacteria, eukaryotic algae, protozoans, fungi and nematodes (Romaní, 2010; Weitere et al., 2018). The community composition is mainly driven by light availability, nutrient concentrations, temperature, pH, oxygen (Salta et al., 2013), grazing pressure (Weitere et al., 2018) and the shear forces experienced within the water bodies (Battin et al., 2003; Risse-Buhl et al., 2017). These factors are often controlled by geographical location (Oberbeckmann et al., 2016) and season (Chen et al., 2019).

MP exhibit surface properties (roughness, free energy, hydrophobicity) distinct from natural particles found in freshwater (Ogonowski et al., 2018). Therefore, microbial community composition on MP might differ from the communities found on natural particles (glass, wood, leaves) originating from the same location (Hoellein et al., 2014). Surface specific attachment of certain bacteria was shown in laboratory studies with limited numbers of bacterial strains (Hossain et al., 2019) or during initial surface colonization (Ogonowski et al., 2018). In addition it has been stated that microbial communities of biofilms growing on MP are enriched with pathogens such as *Vibrio* spp. (McCormick et al., 2014; Wu et al., 2019). However, *Vibrio* spp. are common early colonizers, which are found in high abundance on other surfaces as well (Kesy et al., 2021; Kesy et al., 2019), which questions the statement

of MP as carriers for pathogens in the environment as raised by some authors (Amaral-Zettler et al., 2020; Wu et al., 2019). It remains uncertain whether MP are a unique niche in which specialized bacterial communities, specific to certain polymer types develop. A large meta-analysis indicated that PE particles, collected from various marine locations throughout the world, share at least 13 common and unique (not found on other surfaces) operative taxonomic units (OTU) including members of the families *Microbacteriaceae* and *Sphingomonadaceae* (Oberbeckmann and Labrenz, 2020). However, these unique OTUs only comprised on average 0.47 % of the relative bacterial abundance. Therefore, it is questionable if microbial biofilms found on MP should be called "plastisphere" (Zettler et al., 2013), as this implies differences to biofilms formed on natural surfaces, which could not been shown in a conclusive manner, yet.

After this brief summary on how particle properties shape the MP biofilm community, the viewpoint will be inverted, on how in turn the formation of biofilms affects the properties of MP particles. Under this viewpoint, colonization of submerged surfaces is rather termed biofouling instead of biofilm formation (Rosenhahn et al., 2010). Biofouling covers the process of biofilm formation, followed by the attachment of larger macrofoulers (e.g. mussels, crustaceans). The secondary colonization depends on the properties of the initial biofilms, which provide nutrition and anchoring sites for the macrofoulers (Artham et al., 2009).
Biofouling might alter the transport behaviour of MP by increasing the density (Ye and Andrady, 1991), changing the shape (Shang et al., 2014) or increasing the stickiness of the surface (Michels et al., 2018). The most commonly investigated process is the alteration of density by biofouling. This is facilitated by ballasting material of biogenic origin (e.g. mussels, bryozoans, biofilms, see Table 4) tightly adhering to the particle surface. If sufficient matter is accumulated, even initially buoyant materials such as PE (Kaiser et al., 2019), PP (Chen et al., 2019) or wood (Hess et al., 1999) might start sinking in water. However, this is only possible with ballasting materials having higher densities than the surrounding water and the MP particles. For dense MP polymer types, biofouling with low density biogenic matter might even decrease their settling velocity in water (Ha et al., 2020).

Table 4: Examples for sinking of initially buoyant objects caused by organisms overgrowth (biofouling). Note that the example for the logs (reported by Hess et al., 1999), comes from the Lower Jurassic (185 Ma yrs. ago), were wood was supposed to stay afloat in water for longer time periods compared to modern times. This is often explained by the lacking of shipworms *Teredo* spp. which developed later in the Lower Cretaceous period (Evans and Todd, 1997).

Location	Object	Material	Size	Fouling organism	Time until sinking	Source
China, East lake	Film	HDPE	5x5x0.3 mm 10x10x0.3 mm	algae biofilms	12-30 days >18 days	(Chen et al., 2019)
China, East lake Qinhui River Niushoushan River	Film	PP	5x5x0.32 mm	microbial biofilm	buoyant (44 days)	(Miao et al., 2021)
China, Yellow Sea	Film	LDPE	4x4x0.08 mm	microbial biofilm	buoyant (135 days)	(Tu et al., 2020)
Florida, Biscany Bay	Ballon	Latex	several cm	Porifera (*Mycale americana*)	7 weeks	(Ye and Andrady, 1991)
	Bag	LDPE		Bryozoa (*Schizoporella unicornis*)	7 weeks	
	Web	LDPE		Crustacea (*Balanus venustus*)	7 weeks	
	Rope	PP		Mollusca (*Pteria colymbus*)	7 weeks	
	Tube	LDPE		Chordata (*Ascidia nigra*)	11 weeks	
	Foam	EXPS		Rhodophyta (*Ceramium floridanum*)	buoyant (77 days)	
Germany, Baltic sea Warnow estuary	Sphere	HDPE	1 mm	Mussels (*Mytilus edilus*) microbial biofilms	6 weeks buoyant (98 days)	(Kaiser et al., 2017)
"Germany", Posidonian Sea	Log	Wood	10-20 m	Bivalves (*Pseudamytiloides dubios* Crinoidea (*Seirocrinus subangularis*)	>2 yrs.	(Hess et al., 1999)
Norway, North Sea	Film	LDPE	25x40 cm	calcareous bryozoan brown algae (*Lithoderman* spp.)	3-4 months	(Edlin et al., 1975)
South Africa, False Bay	Films	LDPE HDPE	5x5x0.1 mm 50x50x0.1 mm 5x5x1 mm 50x50x1 mm	diverse macrofoulers: Mussels, hydroids, barnacles bryozoans, ascidians algae,tanaids, amphipods	17 days 49 days 39 days 62 days	(Fazey and Ryan, 2016)
UK, Atlantic	Bags	PE	20x28 cm	microbial biofilms	3 weeks	(Lobelle and Cunliffe, 2011)

The effects of biofouling on initially buoyant materials such as MP was mostly studied in marine settings (see Table 4 for a summary). Biofouling usually leads to settling within few weeks after the object submerged in water. Depending on the

trophic state (Lobelle et al., 2021) and the temperature of water body (Edlin et al., 1975) or the size and shape of the particle (Chubarenko et al., 2016) settling onset might be extended up to several months or years (Hess et al., 1999; Khatmullina and Chubarenko, 2019). Smaller particles are considered as more prone to biofouling due to higher surface to volume ratio (Figure 2, Fazey and Ryan, 2016). Regarding MP shape, spheres are supposed to sink more readily than films or fibers once they are fully covered by a fouling film (see Figure 2).

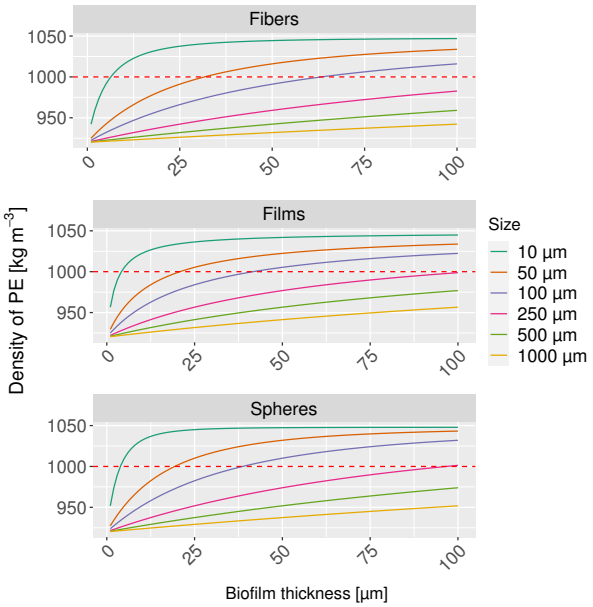

Figure 2: Density increase of PE caused by overgrowth with a uniform biofilm cover (assuming ρ_{biofilm}: 1048 kg m^{-3} from Ha et al., 2020) calculated by iterating (100 times, step size 1 µm) equations provided by Chubarenko et al., 2016. Red dashed line indicates at which biofilm thickness PE of different shapes and sizes become negatively buoyant. Size refers to radius for spheres and fibers or diameter for films. The calculations start with a biofilm coverage of 1 µm thickness. This causes that the smallest particles have a density higher than the density of pristine PE (920 kg m^{-3}) right from the beginning.

The extent of biofouling decreases with water depth (Tu et al., 2020), subsequently defouling and regaining of buoyancy might occur for particles sinking or dispersing out of the euphotic zone (Kooi et al., 2017; Ye and Andrady, 1991). The presence of calcareous macrofoulers was often perceived as prerequisite for the sink-

ing of MP particles (Fazey and Ryan, 2016), as they add substantial biomass with high densities (shells, skeletons) to the fouling film (Kaiser et al., 2017). Common calcareous freshwater biofoulers such as bivalves (*Dreissena*, *Corbicula*), bryozoans and snail or non-calcareous but siliceous sponges can be considered to influence MP in lakes, reservoirs or rivers (Nakano and Strayer, 2014), but have not been reported within plastic associated freshwater biofilms (see Figure 3).

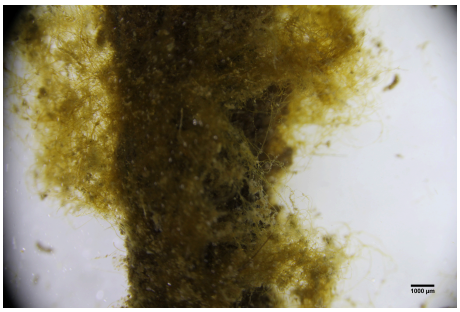

(a) True color binocular image (10x), scale bar: 1000 µm

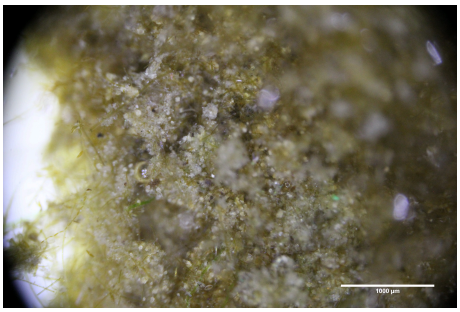

(b) True color binocular image (40x), scale bar: 1000 µm

(c) False color CLSM image (200x), scale bar: 75 µm

Figure 3: Example for an freshwater biofilm developed on a PE plastic film incubated for 2 years in the hypertrophic Beetzsee (Brandenburg an der Havel, Germany). Incubation experiment and image recording were conducted by the author of this thesis. Color coding (C): green (bacteria), pink/purple (cyanobacteria), blue (algae), white (reflection).

In addition, the residence time of MP particles in freshwater reservoirs might not be sufficient for the development of complex biofouling communities with calcareous macrofoulers. Still, the sinking of PP MP after exposure in a freshwater lake and development of microalgae biofilms have been reported recently (Chen et al., 2019). It remains unclear, how the described colonization by small numbers of low density organisms (ρ: 1080 kg m^{-3}) (Guerrero et al., 1985) facilitated the sinking of buoyant MP (Chen et al., 2019). Biofilms might entrap suspended solids (see Figure 3b) from the surrounding water, or biogenic activities could precipitate minerals within the biofilm, which leads to the increased particle density (Chen et al., 2019).
In summary, the extend of biofouling relies mostly on temperature (influenced by seasons) (Chen et al., 2019), water chemistry (trophic state) (Lobelle et al., 2021), hydrodynamic conditions (Risse-Buhl et al., 2017) and presence of specific organisms (Kaiser et al., 2017). Freshwater reservoirs differ with all of these aspects from marine environments. As most studies were conducted in marine settings, a large knowledge gap towards the impact of biofouling on MP in freshwaters, especially freshwater reservoirs was identified. Elucidating the role of biofouling by taking reservoir specific aspects, such as stratification and changing redox conditions, into account, was one of the major challenges of this thesis.

1.5 Iron and calcium mineral formation

The previously mentioned mechanisms aggregation and biofouling are important to understand how biogeochemical processes influence the transport of MP in freshwater reservoirs. In this context the formation of iron and calcium minerals under the influence of reservoir specific redox conditions will be discussed and linked to the aforementioned processes.

The precipitation of iron minerals (mainly iron (oxyhydr)oxides) (Cornell and Schwertmann, 2003)) is a process specific for stratified lakes or freshwater reservoirs. Prerequisite for this is a stable stratification separating the surface water (epilimnion) from the profundal (hypolimnion) by a thermocline (Ladwig et al., 2021). This allows the bottom water to become anoxic due to oxygen consuming processes, such as mineralization of organic matter through respiration. Consequently, ferrous iron (Fe(II)) is released from the sediments via microbial iron reduction (Kappler et al., 2021; Melton et al., 2014) and enriched in the anoxic hypolimnion (Mortimer, 1942). Under neutral to alkaline pH, dissolved ferrous iron will be rapidly oxidized to ferric iron (Fe(III)), when coming into contact with oxygen (Barry et al., 1994). Ferric iron is unstable in water (Sigg and Stumm, 2016), consequently precipitates as amorphous iron (oxyhydr)oxides (Tipping et al., 1981) and forms large, sinking flocs with organic material (iron-organo flocs) originating from the lake water (Deppe and Benndorf, 2002). During stratification this process takes place directly above the pycnocline (Bravidor et al., 2015), but might extend to the whole water column, when the stratification is disrupted by currents or winds (Mortimer, 1942; Oliver et al., 1985). Iron-organo flocs are capable to sorb or enclose dissolved nutrients, such as phosphorus and subsequently transport them down to the sediment through gravitational settling (Deppe and Benndorf, 2002; Sigg and Stumm, 2016). It was found that initially buoyant *Microcystis* spp. colonies also aggregate with sinking iron-organo flocs originating from autumnal lake mixing (Oliver et al., 1985). This indicates the potential of iron flocculation to not only remove dissolved, but also particulate matter from the water column. MP are in the same size range and having similar densities (Chen and Lürling, 2020), compared to cyanobacterial colonies. Hence, they might be prone to iron mediated aggregation and settling in

lakes or reservoirs. This could be even more important for biofouled MP, whose sticky surfaces enhance aggregation processes (Michels et al., 2018). However, the iron (oxyhydr)oxides inside of the flocs are prone to microbial iron redcution, once laying on top of the sediments (Kappler et al., 2021). The dissolution of iron oxides in the sediments is often accompanied by the release of organic matter (Patzner et al., 2020), nutrients (NO_3^-, PO_4^{3-}) and pollutants (metals, organics), formerly bound to the minerals. Whether particulate pollutants such as MP can also be released due to dissolution of the enclosing iron mineral coating, has so far not been investigated.

Calcite precipitation is another important biogenic process in freshwater reservoirs (Dittrich and Koschel, 2002), leading to the formation of dense, calcified biofilms (Merz-Preiß and Riding, 1999) or to release of microcrystals (Thompson et al., 1997) into the water phase. In freshwater reservoirs calcite precipitation is often induced by phototrophs, in particular cyanobacteria, under carbon limiting conditions (Riding, 2006). Carbon limitation might occur during extensive planktonic blooms or inside of biofilms (Riding, 2006), which forces cyanobacteria to take up HCO_3^- instead of the depleted CO_2 for their carbon fixation cycle. In the cytoplasm HCO_3^- is transformed to CO_2, and OH^- is released from the cells into the water (Badger and Price, 2003). This increases the pH in the vicinity of the cells, shifting the carbonic acid equilibrium towards carbonate (CO_3^{2-}) (Lee et al., 2004). As Ca^{2+} originating from the water phase accumulates in associated sheets or surface layers of the cells, formation of calcite ($[Ca^{2+}]_{(aq)} + [CO_3^{2-}]_{(aq)} \longrightarrow [CaCO_3]_{(s)}$) becomes thermodynamically feasible (Riding, 2006).

Calcite is precipitated in proximity to the phototrophic organism, but remains only loosely associated with the cells and can be shed from the cell surface into the water (Martinez et al., 2010). The released sub-micron calcite crystals can reach concentrations up to 2.8 x 10^7 particles l^{-1} (Vanderploeg et al., 1987) in surfaces waters of mesotrophic water bodies (Ortíz-Caballero et al., 2019; Stabel, 1986; Teranes et al., 1999). The minerals are often associated with organic matrices (Riding, 2006) and aggregate with cells or organic material in the lake (Küchler-Krischun and Kleiner, 1990). This leads to flocculation of floating cells or particles and their subsequent transport to the sediments inside of calcite-organo aggregates (Osman-Sigg, 1982).

Calcite formed within biofilms by sessile cyanobacteria is often not released to the surrounding water. Instead minerals might stick to the EPS of the biofilms or encrust the non-motile cyanobacterial cells (Zippel and Neu, 2011). Subsequently calcite can make up 20 - 40 % (Tianzhi et al., 2014; Záray et al., 2005) of freshwater biofilms masses. It can be assumed that calcite rich biofilms (ρ_{Calcite}: 2.7 g cm^{-3}), have a substantial ballasting effect on particles in freshwater reservoirs.

The aggregation of MP particles with mineral flocculants, such as the presented iron hydro(oxides) and calcite crystal might display unique processes influencing the fate of these contaminants in stratified standing freshwater bodies. Further the precipitation of minerals inside of biofilms growing on plastics might also important for governing the sedimentation of initially buoyant polymers.

1.6 Research questions and objectives

The objective of the presented work was to investigate how biogeochemical processes govern the MP transport in freshwater reservoirs. In particular the question, whether biofilm formation and aggregation in combination with mineral precipitation could initiate the sinking of buoyant MP was addressed, by this possibly explaining the surprisingly high concentrations of light density polymers in reservoir sediments. The overarching objective of this work was to further elucidate the potential of standing freshwater bodies to facilitate permanent deposition of MP in their sediments. The objectives can be further summarized into the research questions:

- Does biofilm calcification increase the density of buoyant PE in eutrophic freshwater reservoirs and can calcifying planktonic cyanobacteria aggregate small MP particles?
- Does biofilm formation influence the settling velocity of MP in mesotrophic freshwater reservoirs and is the biofilm formation redox/ depth dependent?
- Lead the aggregation with iron-organo flocs to permanent deposition of MP in reservoir sediments and does the stability of MP in sediments depend on the prevailing redox conditions?
- Is the disintegration of iron-organo flocs connected to microbial iron reduction and subsequently to the release of PE MP?

1.7 Methodological approach

This cumulative dissertation consists of two scientific peer-reviewed papers (Chapter 2 & 3), which have been published in the Journal Water Research and one manuscript (Chapter 4) currently under review in Nature Scientfic Reports (on June 11th 2021). Further one manuscript (Chapter 5) has been submitted (11th of June) to Limnology and Oceanography Letters.
The dissertation opens with a study elucidating the impact of cyanobacterial **calcite precipitation** on MP buoyancy (**Chapter 2**), which was studied working with

biofilms grown on MP incubated in the eutrophic Bautzen reservoir, in combination with laboratory experiments employing *Microcystis* spp. cultures under varying calcium concentrations.

This is followed by the investigation of **biofilm development and sorption of metals** on MP exposed in different depths of the mesotrophic Malter reservoir, during and after the summer stratification (**Chapter 3**). In this study the importance of iron precipitates for the buoycancy of MP became apparent. Hence, the role of **iron-organo flocs** for the sedimentation and subsequent burial of initially buoyant PE MP in sediments, was investigated employing laboratory experiments with natural sediment cores from Bautzen reservoir (**Chapter 4**) and pure culture batch experiments with iron reducing bacteria *Shewanella oneidensis* (**Chapter 5**).

In the last chapter the major findings and their implications for MP in reservoirs are resumed. Further, knowledge gaps, additional research questions, and possible directions of future research are discussed. All practical work was conducted in the Helmholtz-Zentrum für Umweltforschung GmbH - UFZ in Magdeburg. The author of this thesis was involved in the project MikroPlaTas (BMBF: 02WPL1448A), which gave the framework and motivation for the presented investigations.

Chapter 2

Manuscript 1

Interaction of cyanobacteria with calcium facilitates the sedimentation of microplastics in a eutrophic reservoir

Water Research (2021), 189, 116582, doi:10.1016/j.watres.2020.116582

Rico Leiser, Rense Jongsma, Insa Bakenhus, Robert Möckel, Bodo Philipp, Thomas R. Neu and Katrin Wendt-Potthoff

Water Research 189 (2021) 116582

Contents lists available at ScienceDirect

Water Research

journal homepage: www.elsevier.com/locate/watres

Interaction of cyanobacteria with calcium facilitates the sedimentation of microplastics in a eutrophic reservoir

Rico Leiser[a,*], Rense Jongsma[b], Insa Bakenhus[b], Robert Möckel[c], Bodo Philipp[b], Thomas R. Neu[d], Katrin Wendt-Potthoff[a]

[a] Department of Lake Research, Helmholtz Centre for Environmental Research, Brückstraße 3a, 39114 Magdeburg, Germany
[b] Institute of Molecular Microbiology and Biotechnology, Westfälische Wilhelms-Universität Münster (WWU), Corrensstr. 3, 48149 Münster, Germany
[c] Helmholtz-Zentrum Dresden-Rossendorf, Helmholtz Institute Freiberg for Resource Technology, Chemnitzer Str. 40, 09599 Freiberg, Germany
[d] Department of River Ecology, Helmholtz Centre for Environmental Research, Brückstraße 3a, 39114 Magdeburg

ARTICLE INFO

Article history:
Received 26 June 2020
Revised 30 September 2020
Accepted 29 October 2020
Available online 30 October 2020

Keywords:
Microplastic
Reservoirs
Cyanobacteria
Calcite
Biofouling
Biofilms
Sedimentation

ABSTRACT

Low-density microplastics are frequently found in sediments of many lakes and reservoirs. The processes leading to sedimentation of initially buoyant polymers are poorly understood for inland waters. This study investigated the impact of biofilm formation and aggregation on the density of buoyant polyethylene microplastics. Biofilm formation on polyethylene films (4 × 4 × 0.15 mm) was studied in a eutrophic reservoir (Bautzen, Saxony, Germany). Additionally, aggregation dynamics of small PE microplastics (~85 µm) with cyanobacteria were investigated in laboratory experiments. During summer phototrophic sessile cyanobacteria (*Chamaesiphon* spp. and *Leptolyngbya* spp.) precipitated calcite while forming biofilms on microplastics incubated in Bautzen reservoir. Subsequently the density of the biofilms led to sinking of roughly 10% of the polyethylene particles within 29 days of incubation. In the laboratory experiments planktonic cyanobacteria (*Microcystis* spp.) formed large and dense cell aggregates under the influence of elevated Ca^{2+} concentrations. These aggregates enclosed microplastic particles and led to sinking of a small portion (~0.4 %) of polyethylene microplastics. This study showed that both sessile and planktonic phototrophic microorganisms mediate processes influenced by calcium which facilitates densification and sinking of microplastics in freshwater reservoirs. Loss of buoyancy leads to particle sedimentation and could be a prerequisite for the permanent burial of microplastics within reservoir sediments.

1. Introduction

Microplastics (MP) are frequently found in freshwater environments raising concerns about distribution pathways and ecological impacts of this novel contaminant. High loadings of MP are present in lake (Ballent et al., 2016) and reservoir sediments (Di and Wang, 2018), which may act as permanent sinks (Corcoran et al., 2015). The largest share of MP in sediments is often comprised of polyethylene (PE) which has a lower density than water (Ballent et al., 2016). Due to its physical properties this polymer type is expected to stay afloat in the water column instead of settling to the ground (Chubarenko et al., 2016).

After release into the environment, MP density, size and shape can be changed by biofouling (Kaiser et al., 2017) or aggregation with natural particles and planktonic cells (Lagarde et al., 2016). The term biofouling describes the attachment of microorganisms (biofilm formation) and macro-organisms to submerged surfaces (Rosenhahn et al., 2010). In the oceans where calcareous macro-foulers such as mussels (Kaiser et al., 2017), bryozoans (Edlin et al., 1975) or barnacles (Fazey and Ryan, 2016) are commonly found on plastics, biofouling may lead to sinking of buoyant polymers within weeks. The conditions in freshwater lakes differ from the marine environment resulting in fouling films dominated by more soft-bodied organisms (Leiser et al., 2020). Still, formation of cyanobacteria dominated biofilms can lead to the sinking of buoyant polymers (Chen et al., 2019). However, the ballasting effects of cyanobacteria (ρ: 0.990 to 1.055 g cm^{-3}) are considered being insufficient to sink buoyant MP (Li et al., 2016). Therefore it was hypothesized that the density increase originated from minerals trapped or formed inside the biofilm matrix (Chen et al., 2019).

Sessile cyanobacteria as component of aquatic biofilms play a major role in the precipitation of calcite ($CaCO_3$) (Jansson and Northen, 2010) and the subsequent lithification of biofilms (Macintyre et al., 2000) or formation of biogenic tufa (Zippel and Neu, 2011). The finding that dense biofilms ($\rho_{Biofilm} > \rho_{Water}$) may form in lakes (Chen et al., 2019) suggests that sinking of buoyant

* Corresponding author.
E-mail address: rico.leiser@ufz.de (R. Leiser).

https://doi.org/10.1016/j.watres.2020.116582
0043-1354/

MP may be facilitated by biogenic calcite precipitation. Whether the ballasting effects of freshwater biofilms are derived from the microbial biomass or from minerals was investigated in a field study.

Planktonic cyanobacteria are present in many reservoirs (Li et al., 2016) and lakes (Ortíz-Caballero et al., 2019) forming extensive blooms during late summer. *Microcystis* spp. are the most abundant phototrophs in Bautzen reservoir during July and August (Kamjunke et al., 1997). In lake water *Microcystis* spp. are aggregating to large and sinking colonies (Chen and Lürling, 2020) under the influence of dissolved Ca^{2+} (Xu et al., 2016a). These cell aggregates are often exceeding 500 µm in diameter (Feng et al., 2019), possibly enclosing small inorganic particles (Xu et al., 2016b). The question whether such *Microcystis* aggregates form under the influence of Ca^{2+} and subsequently could enclose or sink buoyant MP was studied in lab experiments.

Therefore we investigated interaction of sessile and planktonic cyanobacteria with calcium in regards of their impact on the buoyancy of PE in freshwater reservoirs.

We hypothesized that i) biofilms form on large PE in a eutrophic reservoir leading to a loss in buoyancy ii) buoyancy loss is caused by calcite precipitation iii) planktonic cyanobacteria sink small PE MP through Ca^{2+} induced aggregation. These hypotheses were tested by conducting a field experiment in the eutrophic Bautzen reservoir (Saxony, Germany) and laboratory batch experiments with calcifying cyanobacteria.

2. Material and methods

2.1. Study site

Bautzen reservoir is a freshwater body in the eastern part of Germany, providing water for cooling of coal-fired power stations, fish farming, and agricultural irrigation. It is a large (5.3 km^2) but rather shallow (mean depth 7.4 m) reservoir (Kasprzak et al., 2007), often experiencing strong winds, which sometimes even destroy the summer stratification (Kerimoglu and Rinke, 2013). Bautzen reservoir is eutrophic, with extensive blooms of *Microcystis* spp. (Kamjunke et al., 1997) occurring during summer which results in pH values up to 9.5 in the surface water. One sediment trap (Uwitec, Austria) collecting settling matter was deployed near the deepest point of the reservoir (depth: 12 m) during the year 2018 from May to December and sampled in monthly intervals.

2.2. Plastic material, exposition, and sampling procedure

Squares (4 × 4 × 0.15 mm) made from low-density polyethylene (Goodfellow ET311251, ρ: 0.924 g cm^{-3}) were incubated near the deepest point of the reservoir within a cylindrical stainless steel cage (200 particles, diameter 10 cm, length 25 cm, mesh width 3 mm) (Kettner et al., 2017). The cages had a shading effect which reduced the incoming sunlight intensity by ~33% (Leiser et al., 2020). Particles were sterilized by treatment with ethanol (70% v/v, 10 min) prior to the experiment. The cage was incubated from July 23 to August 21, 2019 (29 days) in 0.5 m depth. Profiles of oxygen concentrations, chlorophyll *a*, pH, temperature (multi-parameter probe, Sea & Sun Technologies, Germany) were measured on both dates (Figure S1).

2.3. Biofilm characterization and sampling procedures

Particles were gently removed from the cage by tweezers or by flushing with reservoir water. Particles for confocal laser scanning microscopy (CLSM) analysis were fixed in 4% v/v formalin solution right after removal from the cage. The other particles were stored in pre-combusted (450°C, 4 h) glass Petri dishes in filtered reservoir water. Additional biofilm samples were taken from the inner wall of the cage and stored in reservoir water as well. These samples were used to characterize the biofilms in regards of dry mass, mineral composition and elemental content. The PE particles were in close proximity to or even enclosed by biofilms growing on the inner cage walls. Given their visual appearance biofilms on PE were not different from biofilms from the inner cage walls (Figure S2). Therefore cage walls biofilms were considered being comparable to PE biofilms in regards of the above mentioned parameters. Most samples (except samples for DNA extraction) were stored at 8°C in the dark until processing. The densities and volumes of three fresh biofilm sub-samples from the inner walls of the cage (300 – 400 mg) and three pooled sunken PE particles were analysed with pycnometers at 25°C. Dry weight (60°C, 24 h) and ash mass (450°C, 24 h) were determined for three individual cage walls biofilm samples. The cell volume of microorganisms (biovolume) within the biofilms of ten buoyant and five sinking PE-particles was analysed via CLSM and image analysis. Particles were examined at five (floating) or ten (sinking) random locations resulting in a total sample size of 50 for each. Calcein assay (Zippel and Neu, 2011) was used to visualize Ca carbonate minerals within the biofilms of two sinking PE particles. Twenty particles for 16S amplicon sequencing were carefully rinsed with DNA-free phosphate-buffered saline (pH 7.4) and stored in liquid nitrogen. Calcium content within the cage walls biofilm dry mass was analysed by ICP-OES (detection limit: 0.1 mg l^{-1}). X-ray diffraction was used to analyse the mineral phase of cage walls biofilm dry mass.

2.4. CLSM imaging

Plastic particles with biofilms were prepared for CLSM as described elsewhere (Leiser et al., 2020). In brief: Particles were mounted and stained (SybrGreen, calcein) in Petri dishes. Imaging was done using a TCS SP5X upright microscope equipped with white laser and 63x NA 0.9 lens (Leica). Calcein staining (1 µg l^{-1}; 2 h, room temperature) was used to visualize divalent cations such as Ca^{2+} and Ca carbonate minerals (Zippel and Neu, 2011). Calcein staining is not specific for Ca^{2+} ions or calcite, and may also react with other divalent cations present in the solution. The calcein stain did not bind to pristine PE particles (data not shown). PE particles were stained with non-toxic iDye PolyPink following established protocols (Karakolis et al., 2019). Bacteria, algae and cyanobacteria were identified via SybrGreen staining, autofluorescence of chlorophyll *a* or phycobilins, respectively (Table S1 for excitation / emission wavelengths). Images were visualised and projected by Imaris (Bitplane) and presented by Photoshop (Adobe). An adaptation of ImageJ was used to semi-quantitatively calculate the biovolumes of algae, bacteria and cyanobacteria cells (Staudt et al., 2004).

2.5. Cyanobacteria cultures and laboratory aggregation experiments

The effect of dissolved Ca^{2+} on the aggregation of MP with cyanobacteria was investigated using non-axenic cultures of *Microcystis* sp. strain BM25 (Schwarzenberger et al., 2013) grown in WC media (Guillard and Lorenzen, 1972) without vitamin solution and silicate. Pre-cultures were grown on a rotary shaker (110 rpm) at room temperature and ambient daylight for 4 weeks prior to the experiment. PE powder (ρ: 0.920 g cm^{-3}; Alfa Aesar 9002-88-4) was sieved through 100 µm and 10 µm stainless steel sieves (Retsch, Germany) to obtain a defined size range of 100 – 10 µm. The mean equivalent spherical diameter (ESD) of the sieved particles was 85 ± 14 µm (n: 60). Particles were stained with iDye PolyPink (Karakolis et al., 2019). Three different Ca^{2+} concentrations (10 mg l^{-1}, 60 mg l^{-1} and, 220 mg l^{-1}) were tested for their potential to aggregate *Microcystis* sp. strain BM25.

Experiments were conducted in triplicates by inoculating 500 ml WC-media with 10 % v/v cyanobacteria pre-culture in airtight 1-liter flasks. Cell concentrations (~10^7 cells ml^{-1}) were chosen to reflect the concentration of *Microcystis* spp. in Bautzen reservoir during summer (~3 -5 $\times$ 10^7 cells ml^{-1}, data provided by the state reservoir administration of Saxony / Landestalsperrenverwaltung des Freistaates Sachsen (LTV)). Right after inoculation, samples for pH, Ca^{2+} and cell counts were taken. Directly afterwards pH was measured using a pH meter (PP-50, Sartorius). Calcium samples were filtered (0.2 µm) and stored at 4°C. Cyanobacteria cells were fixed in Lugol's iodine (5 % w/v iodine) until cell counting. Afterwards 10 mg (6.3 $\times$ 10^4 particles l^{-1}) of PE were added to the flasks. The cultures were then incubated at 23.5°C under constant light (70 W m^{-2}) on roller incubators (10 rpm) until visible aggregates formed. Depending on the Ca^{2+} concentration, aggregates formed within hours to days. Experiments showing no aggregation were stopped after 7 days. Upon termination, samples for Ca^{2+}, pH and cell counts were taken as described above. Aggregates formed within the flasks were photographed and counted employing ImageJ cell counter plugin (Rueden et al., 2017). Furthermore visible aggregates were gently removed using an inverted glass pipette. Twelve aggregates per Ca^{2+} condition (4 per triplicate) were transferred into a coverwell chamber (Thermo Fisher Scientific) for CLSM. Ca^{2+} and fluorescent MP within the sinking aggregates were visualized via CLSM. Density measurements were conducted with 9 aggregates per Ca^{2+} condition (3 per triplicate) in a temperature controlled chamber at 20°C. Aggregates were transferred to ultrapure water (20°C) and titrated with NaI (2 g ml^{-1}, ρ: 1.690 g cm^{-3}) until neutral buoyancy was achieved. The density of the resulting solution was measured with pycnometers. Sinking velocities of 30 individual aggregates (10 per triplicate) were determined in a column (diameter 5 cm) filled with tap water (20°C) and recorded with a camera (13 megapixel, 30 fps). Afterwards the same aggregates were removed from the column and checked for their plastic content under a light microscope. The ESDs of sinking aggregates were calculated from the recorded images using ImageJ. Sunken biomass/aggregates remaining after aggregate selection and sampling were filtered onto a stainless steel sieve (47 mm, pore size 10 µm) to remove non-aggregated cells. The filters were subsequently rinsed three times with ultrapure water. The biomass was dried (60°C, 24 h) and analysed for its mineral content using XRD. Cell concentrations were determined by epifluorescence microscopy after SybrGreen staining. Calcium concentrations in the media were measured via ICP-OES.

2.6. X-ray diffraction

X-ray diffraction was performed using a PANalytical Empyrean diffractometer, equipped with a Co-tube, automatic divergence slit and PIXcel 3D detector. Field samples were sieved (< 4 mm) to remove PE squares and filled into 27 mm sample holders. Measurements were performed from 5 to 80 °2θ with a stepsize of 0.0131 °2θ and total measurement time of 2 h 30 min. The irradiated area on the sample was kept constant at 12 $\times$ 15 mm by means of respective mask and the automatic divergence slit. Samples from laboratory experiments showing low mass on stainless steel filters were prepared on silicon low background holders and measured under the same conditions. Data were evaluated by the use of PANalytical's HighScore software and the BGMN/Profex package v4.0.2 (Doebelin and Kleeberg, 2015).

2.7. DNA extraction, Illumina sequencing and bioinformatics

Total DNA was extracted using the DNA Power Soil Pro Kit (Qiagen) with modifications. Biofilm covered plastic particles were transferred into the PowerBead Pro Tubes containing 800 µl of solution CD1. The tubes were fixed horizontally to a vortex adapter and shaken for one hour for mechanical disruption of bacteria. Afterwards samples were incubated for one hour with 25 μl proteinase K (22 mg ml^{-1}) at 37°C. The extraction was continued following the instructions given by the supplier. Libraries, sequencing and data analysis were performed by Microsynth AG (Balgach, Switzerland). To assess the bacterial diversity, the V4-V5 region of the bacterial 16S rRNA gene was amplified by two-step PCR using the primer pair 515F-Y and 926R (Parada et al., 2016). Libraries were sequenced using a v2 500 cycle kit and the Illumina MiSeq platform. The raw data were submitted to the ENA (European Nucleotide Archive) database and were assigned the BioProject ID: PRJEB38919. Standard statistical analysis and bioinformatics were employed to obtain relative abundance of the bacterial phyla (S3). The OTUs assigned to *Cyanobacteria* were further classified using BLAST analysis (Altschul et al., 1990) using nucleotide database (nt/nr) with uncultured and environmental sample sequences excluded.

2.8. Statistical analysis and programs

Visual MINTEQ (Version 3.1, Royal Swedish Academy of Science) was employed to calculate the saturation indices of calcite ($SI_{calcite}$) in Bautzen reservoir for the years 2018 and 2019 using the default thermodynamic database. The dataset used for modelling contained major water anions, cations, pH, temperature and chlorophyll content of Bautzen reservoir and has been provided by the LTV. Data normality was checked via Q-Q Plots and histograms. F-test was used to test for variance homogeneity prior to conducting t-tests and ANOVA. Differences between datasets were seen as statistically significant for $p < 0.05$. Akaike information criterion method was used to select the best fitting multiple linear models. Residual plots were examined for the validity of the linear models. Non-parametric rank-based tests and median statistics were used for non-normally distributed data. R (R Core Team, 2018) was used for statistical analysis and for the graphs.

3. Results & discussion

3.1. Calcite precipitation in Bautzen reservoir

Summer blooms of phototrophic microorganisms accompanied by high pH values and the decline of dissolved Ca^{2+} in surface water (Figure S3) were observed in 2018 and 2019. Calcium made up between 0.9% and 6.3% of the settling matter during June-July and July-August 2018 (Table S2). Assuming that this Ca was present solely in the form of calcite this mineral accounted for 0.24 – 2.23 g m^{-2} d^{-1} or up to 16.7% of the total settling matter during this time. Bautzen reservoir has a lower potential for calcite precipitation in the surface water compared to lakes such as Baldeggersee (Luzern, Switzerland) producing 10 – 20 g calcite m^{-2} day^{-1} (Teranes et al., 1999) or Lake Constance (Switzerland, Germany, Austria) with 14 g m^{-2} d^{-1} (Stabel, 1988). Calcite precipitation is of high importance for matter flux in many eutrophic and mesotrophic lakes, whereas being less intense in hyper-eutrophic and oligotrophic water bodies (Koschel et al., 1983).

3.2. Field biofilms and microplastic biofouling in Bautzen reservoir

The incubation cage and PE-particles were covered by dense brownish biofilms after the incubation period of 29 days. Whitish minerals (Fig. 1a) covered the biofilms surfaces and calcein stainable minerals were found in close proximity to cyanobacterial cells (Fig. 1b).

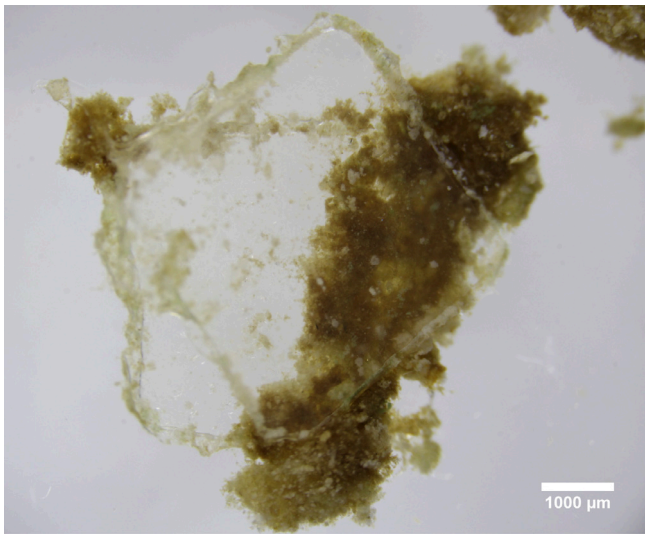

(a)

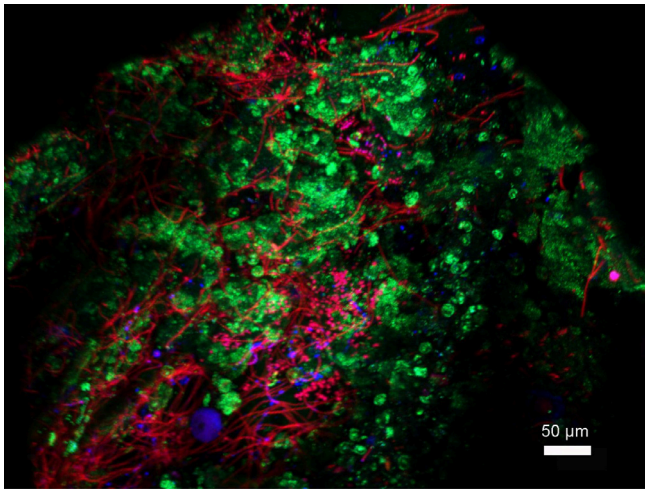

(b)

Fig. 1. Binocular image (white bright field, 10x magnification) (a) showing the biofilm covered PE particles and white mineral precipitation within the covering biofilms. CLSM image (b) showing cyanobacteria, (red, purple) and calcite (green) within the biofilms on PE particles. (For interpretation of the references to color in this figure legend, the reader is referred to the web version of this article.).

This mineralized appearance of the biofilm was reflected by the high dry mass (19.5 ± 3.6%, n: 3) and ash content (91.2 ± 1.9%, n: 3). Mineral phases of the cage walls biofilms were comprised of 98% pure calcite and 2% quartz as shown by XRD analysis (Figure S4). The contents of major elements within the cage walls biofilms dry mass were 0.2% Al, 31.1% Ca, 0.3% Fe, 0.4% Mg, 0.1% Mn, and 0.12% Si. As Ca appeared solely in the form of calcite ($CaCO_3$) this mineral accounted for ~78% of the biofilms dry mass. The calcite content of Bautzen reservoir biofilms was higher compared to biofilms found in Lake Velence (30% calcite) (Záray et al., 2005) and the Sanjiadian reservoir (20 – 40%) (Tianzhi et al., 2014). Thus calcite seems to be a common and major component of biofilms in lakes of different trophic states and water chemistry. The respective wet density of the calcified biofilms was 1.18 g cm^{-3} ± 0.012 (n: 3, 20°C). Given the similarity of cage walls biofilms and PE biofilms (Figure S2) results might be extrapolated to the MP particles. However, it cannot be excluded that biofilm properties slightly differed, which should be considered while interpreting the results.

The community composition within the biofilms of buoyant and sunken PE particles was examined via CLSM and 16S amplicon sequencing. CLSM analysis showed that the sunken particles had significantly higher cell volumes of bacteria (0.43 to 0.007 µm^3 µm^{-2}), cyanobacteria (0.09 to 0.0002 µm^3 µm^{-2}) and algae (0.03 to 0 µm^3 µm^{-2}) if compared with the buoyant particles (Fig. 2). Cyanobacteria occurred either as filamentous colonies of elongated thin cells which were found in 85% of the analysed images (n: 50) or as colonies of rounded cells found in 28% of the images (n: 50). Classification of the 16S rRNA gene sequences revealed a dominance of non-phototrophic bacteria (66% of all sequences, Fig. 3). Still a significant abundance (34%) of cyanobacteria was detected within the calcifying biofilms. Only 12 different bacterial phyla were found on the particles. Such low OTU richness has been described previously as a common feature of microbial biofilms on MP (Amaral-Zettler et al., 2020). The non-phototrophic phyla found in this study have already been described by other authors to colonize MP exposed to river or lake water (Hoellein et al., 2014; Wang et al., 2020; Wu et al., 2019).

Within the cyanobacteria GpI were the most abundant group (26%), followed by GpV (7%), and GpIIa (1%) (Fig. 3). Based on further classification of the sequences using BLAST analysis (Altschul et al., 1990) the groups GpI and GpV could be assigned to *Chamaesiphon* spp. and *Leptolyngbya* spp. According to their morphology, the colonies of rounded cells could belong to *Chamaesiphon* spp. (Kurmayer et al., 2018) whereas the filamentous colonies, which were found in most of the images, resembled *Leptolyngbya* spp. (Arp et al., 2010) cells. Both genera, *Chamaesiphon* spp. (Peraza Zurita et al., 2005) and *Leptolyngbya* spp. (Zippel and Neu, 2011), are common members of calcifying freshwater biofilms (Arp et al., 2010). Especially *Leptolyngbya* spp. has been associated with an increase of $SI_{Calcite}$ and calcite precipitations within stream biofilms (Brinkmann et al., 2015). Further, calcite grains are often found in close proximity or even encrusting cyanobacterial cells (Martinez et al., 2010), which was also observed in our study using calcein staining (Fig. 1b). Hence it is likely that calcite was precipitated by cyanobacteria leading to densification of the biofilms and subsequent sinking of the PE particles. Still heterotrophic bacteria might have influenced the calcite precipitation by providing nucleation sites or releasing Ca^{2+} bound to the organic biofilm matrix (López-García et al., 2005). As algae and diatoms were scarce throughout, occurring in only 10% of the image datasets (n: 50), their influence on calcite precipitation might have been minor.

PE particle buoyancy was tested by observing their upward or downward movement in water. Approximately 20 to 30 particles (10 – 15%) lost their buoyancy at the end of the field experiment. For a minor fraction of PE particles physical disturbance by the sampling procedure led to a certain loss of biofilm and consequently to regaining of their buoyancy. The interior of the cage was covered with biofilms entrapping and hiding some of the PE particles. As a consequence the proportion of sunken particles could not be estimated precisely leading to the conservative number of 20 to 30 sunken particles. The density of the sunken PE-particles was 1.19 g cm^{-3} at 20°C (n: 1), which implies a sharp density increase compared to pristine particles (ρ: 0.924 g cm^{-3}). Biofilm formation has already been reported to sink buoyant MP within 18 days in shallow and high productive lakes (Chen et al., 2019). The authors hypothesized that minerals (calcite, clays) trapped within the biofilms rather than the microbial cells induced sinking of the MP (Chen et al., 2019). In the present study a biofilm volume of 2.68 × 10^{-2} cm^3 (n: 1) was bound to the sunken MP from Bautzen reservoir of which only ~ 1.85 × 10^{-6} cm^3 (n: 50) was accounted for by cells. The main part of the fouling film (collected from cage walls) was comprised of water (around 77% of the weight), organic material (around 2%) and inorganic components (around 21%) with

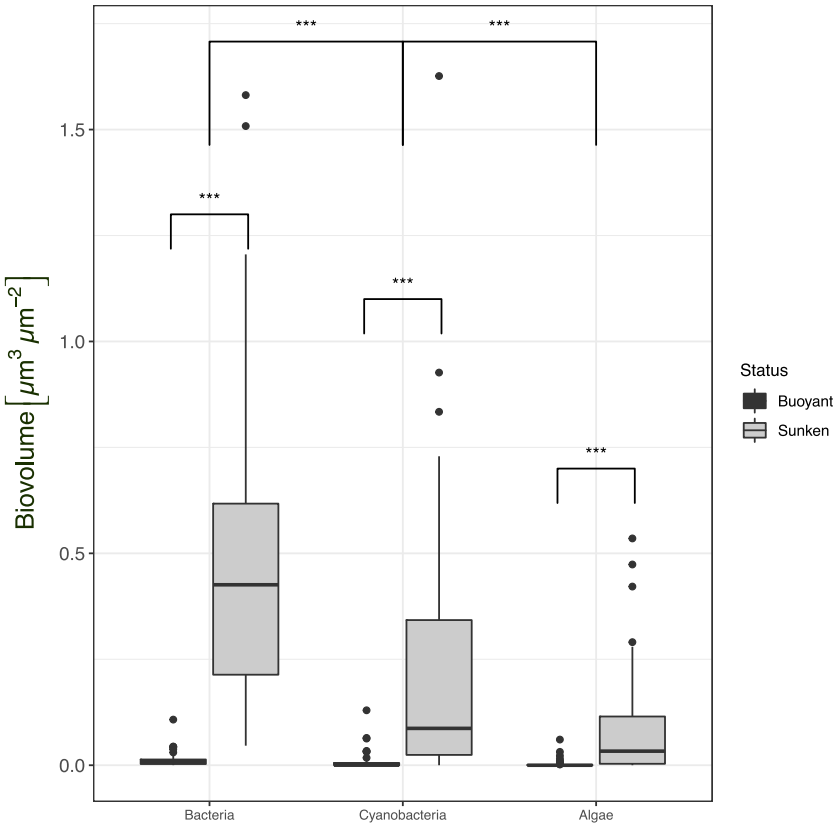

Fig. 2. Biovolumes of bacteria, cyanobacteria and algae cells in biofilms on PE particles retrieved from Bautzen reservoir after 29 days of incubation. Biovolumes were semiquantitatively measured via CLSM followed by image analysis. Significant differences are displayed by asterisks ***: $p < 0.001$.

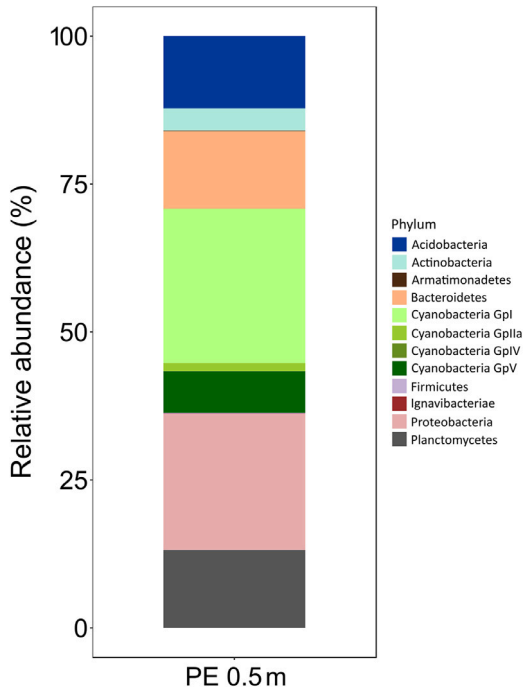

Fig. 3. Bacterial community composition (phylum level) on PE particles exposed in Bautzen reservoir as obtained via 16S sequencing. GpI: Chamaesiphon spp.; GpV: Leptolyngbya spp.; GpIIa: Synechococcus spp.

calcite constituting 17% of the total biofilm weight. Therefore it can be assumed that the contribution of organic matter and microbial cells to the overall biofilm density was minor compared to biogenic calcite.

In marine environments similar studies found that buoyant MP will sink within 2 to 6 weeks (Fazey and Ryan, 2016; Kaiser et al., 2017) due to the development of fouling films on their surfaces. Results of different studies are not easily transferable since the effect of biofouling on MP density is related to particle surface to volume ratio, which is influenced by particle specific size and shape (Chubarenko et al., 2016). MP films are more susceptible towards biofouling than fibers or spheres (Chubarenko et al., 2016), while small particles will lose buoyancy faster than large particles (Fazey and Ryan, 2016). However, the effect of biofouling has only been described for large particles yet. Given by their small size, sub-millimeter MP particles will be colonized by different organisms compared to large plastics (Rogers et al., 2020). Therefore it remains uncertain if findings made for larger plastics can be transferred to small MP (< 1 mm). Hence our finding that calcite formation reduces the buoyancy of large PE films might not be extrapolated to particles smaller than 1 mm. Furthermore it should be considered that the used PE films represented only a small part of the different shapes and size classes of MP found in freshwater. As size and shape influence the surface to volume ratio, these parameters have to be carefully taken into account when transferring the results of this study to other types of particles.

3.3. Calcium, cyanobacteria and MP aggregation in lab experiments

Sinking aggregates of *Microcystis* spp. cells formed under the influence of 220 mg l^{-1} and 60 mg l^{-1} Ca^{2+} after < 2 h and 2 days, respectively, while no aggregates formed under 10 mg l^{-1} Ca^{2+} within 7 days. Each of the experimental approaches reached pH ~ 9.7 at the end of the experiment. Declining of Ca^{2+} concentration was not detected during the experiments. Calcite or other mineral

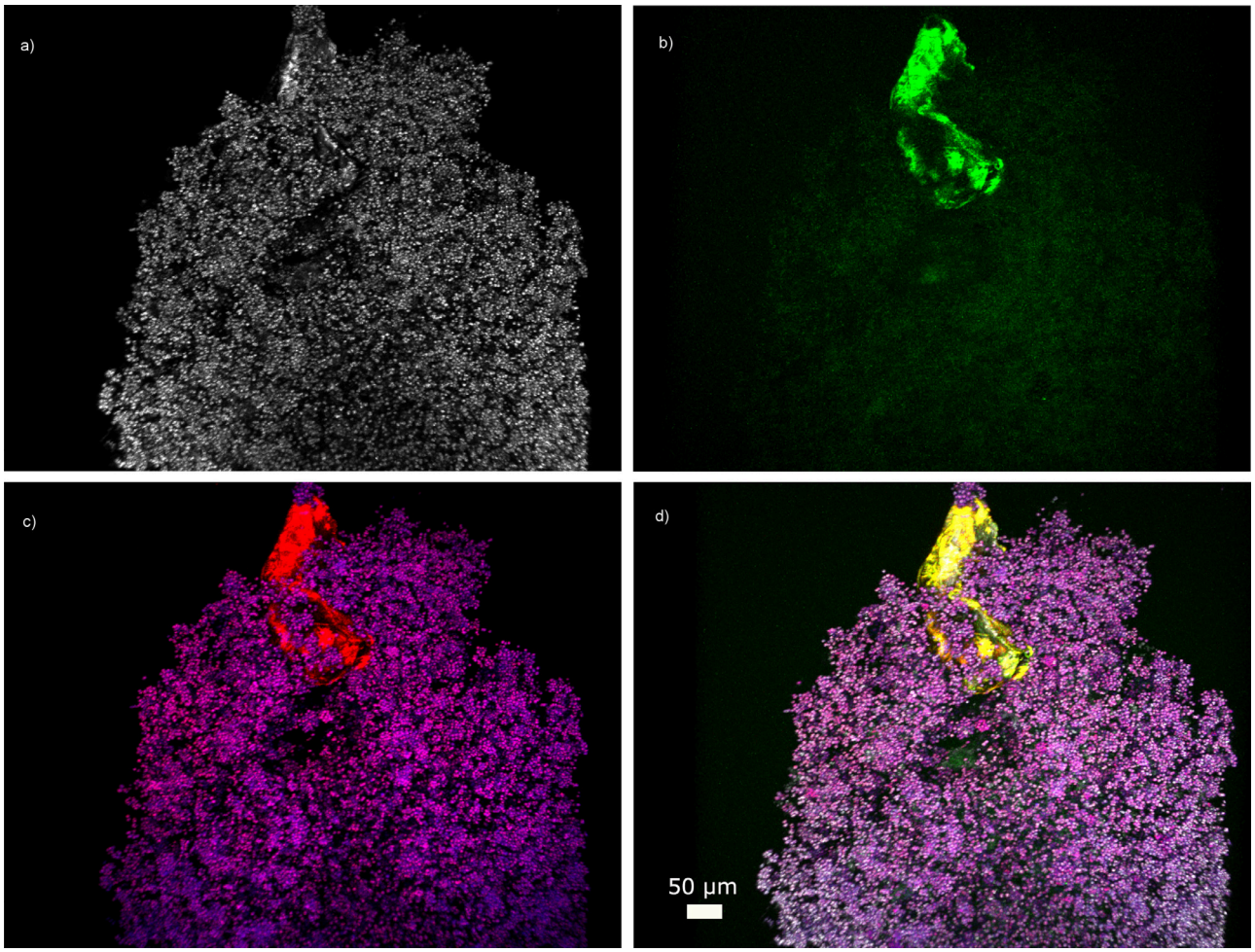

Fig. 4. CLSM images of an aggregate formed during precipitation experiments (60 mg l^{-1} Ca^{2+}), different laser channels are displayed showing a) total reflection (white), b) calcein (green), c) cyanobacteria (purple) and PE (red) and d) the resulting composite image. (For interpretation of the references to color in this figure legend, the reader is referred to the web version of this article.).

phases were not found within the aggregates employing XRD analysis.

PE particles were incorporated into the matrix (Figure S5) or attached to the outer side of the aggregates. Some of the polymer particles were encrusted by calcein stainable matter (Fig. 4). The aggregates formed in 60 mg l^{-1} and 220 mg l^{-1} Ca^{2+} incorporated on average 2 MP particles (mean, n: 60) and subsequently transported them to the bottom of the incubation flasks (Fig. 5). Each flask contained approximately 65 aggregates (mean, n: 5) which in sum incorporated ~130 PE particles (~0.4% of added particles).

Aggregation and settling of MP with eukaryotic algae (Lagarde et al., 2016) and diatoms (Long et al., 2015) have been reported before. So freshwater algae *Chlamydomonas reinhardtii* formed dense aggregates (ρ: 1.2 g cm^{-3}) with polypropylene MP readily sinking in culture media (Lagarde et al., 2016). The aggregates in our study were denser than water (ρ: 1.1 g cm^{-3} for 60 mg l^{-1} Ca^{2+}; 1.05 g cm^{-3} for 220 mg l^{-1} Ca^{2+}) (Fig. 5) and slightly exceeded the density ranges previously reported for cyanobacterial aggregates (1.01 -1.05 g cm^{-3}) (Li et al., 2016). Aggregate densities might be influenced by strain specific excretion of extracellular polymeric substances (EPS) (Li et al., 2016) or formation of gas vacuoles (Xu et al., 2016a). Furthermore, the density of such aggregates strongly depends on other external factors such as the seasons (Li et al., 2016). Under favourable environmental conditions such as high temperature, nutrient loadings or light intensities (Li et al., 2016) cyanobacterial aggregates may stay afloat instead of sinking to the sediments. Multiple linear regression modelling revealed that sinking speed of the aggregates was dependent solely on their size, with larger colonies settling faster than smaller ones. Aggregates in 60 mg l^{-1} Ca^{2+} were significantly larger (mean: 1519 µm, n: 30) than the aggregates formed in 220 mg l^{-1} Ca^{2+} (mean 1262 µm, n: 30). Therefore they were settling approximately 25 % faster than the smaller aggregates (Fig. 5). Regarding the longer incubation time (2 days for 60 mg l^{-1} Ca^{2+} and 1 day for 220 mg l^{-1} Ca^{2+}) this might have been a temporal effect rather than depending on the Ca^{2+} concentration. Considering the sinking velocity of the aggregates (0.0036 m s^{-1} for 60 mg l^{-1} Ca^{2+} and 0.0029 m s^{-1} for 220 mg l^{-1} Ca^{2+}), aggregation with cyanobacteria may transport buoyant small PE to the sediment of Bautzen reservoir within 34 to 42 minutes. However, this might only hold true for MP particles being smaller than the enclosing cyanobacterial aggregates. Large particles (1- 5 mm), such as the PE films used in the field study, are unlikely to be incorporated into the cyanobacterial aggregates (~1 - 1.5 mm). Therefore the results might only be applicable for MP smaller than 100 µm.

Most likely aggregation of cyanobacterial cells was induced by the elevated Ca^{2+} concentrations used in our study. Ca^{2+} ions are suspected to form bridges between the negatively charged cyanobacteria or EPS (Xu et al., 2016a), leading to the formation of cell aggregates (Chen and Lürling, 2020). Furthermore elevated Ca^{2+} concentrations can increase the production of cyanobacteria

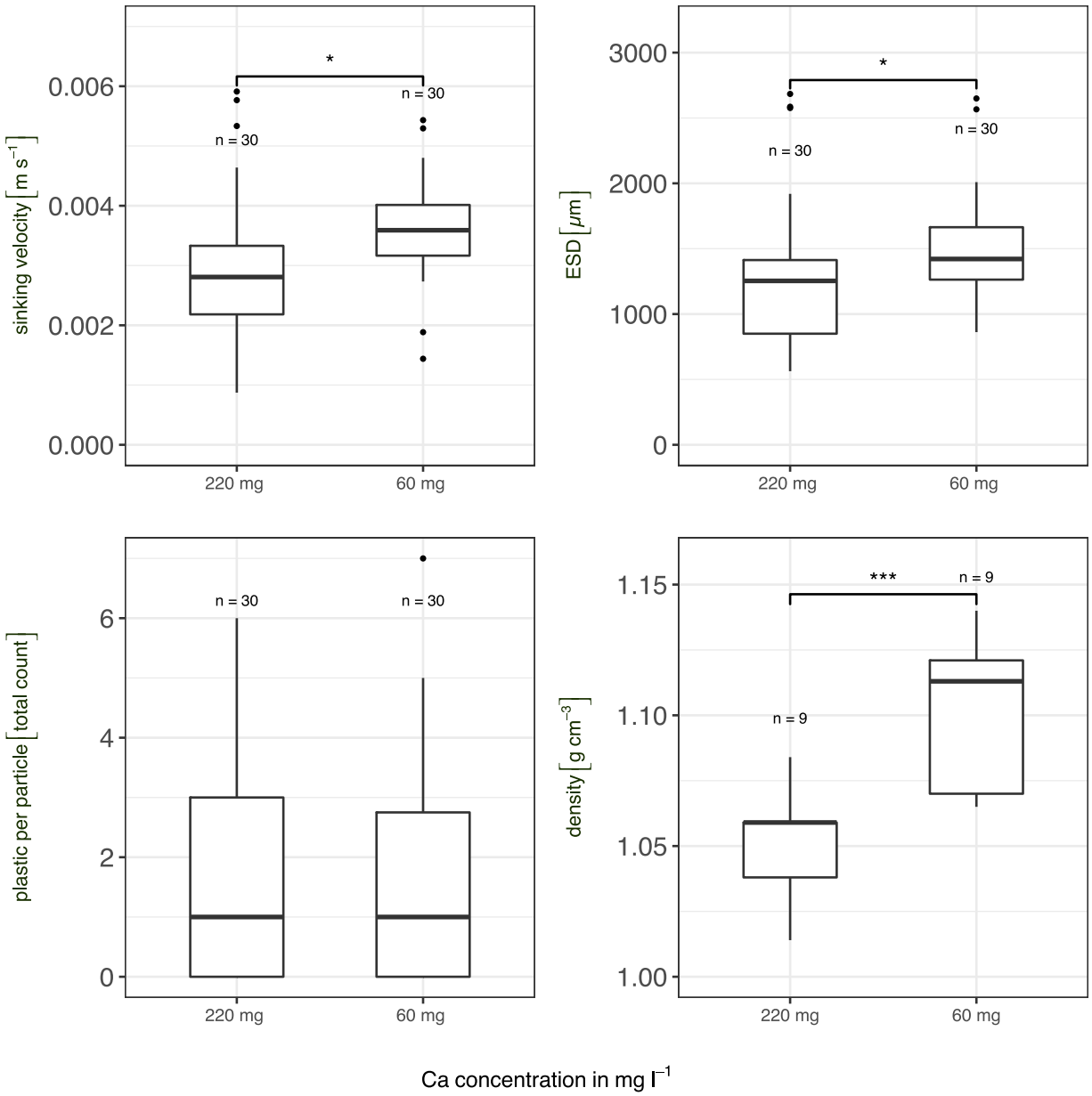

Fig. 5. Properties of cyanobacterial aggregates formed under high (220 mg l^{-1}) and intermediate (60 mg l^{-1}) Ca^{2+} concentrations. Significant differences are displayed as asterisks ***: $p < 0.001$ and *: $p < 0.05$.

EPS (Wang et al., 2011), which plays a crucial role in aggregation processes by providing a sticky, flexible and robust matrix in which cells are embedded (De Oliveira et al., 2020). The assumed bridging role of Ca^{2+} can be supported by the presence of calcein stainable matter within the aggregates (Fig. 4) connecting the cyanobacterial cells. Ca^{2+} concentrations >20 mg l^{-1} are required to induce aggregation of cyanobacterial cells (Chen and Lürling, 2020). Bautzen reservoir has a median Ca^{2+} concentration of 35 mg l^{-1}, which lies in the usual range (10 -120 mg l^{-1} Ca^{2+}) of freshwater bodies (Wang et al., 2011). Correspondingly, large cyanobacterial aggregates / colonies were observed in Bautzen reservoir during the samplings in 2018 and 2019 (Figure S6). This leads to the assumption that the aggregation of cyanobacteria through Ca bridging might be relevant for the fate of small MP in Bautzen reservoir. The Ca^{2+} concentrations used in the lab experiments did not reflect the actual concentrations found in Bautzen reservoir. Still we could show that *Microcystis* spp. aggregate with MP under environmentally relevant Ca^{2+} concentrations (60 mg l^{-1}).

Field and lab experiments described two distinct processes leading to sinking of buoyant PE microplastics in the context of cyanobacterial interaction with calcium. Apparently the formation of biofilms sank proportionally more particles (~ 10 -15%) than the aggregation of small PE with cyanobacteria. However, the low removal efficiency rather resulted from the low concentration of cyanobacterial aggregates (mean: 130 aggregates l^{-1}) than from the number of PE particles incorporated into each of the aggregates (mean: 2). Taking into account that, during cyanobacteria blooms concentrations of 3.5×10^5 aggregates l^{-1} can be reached (Feng et al., 2019), aggregation governs a high potential for MP removal in productive lakes.

4. Conclusions

- A proportion of polyethylene microplastics (~10 - 15% of particles) lost its buoyancy due to biofilm formation after being exposed for 29 days in a eutrophic reservoir

- Biofilms were rich in calcite. Apparently the mineral had a greater effect on biofilm density compared to organic matter or cells
- Cyanobacteria *Chamaesiphon* spp. and *Leptolyngbya* spp. were abundant biofilm members probably facilitating calcite formation in the biofilms
- Planktonic cyanobacteria formed sinking aggregates with small polyethylene microplastics (enclosing ~0.4% of particles) under elevated Ca concentrations

Funding sources

This research was supported by the BMBF project MikroPlaTaS (02WPL1448A). The authors declare no competing financial interest.

Declaration of Competing Interest

The authors declare that they have no known competing financial interests or personal relationships that could have appeared to influence the work reported in this paper.

Acknowledgment

We thank Ute Kuhlicke for her eminent help with confocal microscopy and Corinna Völkner for her expertise in conducting field work. The Landestalsperrenverwaltung des Freistaates Sachsen and Alice Rau are acknowledged for their kind help in providing water data and access to Bautzen reservoir. Furthermore we thank Anke Schwarzenberger for providing *Microcystis* sp. strain BM25 for the lab experiments.

Supplementary materials

Supplementary material associated with this article can be found, in the online version, at doi:10.1016/j.watres.2020.116582.

References

Altschul, S.F., Gish, W., Miller, W., Myers, E.W., Lipman, D.J., 1990. Basic local alignment search tool. J. Mol. Biol. 215, 403–410. doi:10.1016/S0022-2836(05)80360-2.

Amaral-Zettler, L.A., Zettler, E.R., Mincer, T.J., 2020. Ecology of the plastisphere. Nat. Rev. Microbiol. 18, 139–151. doi:10.1038/s41579-019-0308-0.

Arp, G., Bissett, A., Brinkmann, N., Cousin, S., de Beer, D., Friedl, T., Mohr, K.I., Neu, T.R., Reimer, A., Shiraishi, F., Stackebrandt, E., Zippel, B., 2010. Tufa-forming biofilms of German karstwater streams: microorganisms, exopolymers, hydrochemistry and calcification. Geol. Soc. Spec. Publ. 336, 83–118. doi:10.1144/SP336.6.

Ballent, A., Corcoran, P.L., Madden, O., Helm, P.A., Longstaffe, F.J., 2016. Sources and sinks of microplastics in Canadian Lake Ontario nearshore, tributary and beach sediments. Mar. Pollut. Bull. 110, 383–395. doi:10.1016/j.marpolbul.2016.06.037.

Brinkmann, N., Hodač, L., Mohr, K.I., Hodačová, A., Jahn, R., Ramm, J., Hallmann, C., Arp, G., Friedl, T., 2015. Cyanobacteria and diatoms in biofilms of two karstic streams in Germany and changes of their communities along calcite saturation gradients. Geomicrobiol. J. 32, 255–274. doi:10.1080/01490451.2014.901438.

Chen, H., Lürling, M., 2020. Calcium promotes formation of large colonies of the cyanobacterium *Microcystis* by enhancing cell-adhesion. Harmful Algae 92, 101768. doi:10.1016/j.hal.2020.101768.

Chen, X., Xiong, X., Jiang, X., Shi, H., Wu, C., 2019. Sinking of floating plastic debris caused by biofilm development in a freshwater lake. Chemosphere 222, 856–864. doi:10.1016/j.chemosphere.2019.02.015.

Chubarenko, I., Bagaev, A., Zobkov, M., Esiukova, E., 2016. On some physical and dynamical properties of microplastic particles in marine environment. Mar. Pollut. Bull. 108, 105–112. doi:10.1016/j.marpolbul.2016.04.048.

Corcoran, P.L., Norris, T., Ceccanese, T., Walzak, M.J., Helm, P.A., Marvin, C.H., 2015. Hidden plastics of Lake Ontario, Canada and their potential preservation in the sediment record. Environ. Pollut. 204, 17–25. doi:10.1016/j.envpol.2015.04.009.

De Oliveira, T.T.S., Andreu, I., Machado, M.C., Vimbela, G., Tripathi, A., Bose, A., 2020. Interaction of cyanobacteria with nanometer and micron sized polystyrene particles in marine and fresh water. Langmuir 36, 3963–3969. doi:10.1021/acs.langmuir.9b03644.

Di, M., Wang, J., 2018. Microplastics in surface waters and sediments of the Three Gorges Reservoir. China. Sci. Total Environ. 616–617, 1620–1627. doi:10.1016/j.scitotenv.2017.10.150.

Doebelin, N., Kleeberg, R., 2015. Profex: a graphical user interface for the Rietveld refinement program BGMN. J. Appl. Crystallogr. 48, 1573–1580. doi:10.1107/S1600576715014685.

Edlin, G., Lin, L., Kudrna, R., 1975. Plastic films on the bottom of the Skagerack. Nature 255, 735–737. doi:10.1038/253600a0.

Fazey, F.M.C., Ryan, P.G., 2016. Biofouling on buoyant marine plastics: an experimental study into the effect of size on surface longevity. Environ. Pollut. 210, 354–360. doi:10.1016/j.envpol.2016.01.026.

Feng, B., Wang, C., Wu, X., Tian, C., Zhang, M., Tian, Y., Xiao, B., 2019. Spatiotemporal dynamics of cell abundance, colony size and intracellular toxin concentrations of pelagic and benthic *Microcystis* in Lake Caohai, China.. J. Environ. Sci. 84, 184–196. doi:10.1016/j.jes.2019.05.010.

Guillard, R.R.L., Lorenzen, C.J., 1972. Yellow-green algae with chlorophyllide C1,2. J. Phycol. doi:10.1111/j.0022-3646.1972.00010.x.

Hoellein, T., Rojas, M., Pink, A., Gasior, J., Kelly, J., 2014. Anthropogenic litter in urban freshwater ecosystems: distribution and microbial interactions. PLoS One 9. doi:10.1371/journal.pone.0098485.

Jansson, C., Northen, T., 2010. Calcifying cyanobacteria-the potential of biomineralization for carbon capture and storage. Curr. Opin. Biotechnol. 21, 365–371. doi:10.1016/j.copbio.2010.03.017.

Kaiser, D., Kowalski, N., Waniek, J.J., 2017. Effects of biofouling on the sinking behavior of microplastics. Environ. Res. Lett. 12. doi:10.1088/1748-9326/aa8e8b.

Kamjunke, N., Böing, W., Voigt, H., 1997. Bacterial and primary production under hypertrophic conditions. Aquat. Microb. Ecol. 13, 29–35. doi:10.3354/ame013029.

Karakolis, E.G., Nguyen, B., You, J.B., Rochman, C.M., Sinton, D., 2019. Fluorescent dyes for visualizing microplastic particles and fibers in laboratory-based studies. Environ. Sci. Technol. Lett. 6, 334–340. doi:10.1021/acs.estlett.9b00241.

Kasprzak, P., Benndorf, J., Gonsiorczyk, T., Koschel, R., Krienitz, L., Mehner, T., Hülsmann, S., Schultz, H., Wagner, A., 2007. Reduction of nutrient loading and biomanipulation as tools in water quality management: long-term observations on Bautzen Reservoir and Feldberger Haussee (Germany). Lake Reserv. Manag. 23, 410–427. doi:10.1080/07438140709354027.

Kerimoglu, O., Rinke, K., 2013. Stratification dynamics in a shallow reservoir under different hydro-meteorological scenarios and operational strategies. Water Resour. Res. 49, 7518–7527. doi:10.1002/2013WR013520.

Kettner, M.T., Rojas-Jimenez, K., Oberbeckmann, S., Labrenz, M., Grossart, H.P., 2017. Microplastics alter composition of fungal communities in aquatic ecosystems. Environ. Microbiol. 19, 4447–4459. doi:10.1111/1462-2920.13891.

Koschel, R., Benndorf, J., Proft, G., Recknagel, R., 1983. Calcite precipitation as a natural control mechanism of eutrophication. Arch. Hydrobiol. 98, 380–408. doi:10.1007/springerreference_205967.

Kurmayer, R., Christiansen, G., Holzinger, A., Rott, E., 2018. Single colony genetic analysis of epilithic stream algae of the genus *Chamaesiphon* spp. Hydrobiologia 811, 61–75. doi:10.1007/s10750-017-3295-z.

Lagarde, F., Olivier, O., Zanella, M., Daniel, P., Hiard, S., Caruso, A., 2016. Microplastic interactions with freshwater microalgae: hetero-aggregation and changes in plastic density appear strongly dependent on polymer type. Environ. Pollut. 215, 331–339. doi:10.1016/j.envpol.2016.05.006.

Leiser, R., Wu, G.-M., Neu, T.R., Wendt-Potthoff, K., 2020. Biofouling, metal sorption and aggregation are related to sinking of microplastics in a stratified reservoir. Water Res., 115748 doi:10.1016/J.WATRES.2020.115748.

Li, M., Zhu, W., Guo, L., Hu, J., Chen, H., Xiao, M., 2016. To increase size or decrease density? Different *Microcystis* species has different choice to form blooms. Sci. Rep. 6, 1–10. doi:10.1038/srep37056.

Long, M., Moriceau, B., Gallinari, M., Lambert, C., Huvet, A., Raffray, J., Soudant, P., 2015. Interactions between microplastics and phytoplankton aggregates: impact on their respective fates. Mar. Chem. 175, 39–46. doi:10.1016/j.marchem.2015.04.003.

López-García, P., Kazmierczak, J., Benzerara, K., Kempe, S., Guyot, F., Moreira, D., 2005. Bacterial diversity and carbonate precipitation in the giant microbialites from the highly alkaline Lake Van, Turkey.. Extremophiles 9, 263–274. doi:10.1007/s00792-005-0457-0.

Macintyre, I.G., Prufert-Bebout, L., Reid, R.P., 2000. The role of endolithic cyanobacteria in the formation of lithified laminae in Bahamian stromatolites. Sedimentology 47, 915–921. doi:10.1046/j.1365-3091.2000.00327.x.

Martinez, R.E., Gardés, E., Pokrovsky, O.S., Schott, J., Oelkers, E.H., 2010. Do photosynthetic bacteria have a protective mechanism against carbonate precipitation at their surfaces? Geochim. Cosmochim. Acta 74, 1329–1337. doi:10.1016/j.gca.2009.11.025.

Ortíz-Caballero, Z.K., Rentería-Villalobos, M., Montero-Cabrera, M.E., Manjón-Collado, G., Santellano-Estrada, E., Rentería-Monterrubio, A., 2019. Fractionation of chemical species in surface water from El Granero reservoir, Chihuahua, Mexico.. Environ. Earth Sci. 78, 1–13. doi:10.1007/s12665-019-8756-4.

Parada, A.E., Needham, D.M., Fuhrman, J.A., 2016. Every base matters: Assessing small subunit rRNA primers for marine microbiomes with mock communities, time series and global field samples. Environ. Microbiol. 18, 1403–1414. doi:10.1111/1462-2920.13023.

Peraza Zurita, Y., Cultrone, G., Sánchez Castillo, P., Sebastián, E., Bolívar, F.C., 2005. Microalgae associated with deteriorated stonework of the fountain of Bibataurín in Granada, Spain. Int. Biodeterior. Biodegrad 55, 55–61. doi:10.1016/j.ibiod.2004.05.006.

R Core Team, 2018. R: A language and environment for statistical computing.

Rogers, K.L., Carreres-Calabuig, J.A., Gorokhova, E., Posth, N.R., 2020. Micro-by-micro interactions: how microorganisms influence the fate of marine microplastics. Limnol. Oceanogr. Lett. 5, 18–36. doi:10.1002/lol2.10136.

Rosenhahn, A., Schilp, S., Kreuzer, H.J., Grunze, M., 2010. The role of "inter" surface chemistry in marine biofouling prevention. Phys. Chem. Chem. Phys. 12, 4275–4286. doi:10.1039/c004746p.

Rueden, C.T., Schindelin, J., Hiner, M.C., DeZonia, B.E., Walter, A.E., Arena, E.T., Eliceiri, K.W., 2017. ImageJ2: ImageJ for the next generation of scientific image data. BMC Bioinformatics 18, 1–26. doi:10.1186/s12859-017-1934-z.

Schwarzenberger, A., Sadler, T., Von Elert, E., 2013. Effect of nutrient limitation of cyanobacteria on protease inhibitor production and fitness of *Daphnia magna*. J. Exp. Biol. 216, 3649–3655. doi:10.1242/jeb.088849.

Stabel, H.-H., 1988. Algal control of elemental sedimentary fluxes in Lake Constance. In: SIL Proceedings, 23, pp. 700–706. doi:10.1080/03680770.1987.11899696 1922-2010.

Staudt, C., Horn, H., Hempel, D.C., Neu, T.R., 2004. Volumetric measurements of bacterial cells and extracellular polymeric substance glycoconjugates in biofilms. Biotechnol. Bioeng. 88, 585–592. doi:10.1002/bit.20241.

Teranes, J.L., McKenzie, J.A., Bernasconi, S.M., Lotter, A.F., Sturm, M., 1999. A study of oxygen isotopic fractionation during bio-induced calcite precipitation in eutrophic Baldeggersee, Switzerland.. Geochim. Cosmochim. Acta 63, 1981–1989. doi:10.1016/S0016-7037(99)00049-6.

Tianzhi, W., Yunkai, L., Mingchao, L., Peiling, Y., Zhihui, B., 2014. Biofilms on the surface of gravels and aquatic plants in rivers and lakes with reusing reclaimed water. Environ. Earth Sci. 72, 743–755. doi:10.1007/s12665-013-2998-3.

Wang, S., Xue, N., Li, W., Zhang, D., Pan, X., Luo, Y., 2020. Selectively enrichment of antibiotics and ARGs by microplastics in river, estuary and marine waters. Sci. Total Environ. 708, 134594. doi:10.1016/j.scitotenv.2019.134594.

Wang, Y.W., Zhao, J., Li, J.H., Li, S.S., Zhang, L.H., Wu, M., 2011. Effects of calcium levels on colonial aggregation and buoyancy of Microcystis aeruginosa. Curr. Microbiol. 62, 679–683. doi:10.1007/s00284-010-9762-7.

Wu, X., Pan, J., Li, M., Li, Y., Bartlam, M., Wang, Y., 2019. Selective enrichment of bacterial pathogens by microplastic biofilm. Water Res. 165, 114979. doi:10.1016/j.watres.2019.114979.

Xu, H., Lv, H., Liu, X., Wang, P., Jiang, H., 2016a. Electrolyte cations binding with extracellular polymeric substances enhanced *Microcystis* aggregation: implication for *Microcystis* bloom formation in eutrophic freshwater lakes. Environ. Sci. Technol. 50, 9034–9043. doi:10.1021/acs.est.6b00129.

Xu, H., Yang, C., Jiang, H., 2016b. Aggregation kinetics of inorganic colloids in eutrophic shallow lakes: influence of cyanobacterial extracellular polymeric substances and electrolyte cations. Water Res. 106, 344–351. doi:10.1016/j.watres.2016.10.023.

Záray, G., Kröpfl, K., Szabó, K., Taba, G., Ács, É., Berlinger, B., Dogan, M., Salih, B., Akbulut, A., 2005. Comparison of freshwater biofilms grown on polycarbonate substrata in Lake Velence (Hungary) and Lake Mogan (Turkey). Microchem. J. 79, 145–148. doi:10.1016/j.microc.2004.08.012.

Zippel, B., Neu, T.R., 2011. Characterization of glycoconjugates of extracellular polymeric substances in tufa-associated biofilms by using fluorescence lectin-binding analysis. Appl. Environ. Microbiol. 77, 505–516. doi:10.1128/AEM.01660-10.

Chapter 3

Manuscript 2

Biofouling, metal sorption and aggregation are related to sinking of microplastics in a stratified reservoir

Water Research (2020), 177, 115748, doi.org:10.1016/J.WATRES.2020.115748

Rico Leiser, Gi-Mick Wu, Thomas R. Neu and Katrin Wendt-Potthoff

Water Research 176 (2020) 115748

Contents lists available at ScienceDirect

Water Research

journal homepage: www.elsevier.com/locate/watres

Biofouling, metal sorption and aggregation are related to sinking of microplastics in a stratified reservoir

Rico Leiser [a, *], Gi-Mick Wu [b], Thomas R. Neu [c], Katrin Wendt-Potthoff [a]

[a] Department of Lake Research, Helmholtz Centre for Environmental Research, Brückstraße 3a, 39114, Magdeburg, Germany
[b] Helmholtz Centre for Environmental Research, Permoserstraße 15, 04318, Leipzig, Germany
[c] Department of River Ecology, Helmholtz Centre for Environmental Research, Brückstraße 3a, 39114, Magdeburg, Germany

ARTICLE INFO

Article history:
Received 13 October 2019
Received in revised form
14 March 2020
Accepted 20 March 2020
Available online 25 March 2020

Keywords:
Microplastics
Reservoirs
Biofouling
Aggregation
Microscopy
Sinking

ABSTRACT

Microplastic particles entering aquatic systems are rapidly colonized by microbial biofilms. The presence of microbial biomass may cause sinking of particles and as a consequence prevent their transport to the oceans. We studied microbial colonization of different polymer particles exposed in the epi-, meta- and hypolimnion of a freshwater reservoir during late summer for 47 days. Parameters measured included biofilm formation, metal sorption and sinking velocities. Microbial biofilms contained bacteria, cyanobacteria and algae as well as inorganic particles such as iron oxides. Regardless of biofilm thickness and biovolumes of different biofilm constituents, single polyethylene (PE) particles stayed buoyant, whereas the sinking velocity of single polystyrene (PS) and polyethylene terephthalate (PET) particles did not change significantly compared to initial values. During exposition, a mixing event occurred, by which anoxic, iron-rich water from the hypolimnion was mixed with water from upper layers. This induced aggregation and sinking of hypolimnetic PE particles together with organic matter, cyanobacteria colonies and iron minerals.

1. Introduction

Microplastics (MP) are one of the widely distributed man-made pollutants, found in nearly any place of the earth. Zones with reduced flow velocities such as point bars, impoundments and reservoirs allow particles to settle down to the sediment (Watkins et al., 2019), reducing the plastic load of streams (Castañeda et al., 2014). As a consequence, high concentrations of MP are found in sediments of natural lakes (Anderson et al., 2017) and man-made reservoirs (Zhang et al., 2015), which may even act as permanent sink (Corcoran et al., 2015). Elucidating the factors governing particle settling in zones with reduced flow, such as reservoirs, is therefore crucial for a comprehensive understanding of MP transport in the environment.

Microplastic particles are rapidly colonized by various microorganisms like bacteria, cyanobacteria and microalgae when submerged in freshwater. This leads to the development of a biofilm comprising microbial communities distinct from the surrounding water (Zettler et al., 2013). Environmental conditions such as pH, temperature, light/oxygen availability or dissolved nutrients mainly determine which organisms may occur within a biofilm; whereas the surface properties seem to be less influential than these external factors (McCormick et al., 2014; Oberbeckmann et al., 2016). However, if incubated under the same environmental conditions, differences between microbial community composition and biofilm density can be observed among different surfaces (Parrish and Fahrenfeld, 2019).

The settling of particles is influenced by their shape, size and density (Chubarenko et al., 2016; Kowalski et al., 2016). Particles denser than water and above 5 μm in diameter will eventually settle down by gravitational force within a few meters after being submerged in water. Particles less dense than water or below 5 μm in size may stay buoyant or even float at the surface if not altered by environmental processes (Besseling et al., 2017). For further transport, aggregation with natural materials and colonization by organisms play a crucial role by increasing the size and density of these particles. In oceans, the aggregation of buoyant MP with algae (Long et al., 2015) and marine snow (Michels et al., 2018) leads to rapid settling. Coverage of larger particles with calcareous macroorganisms, which is often referred to as biofouling, also sinks buoyant plastic polymers (Kaiser et al., 2017).

* Corresponding author.
E-mail address: rico.leiser@ufz.de (R. Leiser).

https://doi.org/10.1016/j.watres.2020.115748
0043-1354/

Conditions in freshwater differ from the marine environment with regard to physical (currents/waves, tides, wind, temperature), chemical (pH, salinity, oxygen availability, nutrients/metals) and biological parameters. Additionally, the residence time in freshwater reservoirs is by magnitudes lower than in the ocean, leading to the assumption that extensive aging and biofouling by heavy calcareous organisms is unlikely to take place. Transfer of buoyant MP to reservoir sediments may therefore rely rather on mechanisms distinct from those observed in marine environments (Besseling et al., 2017). During summer, many reservoirs become stratified and partly anoxic, leading to the reduction of iron oxides to ferrous iron. Lake mixing leads to the autoxidation of ferrous iron and formation of iron oxide colloids in the water column (Tipping et al., 1981). These colloids are known to sink together with algae and cyanobacteria by forming sticky agglomerates with the cells (Oliver et al., 1985).

We hypothesize that this aggregation may also be relevant for MP during mixing. Stratified reservoirs, which exhibit gradients of redox potential and oxygen availability, may therefore provide an ideal setting to study the factors governing biofilm development and plastic sedimentation which are presently not well understood. We characterized biofilm formation on PE, PET and PS in the stratified mesotrophic Malter reservoir during late summer. Other factors such as aggregation with freshwater algae and cyanobacteria or sorption of metals were considered as well. The following hypotheses were tested: i) incubation depth and time influence biofilm composition; ii) biofilm covered MP sorb metal oxides; iii) aggregation or biofouling influence MP settling in stratified reservoirs.

2. Materials and methods

2.1. Location

The mesotrophic Malter reservoir (0.84 km^2, 335 m above sea level) is located in eastern Germany (Dippoldiswalde, Saxony). Its maximum depth is 16–20 m and the maximum storage capacity is 9.6 million m^3. Due to continuous discharge during summer, the water level may drop by several meters. In summer the water column is stratified with an anoxic hypolimnion separated from the oxic epilimnion by a thermocline at 8 m depth in 2018 (Fig. S1 and Table S1). Autumnal mixing usually occurs during September restoring oxic conditions near the bottom (Müller et al., 2000).

2.2. Plastic material and incubation conditions

Three different polymer foils in research quality and free of stabilizers, PE (ρ: 0.924 g cm^{-3}, contact angle: 99.2 ± 4.1°, ET311251), PS (ρ: 1.05 g cm^{-3}, contact angle: 91.7 ± 4.6°, ST311125), and PET (ρ: 1.4 g cm^{-3}, contact angle: 84.3 ± 3.4°, ES301425) were purchased from GoodFellow (Hamburg, Germany). Foil thicknesses were 0.125 mm for PS/PET and 0.15 mm for PE. Polymer squares (4 × 4 mm) were obtained employing a multiple puncher (Pavo HD Wire Binder), using sterile techniques (ethanol-sterilized puncher and lab cloths, laminar flow bench). PS particles exhibited a curved shape, whereas PE and PET particles were even. The cutting edges of the particles were rougher compared to the uncut foil. The squares and foils were stored at 20 °C in a dry, dark place.

In order to incubate the particles in Malter reservoir, 500 particles of each polymer (PE, PS, PET) were transferred to individual closed stainless steel cages (cylindrical shape, diameter 10 cm, length 25 cm, mesh width 3 mm) each containing just a single polymer type (Arias-Andres et al., 2018). Particles were distributed to the cages as follows: 3 × 500 particles (three individual cages containing PE, PET or PS) in the epilimnion, 3 × 500 in the metalimnion and 9 × 500 (in 3 × 3 cages with PE, PET or PS) in the hypolimnion (Fig. S2). Cages were incubated from August 30 to October 16, 2018, with three samplings after 6 days (09/05), 22 days (09/21) and 47 days (10/16). Three incubation depths at 0.5 m (epilimnion, O_2 saturation > 100%, light), 8 m (metalimnion, O_2 saturation 80%, no light) and 16 m (hypolimnion, O_2 saturation 0%, no light) were chosen according to prevailing oxygen concentrations (multi-parameter probe, Sea & Sun Technologies, Germany) and light intensities (Licor 1400, Li-cor Biosciences, Germany) on August 30 (Fig. S1a). Cages were lifted to the surface for sampling and particles were gently transferred using tweezers or flushing with reservoir water to pre-combusted (450 °C, 4 h) glass Petri dishes filled with water from the incubation depth. The hypolimnion was anoxic during the initial stage of the experiment (Fig. S1). To avoid repeated oxygen exposure of anaerobic organisms during lifting of the cages for sampling, additional cages on separate ropes were deployed in the hypolimnion so that for each sampling previously un-sampled cages were used. Some PS particles were flushed out of the cages, leading to missing values of crystal violet staining in the epilimnion and metalimnion for day 47. All samples were stored in the dark at 4 °C until processing in the laboratory. Samples for confocal laser scanning microscopy (CLSM) were preserved in 4% formalin solution, and particles for iron/manganese measurement were directly placed in glass vials with hydroxyl ammonium chloride-hydrochloric acid (0.5 M/1 M). Particles used to determine the sinking velocity and for conducting crystal violet staining were transported in reservoir water.

2.3. CLSM imaging

At every sampling date 10 randomly chosen particles per polymer were taken from each incubation depth, and 5 random locations on each of them were examined via CLSM. Samples were washed in tap water and mounted in a 5 cm Petri dish. For this purpose the plastic squares were glued with silicone adhesive to the bottom of the dish. Nucleic acid staining was done with SybrGreen (dilution 1:1000). After staining for 5 min the Petri dish was flooded with tap water. For CLSM a TCS SP5X with upright microscope and super continuum light source was available. The system was controlled by LAS AF version 2.4.1. Samples were examined by using a long working distance 63x NA 0.9 water immersible objective lens. Excitation was at 490, 561 and 633 nm. Emission was recorded sequentially from 480 to 500 nm (reflection), 510–580 nm (SybrGreen) together with 650–720 nm (autofluorescence of chlorophyll *a*) and separately from 575 to 650 nm (autofluorescence of phycobilins). Datasets were recorded without average and a step size of 1 μm. For visualisation Imaris (Bitplane) version 9.3 was employed. Projected image data sets were printed from photoshop (Adobe). Calculations of cell biovolumes contained in the digital images were done with an adapted version of ImageJ (Staudt et al., 2004). Extracellular polymeric substances (EPS) were visualized by the glycoconjugate binding lectin AAL-A568 (Vector Laboratories, Burlingame, USA).

2.4. Iron and manganese analysis

Iron and manganese were determined by extracting 15 pooled particles per sampling date, depth, and polymer type with 2 ml hydroxyl ammonium chloride-hydrochloric acid solution (0.5/1 M) for 24 h in an overhead shaker (120 rpm). Iron was subsequently measured by ferrozine assay (Stookey, 1970) at 562 nm using a spectrophotometer (Agilent Cary 60 UV-VIS). Briefly, 50 μl of acidic, centrifuged sample (10 min, 15000 rpm) was added to 950 μl ferrozine solution (50 mM HEPES, 1 mg ml^{-1} ferrozine, pH 7.0) and incubated for 10 min prior to the measurement. If optical density

exceeded 1.0 the remaining sample was diluted with acidified ultra-pure H_2O prior to the addition of ferrozine. Manganese was measured using the formaldoxime method adapted from Burlage et al. (1998), Goto et al. (1962) and Brewer and Spencer (1971). The following solutions were prepared: (1) TRIS-Buffer (5 M TRIS-HCl, pH 9.0 adjusted with H_2SO_4), (2) formaldoxime (20 g hydroxyl ammonium chloride in 450 ml ultrapure H_2O, addition of 10 ml 10% formaldehyde, filled up to 500 ml), (3) 0.1 M EDTA in water and (4) 10% hydroxyl ammonium chloride in water. One ml of TRIS solution was added to an Eppendorf tube followed by addition of 100 µl supernatant from the centrifuged sample. Then 100 µl of formaldoxime was added, followed by 2 min of incubation at room temperature. To remove dissolved ferrous iron, 100 µl EDTA and 200 µl hydroxyl ammonium chloride solution were added separately, subsequently the solution was incubated at room temperature for 10 min and measured at 450 nm (Agilent Cary 60 UV-VIS).

2.5. Crystal violet staining

Crystal violet staining was conducted to quantify total biofilm mass (Arias-Andres et al., 2018), as the dye stains both cells and the biofilm EPS (Xu et al., 2016). On each sampling date 8 particles from each depth and of every polymer type were stained. During the procedure some particles were lost leading to lower sample numbers (Fig. 2). Briefly, particles were dried (60 °C, 24 h), stained with 250 µl crystal violet (0.3% in ultrapure water) for 15 min, washed 4 times with ultrapure water and de-stained with 200 µl ethanol (97%). The ethanol-crystal violet solution was measured at 595 nm (OD_{595}) using a multiplate reader (Thermo Fisher Multiscan RC). Samples showing optical densities higher than 1.00 were diluted with 97% ethanol.

2.6. Measurement of sinking velocities

Sinking velocities were determined within 12 h after sampling. A sinking column (0.15 m × 2 m) filled with deionized water and placed in a climate chamber (20 °C) was used. The water was filled 2–3 days in advance to avoid currents and temperature differences in the column. The time needed to settle 50 cm through the column was measured using a stop watch (Kaiser et al., 2017). Particles were placed carefully beneath the water surface using tweezers and then allowed to settle for 30 cm in order to reach their terminal velocity before measurement was started. Particles settling close to the tube walls were excluded from data analyses. Multicellular organisms attached to sinking polymers were identified via binocular and a field guide (Streble and Krauter, 1988) to the family level.

2.7. Analysis of iron colloids

Iron colloids resulting from reservoir mixing were obtained by centrifuging two water samples retrieved on September 21 (10 min, 15000 rpm). The resulting pellets were dried (60 °C for 24 h) and iron and manganese were analysed according to methods described in 2.4. The remaining solids were washed three times with acidified water (pH 1.8) and centrifuged/dried again (60 °C, 24 h) to determine the acid soluble fraction. Afterwards the ash content was determined by combusting the sample at 450 °C for 24 h. One aggregate formed by PE and iron colloids was treated similarly and analysed for its iron and manganese content.

2.8. Data analysis

The critical thickness and mass of an attached fouling film in order to overcome a PE squares buoyancy was calculated following Chubarenko et al. (2016):

$$d_{film} = \frac{h}{2} * \frac{\rho_w - \rho_0}{\rho_f - \rho_w} \quad (1)$$

$$m_f = a^2 * d * \rho_f \quad (2)$$

With ρ_0: Density of unfouled PE particle (920 kg m^{-3}); ρ_f: Density of the fouling film (different densities, Table S2); ρ_w Density of water (1000 kg m^{-3}); h : Height of the particle (1.5×10^{-4} m); d_{film}: Thickness of the fouling film; m_f: Mass of fouling film needed to sink PE; a: Length of LDPE particle (4×10^{-3} m).

Results were compared among sampling dates and depths using non-parametric bootstrapping (Efron and Tibshirani, 1986) because assumptions of the ANOVA were not satisfied. For each comparison, we reported the median difference of 10000 bootstrapped samples with 95% confidence intervals. Differences in medians containing values other than zero were regarded as significantly different from each other by 95% chance. Software R (R Core Team, 2018) was used for all statistical analysis.

3. Results

3.1. Biovolumes analysed by CLSM

Biovolumes of three phylogenetic groups (bacteria, cyanobacteria and algae) were analysed for three different reservoir depths (epilimnion, metalimnion and hypolimnion) and time intervals (day 6, day 22 and day 47). Cages from the epilimnion were covered with visible biofilms after 47 days, whereas no visible biofilm formation was observed on cages from the metalimnion and hypolimnion.

The cellular components of the biofilms on day 6 consisted predominantly of bacteria (Fig. 1). PET had fewer bacteria compared to PS/PE in the metalimnion and to PE in the epilimnion, while PS had significantly more bacteria than PE and PET in the hypolimnion. Cyanobacteria and algae were scarce throughout, nonetheless small but statically significant differences among the polymers were found (Fig. 1b and c).

On day 22 (Fig. 1) biofilms were again dominated by bacteria. PE showed the highest bacterial biovolume of all polymers in each incubation depth (Fig. 1a). PS had higher values than PET in the epilimnion and metalimnion, but lower bacterial biovolumes in the hypolimnion compared to PET. Cyanobacteria biovolumes were again negligible. Some algae were found on PS exceeding PE and especially PET in the epi- and metalimnion. In the hypolimnion PE had remarkably higher algae biovolumes than PET and PS.

Biovolumes on day 47 were distinct from the previous sampling dates, and characterized by higher shares of phototrophic organisms in the epilimnion. Bacterial biovolume showed less pronounced differences between the surfaces than before. Cyanobacteria in the epilimnion made up a significant proportion of the phototrophic biovolume. Comparing the surfaces, PET and PS showed the highest volumes, while PE only reached around 5% of the cyanobacteria biovolume found on PET or PS. In the metalimnion cyanobacteria were scarce throughout. In the hypolimnion cyanobacteria biovolume was low but significantly different between surfaces (Fig. 1c). Substantial algae biovolumes were found on all polymers in the epilimnion with PET/PS significantly exceeding PE. Few algae occurred in the metalimnion and hypolimnion although some significant differences were found (Fig. 1b).

The biovolumes of bacteria, cyanobacteria and algae increased over time on all polymers in each of the incubation depths. Remarkably, algal biovolumes increased by at least one order of magnitude between day 22 and day 47 in the epilimnion. No

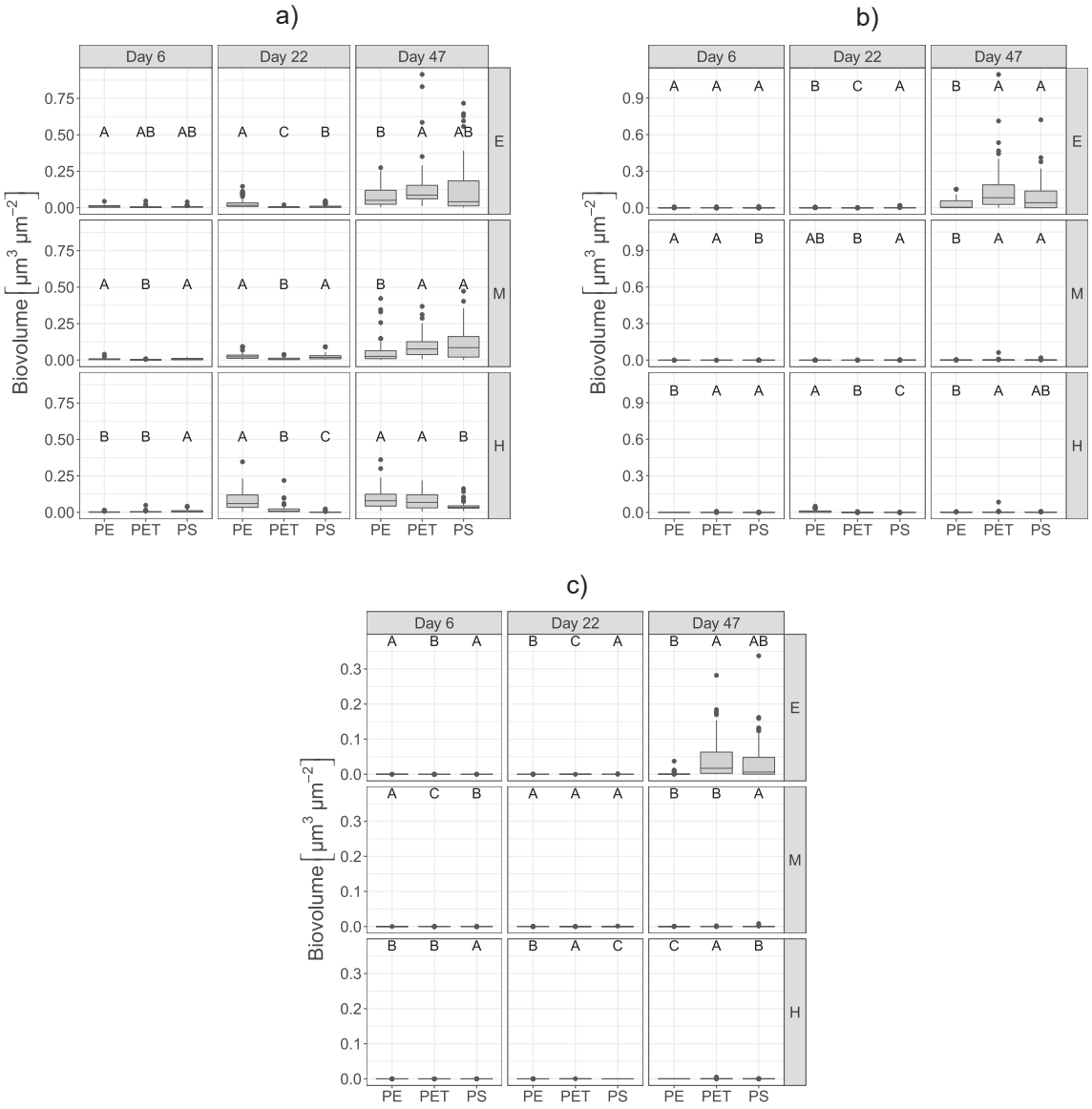

Fig. 1. Biovolumes of bacteria (a), algae (b) and cyanobacteria (c) in epilimnion (E), metalimnion (M) and hypolimnion (H) over 47 days of exposure. Sample sizes were 50 for each polymer. Groups significantly different from each other (with 95% confidence) are highlighted with letters in alphabetical order beginning with the highest value in each individual panel.

general differences regarding the final bacterial biovolumes were found at day 47. However, PE tended to have lower biovolumes of phototrophic organisms than the other surfaces.

3.2. Biofilms analysed by crystal violet staining

On day 6 the biofilm was not well established, with OD_{595} values being low for all polymers (Fig. 2), but still significantly higher than the pristine particles used as blanks. Differences between the polymers were scarce with only PET exhibiting lower OD_{595} values than PE in all samples on day 22 and day 47. Biofilm mass on PS on day 22 was equal to that on PE in the epilimnion and metalimnion but lower than on PE in the hypolimnion. PS values were equal to PET values on day 22 except for the epilimnion. OD_{595} was highest at day 47 for all sampled polymers, which indicates an increase of stainable molecules over the incubation time.

The OD_{595} values showed a positive linear correlation with their respective total biovolumes (sum of algae, bacteria and cyanobacteria) derived from CLSM imaging. The increase of OD_{595} per biovolume was higher for PE than for PET, as expressed by a steeper regression line. Therefore higher OD_{595} values would result from similar or lower biovolume on PE compared to PET (Fig. S3, Table S3).

3.3. Metal concentrations on MP

Iron and manganese (detection limit 0.3 µg mg^{-1}) were found on all tested biofilm-covered MP. On day 6 and 22 no manganese was detected, but after 47 days manganese was found on every polymer in most incubation depths. PE showed the highest manganese sorption, exceeding 0.63 µg mg^{-1} in the epilimnion.

In contrast, iron was detected from day 6 on at all polymers. On day 22 substantial iron sorption was observed in the hypolimnion (Fig. 3). The highest iron concentration occurred on PE on day 47 in the epilimnion (1.64 µg mg^{-1}).

At least for PE metal concentrations increased substantially over

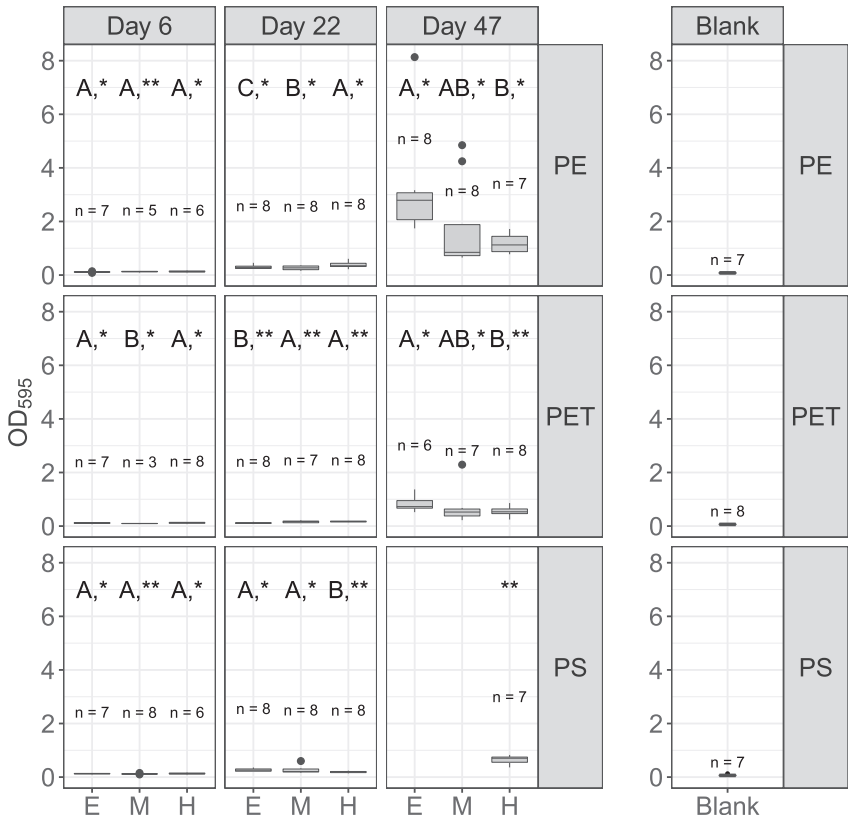

Fig. 2. Effect of incubation depth and exposure time on the total biofilm mass (crystal violet staining, OD_{595}). Pristine particles were used as blanks. Values for PS are missing on day 47 for the epilimnion and metalimnion due to sample loss. Letter display significant differences (with 95%confidence) between the surface in each panel in horizontal direction, stars (with * > **) mark significant difference between the incubation depths of a single polymer in vertical direction.

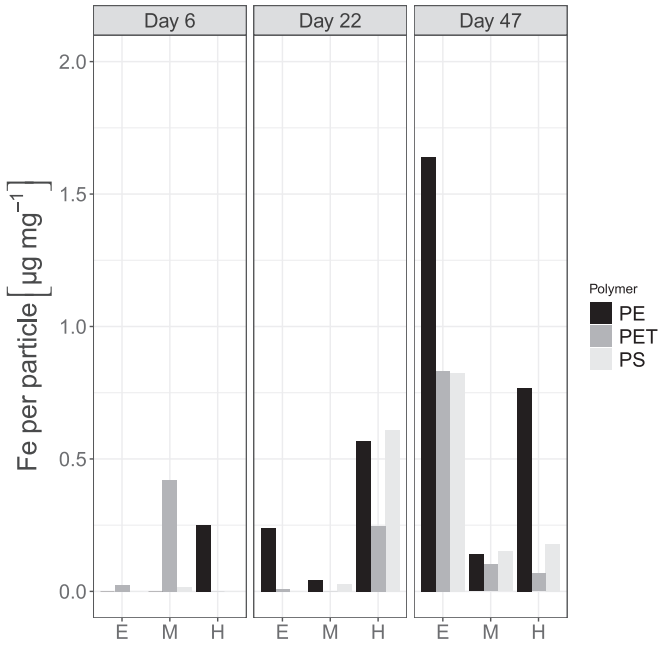

Fig. 3. Iron concentrations on plastic polymers during exposure in Malter reservoir. Missing values indicate no measurable iron present at the particular time point or depth. The values were calculated by dividing the measured concentrations by particle weight (15 particles weighing 1.93 (PS), 2.63 (PET) and 2.2 mg (PE) each).

the incubation time. Sorption of iron exceeded that of manganese on all polymers. As the data display an integrated mean of 15 particles per measurement no statistical analysis was conducted.

3.4. Sinking velocity of particles

During the experiment no sinking of single PE particles regardless of incubation depth or time occurred and so no sinking velocities were recorded.

The terminal sinking velocities of PET squares were roughly three times higher than those of PS, with values of 0.028 m s^{-1} compared to 0.0075 m s^{-1} respectively (Fig. 4). No substantial differences between incubated particles and the control pristine particles of PET and PS were observed (Table S4). Small differences between some incubation depths or sampling dates were occurring (Table S4). On day 47, larger organisms such as hydras and cladocerans were attached to the surface of 9% of the PS particles and 10% of the PET particles used in the sinking experiment. These organisms influenced the sinking speed of PS slightly by accelerating the sinking speed by 4% (median of particles with attached multicellular organisms: 0.008 m/s, n: 4) and decreased the sinking speed of PET by 1% (median: 0.0276, n: 6) compared to particles with no attached larger organisms. On day 6 and day 22 no such organisms were observed on the particles.

3.5. Mixing event and aggregation of MP with iron colloids

Oxygen intruded into the anoxic hypolimnion of the stratified Malter reservoir between September 5 (day 6) and September 21 (day 22) (Fig. S1b and c). Substantial amounts of brownish-red iron

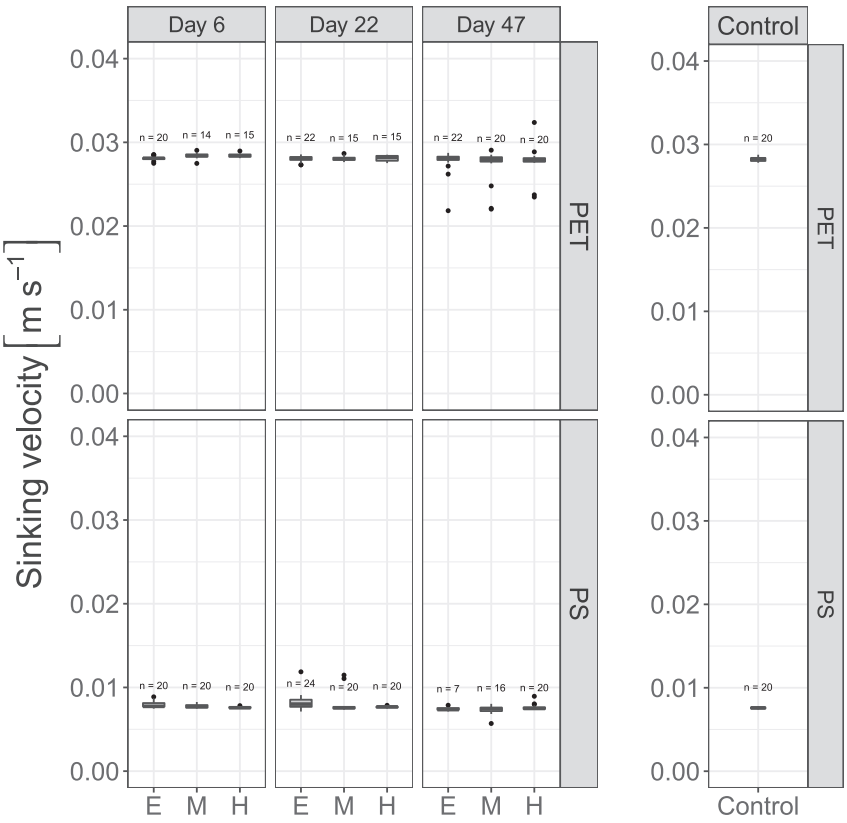

Fig. 4. Sinking velocity of PET and PS in deionized water (20 °C) after incubation in Malter reservoir. The control displays settling velocities of unexposed (pristine) particles.

flocs (Fig. 5a) floated freely in the whole water column on September 21. These reservoir-borne iron colloids consisted of approximately 12% per weight iron, 40% per weight organics, and 38% per weight ash content referring to the dry mass. The acid soluble fraction was 26% per weight which corresponds well to the mass of 27% Fe_2O_3 x 0.5 H_2O stoichiometrically calculated from the measured iron content. The colloids were not observed at day 47 (October 16). Aggregation of four PE particles with iron colloids was observed in the hypolimnion (Fig. 5a and b). The formed aggregate was stable enough for being transferred by tweezers without breaking apart. Its density was higher than water; subsequently it sank down to the bottom of a water filled storage container. Non-agglomerated PE particles retrieved from the hypolimnion on that day remained buoyant. The biofilm on the aggregate showed higher biovolumes of bacteria, algae and cyanobacteria compared to any other surface (Fig. 5c). The agglomerate was of brownish color, indicating the presence of iron which made up approximately 3% Fe (11 μg mg^{-1}) of the total dry mass. Small amounts of manganese reaching <1% (0.07 μg mg^{-1}) of the total dry mass were measured as well.

4. Discussion

In this study we measured biofilm formation and sorption of metals to different polymers in MP size in order to investigate the effects on their sinking behavior. Employing CLSM, crystal violet staining and spectrophotometric methods, we found microbial biofilm formation to be not sufficient for promoting the sinking of single MP particles in Malter reservoir during late summer. Sinking through aggregation with iron colloids and biomass (cells/EPS) was observed after reservoir mixing in a single case.

Contrary to our findings, biofouling with cyanobacteria was found to sink polypropylene particles in a eutrophic tropical lake (Chen et al., 2019). The authors hypothesized that the binding of inorganic material contributed more significantly to the mass of the fouling film than the phototrophic cells (Chen et al., 2019). Differences to our results can be explained by distinct environmental conditions in Malter reservoir such as lower concentrations of chlorophyll *a* (41 μg/l vs. 120 μg l^{-1}), phosphate (0.03 vs. 0.214 mg l^{-1}), ammonia (0.07 vs. 0.41 mg l^{-1}), and suspended solids (4 vs. 35 mg l^{-1}). Regarding the different conditions, biofouling will be more intense in warm, nutrient-rich, shallow lakes compared to temperate, nutrient-poor, deep reservoirs. The absence of calcareous macrofoulers which is considered as a major factor promoting sinking of MP in marine environments (Kaiser et al., 2017) may also explain low impact of biofouling on the particle densities in this study.

However it cannot be excluded that more extensive biofouling occurs during different seasons and may facilitate MP sinking in Malter reservoir. Biofilm formation may strongly influence aggregation dynamics and subsequently the sinking of MP by increasing the stickiness, surface charge or altering the morphology (e.g. lobes, filaments) of the particles. Aggregation with inorganic and organic particles is considered as another important process that determines the environmental fate of MP (Besseling et al., 2017). Sticky organic material such as marine snow (Porter et al., 2018), biogenic particles (Michels et al., 2018), EPS (Summers et al., 2018), organo-mineral particulate matter (Möhlenkamp et al., 2018) and marine (Long et al., 2015) or freshwater microalgae (Lagarde et al., 2016) can sink buoyant MP through formation of large hetero-aggregates. Most studies used laboratory set-ups employing conditions favoring aggregation such as low shear stress and high particle concentrations (10^1-10^4 particles ml^{-1}) (Möhlenkamp et al., 2018) which may not reflect natural conditions. Currents,

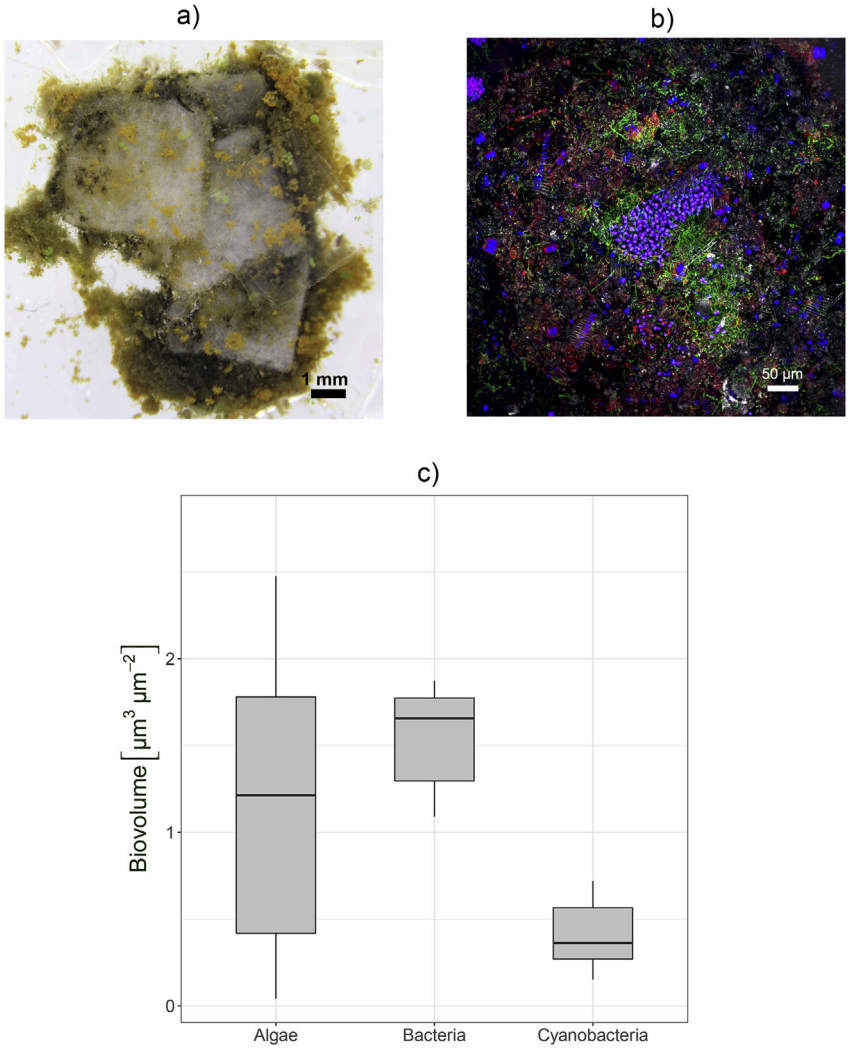

Fig. 5. Images and biovolumes of PE aggregate from hypolimnion at day 22. a) bright light microscopy (10x magnification), b) CLSM image stained with lectin to visualize EPS, c) biovolumes of algae, bacteria and cyanobacteria within the aggregate. Coding for CLSM: green (bacterial cells), purple (cyanobacteria), blue (algae), and red (EPS). (For interpretation of the references to color in this figure legend, the reader is referred to the Web version of this article.)

grazing, microbial degradation and ingestion by larger organisms could lead to rapid break-up or consumption of such aggregates in nature (Cole et al., 2016). In this study aggregation of PE with organo-mineral matter was observed. The formation right after mixing indicates that iron oxide containing colloids induced the aggregation of PE with organic matter and cells of cyanobacteria, algae and bacteria. Iron colloid formation is an important process capable to aggregate and sink buoyant cyanobacteria in natural lakes after mixing (Oliver et al., 1985). Given that only 4 large microplastic particles aggregated with such colloids; this study cannot provide sufficient data on the importance and implications of this mechanisms for the fate of MP in reservoirs. Furthermore it should be considered that reservoir mixing is no prerequisite for the aggregation and subsequent settling of MP in the environment.

Considering the oxic conditions of the hypolimnion prevailing at least since day 22, the majority of iron and manganese should have been present as metal oxides. Oxide minerals such as ferrihydrite (Fe_5HO_8 x 4 H_2O), magnetite (Fe_3O_4) or manganese (IV) oxide (MnO_2) exhibit a high specific density and may influence the density of MP particles. The density change of PE particles (4 × 4 × 0.15 mm) covered by a "fouling film" was calculated by using the specific density of these minerals as input variable (Chubarenko et al., 2016). Afterwards the mass of fouling films comprising ferrihydrite, magnetite, manganese oxide or bacteria needed to sink the PE particle ($\rho_{PE} > \rho_{Water}$) were determined following equation (2). Accordingly, the mass concentrations needed to sink PE are 54 µg mg^{-1} magnetite, 58 µg mg^{-1} ferrihydrite, 55 µg mg^{-1} manganese oxide and 131, 156 or 218 µg mg^{-1} bacteria (with different $\rho_{Bacteria}$, Table S2). The maximum iron concentration found on buoyant PE (1.64 µg mg^{-1}) corresponded to 2.2 µg mg^{-1} ferrihydrite or 2.1 µg mg^{-1} magnetite whereas the maximum manganese concentration (0.64 µg mg^{-1}) corresponded to 0.94 µg mg^{-1} manganese oxide. Therefore, the mass concentration of metals bound to freely floating PE particles was at least one order of magnitude too low to overcome their buoyancy. The sinking aggregated PE particles showed iron concentrations of 11 µg mg^{-1} corresponding to 16.4 µg mg^{-1} ferrihydrite or 15.2 µg mg^{-1} magnetite. Biovolume (in μm^3 μm^{-2}) of bacteria, cyanobacteria and algae can be converted to cells mass per particle by multiplying with the particle surface area (1.6 × 10^7 μm^2) and the specific density of microbial biomass (Table S2). Buoyant PE particles contained approximately 8 µg mg^{-1} total biomass (for $\rho_{Biomass}$: 1500 kg m^{-3}) while the microbial biomass on the sunken PE agglomerate made up 149, 138 or 124 µg mg^{-1} depending on the

specific density of microbial biomass applied. The biomass calculated for the sunken agglomerated PE was in good agreement with the 131 μg mg^{-1} (for $\rho_{Biomass}$: 1500 kg m^{-3}) (Chubarenko et al., 2018) theoretically needed to sink buoyant PE particles. Assuming lower $\rho_{Bacteria}$ the results deviated slightly (156 μg mg^{-1} for $\rho_{Biomass}$: 1388 kg m^{-3}) (Besseling et al., 2017) or moderately (218 μg mg^{-1} for $\rho_{Biomass}$: 1250 kg m^{-3}) (Kooi et al., 2017) from the biomass theoretically required for sinking. However it should be considered that most of the aggregate organic mass was not quantified via CLSM as EPS was not assessed with the used technique. Nonetheless ballasting effects of microorganisms considerably exceeded the effect of metal oxides, comprising a likely reason for the observed loss in buoyancy. This leads to the assumption that the aggregation of freshwater microorganisms can sink MP if sufficient biomass is provided. However, under low bio-productivity or low temperature conditions the critical mass to sink the MP may not be reached within reasonable timescales.

The extent of EPS production within the biofilms seemed to differ between the polymers, as shown via crystal violet assay. Algae and cyanobacteria cells were present in lower densities on PE compared to PET and PS as seen from CLSM imaging. This may indicate that these organisms had to put more effort into attachment to PE surfaces than to PET/PS. Low attachment efficiency leads to environmental stress (Vosshage et al., 2018) and ultimately to more EPS production by the stressed cells (Scott et al., 2014). Therefore the fewer but stressed cells on PE could have produced more EPS than the cells on PET.

Regarding the occurrence of metals on biofilm covered MP, PE showed higher concentrations of iron and manganese compared to the other polymers. Concentrations of Fe and Mn exceeded up to 100 times (Fe) or 10 times (Mn) the concentrations found on beached plastic pellets at British shores (Ashton et al., 2010; Holmes et al., 2012) and plastics exposed to seawater for several months (Rochman et al., 2014). Lower ionic strength and the higher abundance of Fe/Mn in freshwater water may explain the higher MP metal concentrations found in this study. According to previous studies long-term metal sorption to plastics does not differ between polymer types (Rochman et al., 2014). The metal sorption is rather controlled by the biofilm thickness and the available binding places therein (Rochman et al., 2014; van Hullebusch et al., 2003). In our study, PE showed the highest crystal violet stainable biomass of all polymers. PE may therefore have provided more binding places for metals within the EPS matrix, leading to the highest measured iron and manganese concentrations.

The polymers were enclosed in steel cages during the experiment. For PS and PET this produces artificial conditions, as particles of the used size will settle down to the sediment within 10 (PET) to 30 min (PS) assuming a mean water depth of 16 m and no other currents or mixing. However, polymers with mechanically changed properties such as PET bottles with trapped air inside or expanded PS may stay afloat for a longer time-span than the particles used in this experiment. This makes the description of biofilm formation on PS and PET in the upper reservoir parts environmentally relevant even though the particles are not buoyant. Conditions for biofilm formation may differ between the interior of the cages and the open reservoir water, as larger grazing organisms were excluded by the mesh size. Furthermore the cages had a shading effect reducing the light intensity by 33%. Due to biofilm formation on the cages this shading effect could have been even stronger than the 33% measured for blank cages. Reservoirs and especially their hypolimnia experience very low currents. For this reason, biofilms are only loosely bound to their carriers, making biofilm loss due to shear stress likely. This may partly explain the high variability of biovolumes on particles of the same material and exposure time. Formation of hetero-aggregates between PE and organo-mineral matter was only observed in the hypolimnion. Therefore, the possible sinking of PE floating at the water surface could not be proven directly. Only one aggregate with four PE particles has been observed hence coincidence cannot be excluded. The experiment was conducted from late summer to autumn which includes lowering of temperatures and light intensities during this time. As the extent of biofouling depends on season (Chen et al., 2019), it cannot be excluded that biofouling-induced sinking may occur during other times of the year.

5. Conclusions

- Late summer biofilm development within a temperate mesotrophic reservoir was not sufficient to facilitate sinking of buoyant MP or increasing the settling velocity of dense MP
- Biofilms grown on PET and PS microplastics in the mesotrophic reservoir contained more phototrophic microorganisms than those on PE microplastics
- Manganese and iron sorbed to biofilm covered microplastics in substantial amounts

Declaration of competing interest

The authors declare that they have no known competing financial interests or personal relationships that could have appeared to influence the work reported in this paper.

Acknowledgements

We thank Ute Kuhlicke for extensive microscopy work and excellent advice, and Corinna Völkner, Martin Wieprecht, Franziska Reggelin and Jana Reichenbach for eminent help with field and laboratory work. Therese Kettner is acknowledged for providing the steel cages. We also thank the Landestalsperrenverwaltung des Freistaates Sachsen (LTV; especially Alice Rau) for providing access to the reservoir and water quality data. The critical comments of anonymous reviewers helped to improve the manuscript. This research was supported by the BMBF project MikroPlaTaS (02WPL1448A).

Appendix A. Supplementary data

Supplementary data to this article can be found online at https://doi.org/10.1016/j.watres.2020.115748.

References

Anderson, P.J., Warrack, S., Langen, V., Challis, J.K., Hanson, M.L., Rennie, M.D., 2017. Microplastic contamination in Lake Winnipeg, Canada. Environ. Pollut. 225, 223–231. https://doi.org/10.1016/j.envpol.2017.02.072.

Arias-Andres, M., Kettner, M.T., Miki, T., Grossart, H.-P., 2018. Microplastics: new substrates for heterotrophic activity contribute to altering organic matter cycles in aquatic ecosystems. Sci. Total Environ. 635, 1152–1159. https://doi.org/10.1016/j.scitotenv.2018.04.199.

Ashton, K., Holmes, L., Turner, A., 2010. Association of metals with plastic production pellets in the marine environment. Mar. Pollut. Bull. 60, 2050–2055. https://doi.org/10.1016/j.marpolbul.2010.07.014.

Besseling, E., Quik, J.T.K., Sun, M., Koelmans, A.A., 2017. Fate of nano- and microplastic in freshwater systems: a modeling study. Environ. Pollut. 220, 540–548. https://doi.org/10.1016/j.envpol.2016.10.001.

Brewer, P.G., Spencer, D.W., 1971. Colorimetric determination of manganese in anoxic waters. Limnol. Oceanogr. 16, 107–110. https://doi.org/10.4319/lo.1971.16.1.0107.

Burlage, R., Atlas, R., Stahl, D., 1998. Techniques in Microbial Ecology, first ed. Oxford University Press. https://doi.org/10.1016/s0580-9517(08)x7011-4.

Castañeda, R.A., Avlijas, S., Anouk Simard, M., Ricciardi, A., 2014. Microplastic pollution in St. Lawrence River sediments. Can. J. Fish. Aquat. Sci. 71, 1767–1771. https://doi.org/10.1139/cjfas-2014-0281.

Chen, X., Xiong, X., Jiang, X., Shi, H., Wu, C., 2019. Sinking of floating plastic debris caused by biofilm development in a freshwater lake. Chemosphere 222,

856–864. https://doi.org/10.1016/j.chemosphere.2019.02.015.
Chubarenko, I., Bagaev, A., Zobkov, M., Esiukova, E., 2016. On some physical and dynamical properties of microplastic particles in marine environment. Mar. Pollut. Bull. 108, 105–112.
Chubarenko, I., Esiukova, E., Bagaev, A., Isachenko, I., Demchenko, N., Zobkov, M., Efimova, I., Bagaeva, M., Khatmullina, L., 2018. Behavior of Microplastics in Coastal Zones, Microplastic Contamination in Aquatic Environments. https://doi.org/10.1016/B978-0-12-813747-5.00006-0.
Cole, M., Lindeque, P.K., Fileman, E., Clark, J., Lewis, C., Halsband, C., Galloway, T.S., 2016. Microplastics alter the properties and sinking rates of zooplankton faecal pellets. Environ. Sci. Technol. 50, 3239–3246. https://doi.org/10.1021/acs.est.5b05905.
Corcoran, P.L., Norris, T., Ceccanese, T., Walzak, M.J., Helm, P.A., Marvin, C.H., 2015. Hidden plastics of Lake Ontario, Canada and their potential preservation in the sediment record. Environ. Pollut. 204, 17–25. https://doi.org/10.1016/j.envpol.2015.04.0093.
Efron, B., Tibshirani, R., 1986. Bootstrap methods for standard errors, confidence intervals, and other measures of statistical accuracy. Stat. Sci. 1, 54–75. https://doi.org/10.1214/ss/1177013815.
Goto, K., Komatsu, T., Furukawa, T., 1962. Rapid colorimetric determination of manganese in waters containing iron. Anal. Chim. Acta 27, 331–334. https://doi.org/10.1016/S0003-2670(00)88510-4.
Holmes, L.A., Turner, A., Thompson, R.C., 2012. Adsorption of trace metals to plastic resin pellets in the marine environment. Environ. Pollut. 160, 42–48. https://doi.org/10.1016/j.envpol.2011.08.052.
Kaiser, D., Kowalski, N., Waniek, J.J., 2017. Effects of biofouling on the sinking behavior of microplastics. Environ. Res. Lett. 12 https://doi.org/10.1088/1748-9326/aa8e8b.
Kooi, M., Van Nes, E.H., Scheffer, M., Koelmans, A.A., 2017. Ups and downs in the ocean: effects of biofouling on vertical transport of microplastics. Environ. Sci. Technol. 51, 7963–7971. https://doi.org/10.1021/acs.est.6b04702.
Kowalski, N., Reichardt, A.M., Waniek, J.J., 2016. Sinking rates of microplastics and potential implications of their alteration by physical, biological, and chemical factors. Mar. Pollut. Bull. 109, 310–319. https://doi.org/10.1016/j.marpolbul.2016.05.064.
Lagarde, F., Olivier, O., Zanella, M., Daniel, P., Hiard, S., Caruso, A., 2016. Microplastic interactions with freshwater microalgae: hetero-aggregation and changes in plastic density appear strongly dependent on polymer type. Environ. Pollut. 215, 331–339. https://doi.org/10.1016/j.envpol.2016.05.006.
Long, M., Moriceau, B., Gallinari, M., Lambert, C., Huvet, A., Raffray, J., Soudant, P., 2015. Interactions between microplastics and phytoplankton aggregates: impact on their respective fates. Mar. Chem. 175, 39–46. https://doi.org/10.1016/j.marchem.2015.04.003.
McCormick, A., Hoellein, T.J., Mason, S.A., Schluep, J., Kelly, J.J., 2014. Microplastic is an abundant and distinct microbial habitat in an urban river. Environ. Sci. Technol. 48, 11863–11871. https://doi.org/10.1021/es503610r.
Michels, J., Stippkugel, A., Lenz, M., Wirtz, K., Engel, A., 2018. Rapid aggregation of biofilm-covered microplastics with marine biogenic particles. Proc. Biol. Sci. 285, 20181203 https://doi.org/10.1098/rspb.2018.1203.
Möhlenkamp, P., Purser, A., Thomsen, L., 2018. Plastic microbeads from cosmetic products: an experimental study of their hydrodynamic behaviour, vertical transport and resuspension in phytoplankton and sediment aggregates. Elementa 6. https://doi.org/10.1525/elementa.317.
Müller, J., Ruppert, H., Muramatsu, Y., Schneider, J., 2000. Reservoir sediments - a witness of mining and industrial development (Malter Reservoir, eastern Erzgebirge, Germany). Environ. Geol. 39, 1341–1351. https://doi.org/10.1007/s002540000117.
Oberbeckmann, S., Osborn, A.M., Duhaime, M., 2016. Microbes on a bottle: substrate, season and geography influence community composition of microbes colonizing marine plastic debris. PLoS One 11, 1–24. https://doi.org/10.1371/journal.pone.0159289.
Oliver, R.L., Thomas, R., Reynold, C.S., Walsby, A.E., 1985. The sedimentation of buoyant *Microcystis* colonies caused by precipitation with an iron- containing colloid. Proc. R. Soc. B 223, 511–528. https://doi.org/10.1098/rspb.1985.0016.
Parrish, K., Fahrenfeld, N.L., 2019. Microplastic biofilm in fresh- and wastewater as a function of microparticle type and size class. Environ. Sci. Water Res. Technol. 5, 495–505. https://doi.org/10.1039/c8ew00712h.
Porter, A., Lyons, B.P., Galloway, T.S., Lewis, C., 2018. Role of marine snows in microplastic fate and bioavailability. Environ. Sci. Technol. 52, 7111–7119. https://doi.org/10.1021/acs.est.8b01000.
R Core Team, 2018. R: A Language and Environment for Statistical Computing.
Rochman, C.M., Hentschel, B.T., Teh, S.J., 2014. Long-term sorption of metals is similar among plastic types: implications for plastic debris in aquatic environments. PLoS One 9. https://doi.org/10.1371/journal.pone.0085433.
Scott, C.E., Jackson, D.A., Zimmerman, A.P., 2014. Environmental and algal community influences on benthic algal extracellular material in Lake Opeongo, Ontario. Freshw. Sci. 33, 568–576. https://doi.org/10.1086/675811.
Staudt, C., Horn, H., Hempel, D.C., Neu, T.R., 2004. Volumetric measurements of bacterial cells and EPS glycoconjugates in biofilms. Biotechnol. Bioeng. 88, 585–592doi. https://doi.org/10.1002/bit.20241.
Stookey, L.L., 1970. Ferrozine - a new spectrophotometric reagent for iron. Anal. Chem. 42, 779–781. https://doi.org/10.1021/ac60289a016.
Streble, H., Krauter, D., 1988. Das Leben im Wassertropfen. Mikroflora und Mikrofauna des Süßwassers, eighth ed. Kosmos Stuttgart.
Summers, S., Henry, T., Gutierrez, T., 2018. Agglomeration of nano- and microplastic particles in seawater by autochthonous and de novo-produced sources of exopolymeric substances. Mar. Pollut. Bull. 130, 258–267. https://doi.org/10.1016/j.marpolbul.2018.03.039.
Tipping, E., Woof, C., Cooke, D., 1981. Iron oxide from a seasonally anoxic lake. Geochem. Cosmochim. Acta 45, 1411–1419. https://doi.org/10.1016/0016-7037(81)90275-1.
van Hullebusch, E.D., Zandvoort, M.H., Lens, P.N.L., 2003. Metal immobilisation by biofilms: mechanisms and analytical tools. Rev. Environ. Sci. Biotechnol. 2, 9–33. https://doi.org/10.1023/B:RESB.0000022995.48330.55.
Vosshage, A.T.L., Neu, T.R., Gabel, F., 2018. Plastic alters biofilm quality as food resource of the freshwater gastropod *Radix balthica*. Environ. Sci. Technol. 52, 11387–11393. https://doi.org/10.1021/acs.est.8b02470.
Watkins, L., McGrattan, S., Sullivan, P.J., Walter, M.T., 2019. The effect of dams on river transport of microplastic pollution. Sci. Total Environ. 664, 834–840. https://doi.org/10.1016/j.scitotenv.2019.02.028.
Xu, Z., Liang, Y., Lin, S., Chen, D., Li, B., Li, L., Deng, Y., 2016. Crystal violet and XTT assays on *Staphylococcus aureus* biofilm quantification. Curr. Microbiol. 73 (4), 474–482. https://doi.org/10.1007/s00284-016-1081-1.
Zettler, E.R., Mincer, T.J., Amaral-Zettler, L.A., 2013. Life in the “plastisphere”: microbial communities on plastic marine debris. Environ. Sci. Technol. 47, 7137–7146. https://doi.org/10.1021/es401288x.
Zhang, K., Gong, W., Lv, J., Xiong, X., Wu, C., 2015. Accumulation of floating microplastics behind the Three Gorges Dam. Environ. Pollut. 204, 117–123. https://doi.org/10.1016/j.envpol.2015.04.023.

Chapter 4

Manuscript 3

Burial of microplastics in freshwater sediments facilitated by iron-organo flocs

submitted to *Nature Scientific Reports* on May 6th 2021,(status on June 11th 2021: Under review)

Rico Leiser, Maja Schumann, Tallent Dadi and Katrin Wendt-Potthoff

Abstract

Microplastics are ubiquitous in standing freshwater bodies, subsequently lakes and reservoirs may be important sinks for these contaminants. However, the mechanisms governing microplastics deposition and their interactions with the sediments are understudied. We demonstrate how aggregation-based transport facilitates the sinking and infiltration of buoyant microplastics into freshwater reservoir sediments by employing experiments with intact sediment cores. Buoyant polyethylene microplastics were rapidly (1 - 4 hours) incorporated into sinking iron-organic aggregates, followed by swift deposition into sediments. Ingression of microplastic bearing flocs into sediments was completed within 6 days and led to stable deposition of the incorporated particles for at least 2 months. Most microplastics were deposited in the top 2 centimeter of the sediments and few particles (5 - 15 %) were re-released into the water. Our results show at least 85 % burial of microplastics, indicating the significant role of standing freshwaters in reducing microplastic loads to the oceans.

Introduction

Microplastics (MP) are particulate anthropogenic pollutants ($<$ 5 mm) frequently found in the sediments of many lakes (Turner et al., 2019) and reservoirs (Di and Wang, 2018) worldwide. Most of these plastics originate from rivers, flowing into the standing water bodies. The reduction of flow velocity leads to the settling of MP (Watkins et al., 2019), alongside with other particulate matter (Franzen, 1985) into the sediments (Enders et al., 2019). However, this only holds true for MP particles with high densities ($\rho > 1.0$ g cm^{-3}) allowing sedimentation in water (Chubarenko et al., 2016). Still, initially floating, low density ($\rho < 1.0$ g cm^{-3}) polymer types such as polyethylene (PE) are among the most common MP retrieved from freshwater sediments (Merga et al., 2020). This implies the existence of processes governing the sedimentation of buoyant MP in freshwater lakes and reservoirs.

Such processes are aggregation (Michels et al., 2018), biofouling (Kaiser et al., 2017) and mineral formation (Leiser et al., 2021) affecting both high and low density MP. The MP particles may aggregate with microalgae cells (Lagarde et al., 2016),

cyanobacteria (Leiser et al., 2021), diatoms (Long et al., 2017) or transparent exopolymeric particles (Michels et al., 2018) (TEP) leading to the sinking of initially buoyant polymers.

Large sinking aggregates (> 1 mm) comprised of organic debris and inorganic particles (Grossart et al., 1997) are commonly found in lakes referring to as lake snow (Grossart and Simon, 1993). Depending on the prevailing biogeochemical conditions "lake snow" may contain high proportions of iron oxy(hydroxides) (Elliott and Warren, 2014; Reiche et al., 2011). The organic matter in such flocs consists of microbes (Plach et al., 2011) and of co-precipitated dissolved or particulate organic carbon from the water (Pizarro et al., 1995). Especially during lake stratification (Bravidor et al., 2015) or autumnal lake mixing (Oliver et al., 1985) such iron-organo aggregates can be present in the water column.

Iron-rich aggregates are usually formed at the upper part of the oxycline where anoxic water rich in ferrous iron comes into contact with oxic water. This leads to the oxidation of the ferrous to ferric iron (Cornell and Schwertmann, 2003) which subsequently precipitates in the form of amorphous iron oxy(hydroxides) colloids (Tipping et al., 1981). These colloids form large and sinking flocs by aggregating with the organic material present in lake water (Reiche et al., 2011). Such flocs may also be formed by the rapid breakdown of lake summer stratification (Mortimer, 1942). This results in the complete mixing of the anoxic hypolimnion with the oxic epilimnion. The resulting iron-organo flocs are dispersed through the whole water column and co-precipitate microbial cells (Oliver et al., 1985), nutrients (Deppe and Benndorf, 2002) or heavy metals (Díez et al., 2007). It was previously reported that lake mixing leads to aggregation of buoyant planktonic *Microcystis* colonies with iron flocs, transporting them to the sediment (Oliver et al., 1985). These mixing events might even aggregate and sink buoyant MP through aggregating with iron containing colloids (Leiser et al., 2020). However the fate of the MP particles in the sediment is not known.

Iron flocs formed in lakes are susceptible to microbial iron reduction (Elliott and Warren, 2014) especially once they reach the sediment(Venkateswaran et al., 1999). Reduction might lead to the dissolution of the ballasting iron oxy(hydroxides), followed by floc disintegration (Oliver et al., 1985) and, if MP is enclosed, to MP

liberation. Hence post-deposition floc stability might be crucial for the permanent removal of MP from the water-column. Iron reduction is more intense during summer anoxia compared to times in which the hypolimnion is oxygenated (Wendt-Potthoff et al., 2014). Therefore iron floc stability and MP release might depend on the prevailing redox condition in the hypolimnion.

In this study, we explored how the aggregation of PE MP into sinking iron-organo flocs affect their long-term deposition in freshwater reservoir sediments, which is a crucial step for the complete understanding of this globally important MP sink. We hypothesized that iron-organo floc formation can be simulated in lab and that the incorporation of PE MP into such aggregates leads to sinking of this buoyant polymer. In addition, we assumed that size and shape of the particles govern their enclosure rate into iron flocs. This was tested by amending surface water from a eutrophic reservoir with the iron flocculent Fe(II)SO_4 and PE MP of three different shapes (fragments of 4 different size classes, fibers and spheres). Further we tried to elucidate the fate of such MP bearing iron-organo flocs once reaching the sediments of the water body. The first few mm of sediments and the over-laying water column of lakes and reservoirs might be anoxic or oxic, depending on the season. With iron being a redox-sensitive element, we hypothesized that iron-organo-flocs containing PE MP laying on-top of sediments will be stable under oxic conditions, while being disintegrated under anoxic conditions leading to MP release. This was tested with sediment cores from a eutrophic reservoir, which allow lab simulation of natural sediment processes due to their intact sediment surfaces. By addition of MP bearing iron-organo flocs to these sediment cores, we aimed to reassemble the route of MP initially floating in the water-body, into the sediments via an aggregation based transport mechanism.

Results

Iron-organo flocs formed by $FeSO_4$ oxidation and their characteristics

The addition of 100 or 300 µM $FeSO_4$ to filtered Bautzen reservoir water led to the formation of large and sinking iron containing flocs within < 1 h. (300 µM Fe) to 3-4 h. (100 µM Fe) (Figure S 1). The flocs formed by 100 µM Fe were generally fewer, smaller and had a lower density (Table 1) than the 300 µM Fe flocs. They were of reddish color emphasizing the high content of Fe (oxy)hydroxides (Figure S2).

Table 1: Properties of flocs formed after addition of 100 µM and 300 µM Fe. Inorganic, organic and Fe contents refer to the wet mass of the flocs. Displayed are the means and standard deviation of 6 replicates, except for equivalent spherical diameter (ESD) (Kaiser et al., 2019) which was calculated from 30 individual flocs.

Parameter	100 µM Fe(II)	300 µM Fe(II)
Water content [%]	94.41 ± 0.9	96.1 ± 0.8
Dry mass [%]	5.6 ± 0.9	3.9 ± 0.8
Inorganics [%]	3.0 ± 0.5	2.6 ±0.6
Organics [%]	2.6 ± 0.5	1.3 ± 0.2
Fe [%]	2.1 ± 0.7	2.9 ± 0.4
ESD [µm]	502 ± 132	3919 ± 700
Density [g cm^{-3}]	1.005 ± 0.0006	1.015 ± 0.0016

The main component was water (>90 %), while dry mass consisted of similar ratios of organic to inorganic components. The 300 µM Fe flocs had a significantly lower content of organics compared to the 100 µM flocs (ANOVA, $p < 0.05$). The inorganic content of the flocs was mainly comprised of Fe, the organics consisted primarily of extracellular polymeric substances (EPS) enclosing microbial cells and minerals (Fig. 1). The sticky EPS can be considered as binding agent gluing the cells and iron minerals together, thereby shaping the flocs' gel-like appearance (Figure 1a). Most cells within the flocs were identified as bacteria using Confocal Laser Scanning Microscopy (CLSM) technique, but also small numbers of eukaryotic algae

and cyanobacteria were present (Fig. 1b).

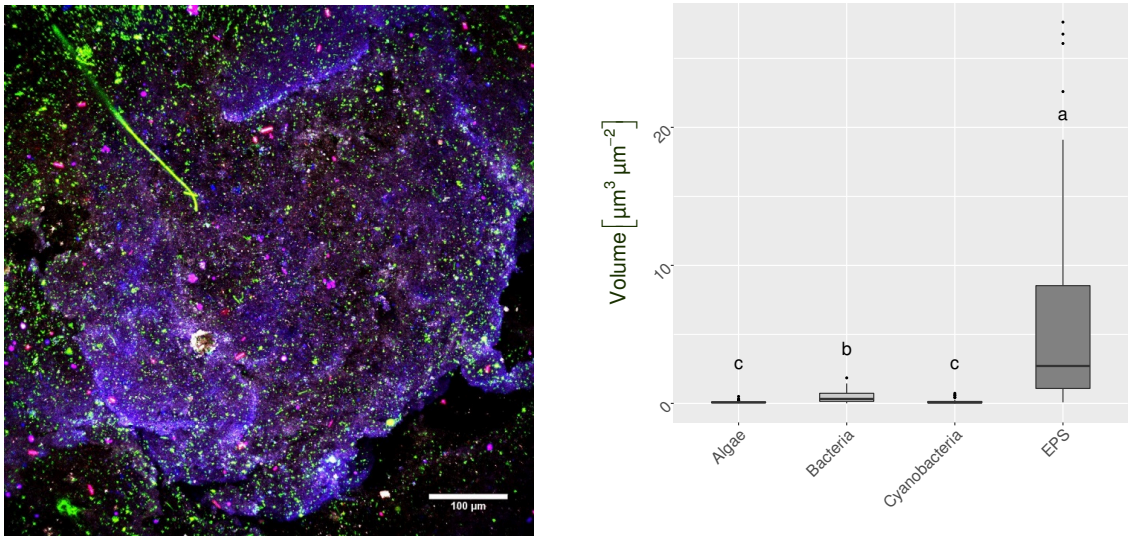

(a) (b)

Figure 1: Results of floc analysis via CLSM, with a) a representative iron-organo floc image showing bacteria (green), EPS (purple), cyanobacteria (pink) and algae (blue) and b) the biovolumes of different microbial groups and EPS within 300 µM Fe flocs.The biovolumes were semi-quantitatively calculated from 50 individual images. Statistically significant differences (non-parametric bootstrapping, 95 % confidence) are displayed by small letters.

Aggregation of different MP shapes into iron-organo flocs

Flocs formed by the addition of 300 µM Fe aggregated PE MP irrespective of their shape (Figure 2a). Spheres and small fragments (10 - 100 µm) were incorporated more readily than fibers (Table S3 Figure 2a). Only very few of the mid-sized fragments (100 - 250 µm) and almost none of the two largest fragment fractions (250 - 500 µm and $>$ 500 µm) were taken up by the iron flocs (Table S3 Figure 2a). The floc sizes showed high variability with means ranging from 2632 $\pm$ 1666 µm (median 2263 µm, n: 30) for spheres to 6270 $\pm$ 1666 µm (median 5650 µm, n: 30) for fibers (Figure 2b). Flocs formed with fibers had a pronounced elongated shape and contained macroscopic structures of entangled fibers (Figure S4). Beside this there were no clear differences in size between flocs with MP or without MP (Figure

2b). By contrast, the presence of MP significantly reduced the sinking velocity of the flocs (Figure 2c). The mean sinking velocities of the flocs ranged from 0.006 ± 0.0018 m s^{-1} (median 0.0059 m s^{-1}, n: 30) for fragments 10 – 100 µm to 0.01 ± 0.0017 m s^{-1} (median 0.0101 m s^{-1}, n: 30) for no MP. However, given the high variability of the data the absolute difference between the sinking velocities can be considered as minor, although being statistically significant. Flocs formed by 100 µM Fe also aggregated PE spheres but showed lower precipitation of MP (28 % of added spheres, mean, n: 3) compared to the 300 µM Fe flocs (99 %, mean, n: 3). The lower aggregation efficiency was linked to the lower amount of flocs which were precipitated by this treatment (Table S3). Normalized to the total mass of flocs the aggregation efficiency was similar for the 100 µM Fe (7.4 spheres per mg floc, mean, n:3) compared to the 300 µM Fe treatment (7.3 spheres per mg floc, mean, n: 3).

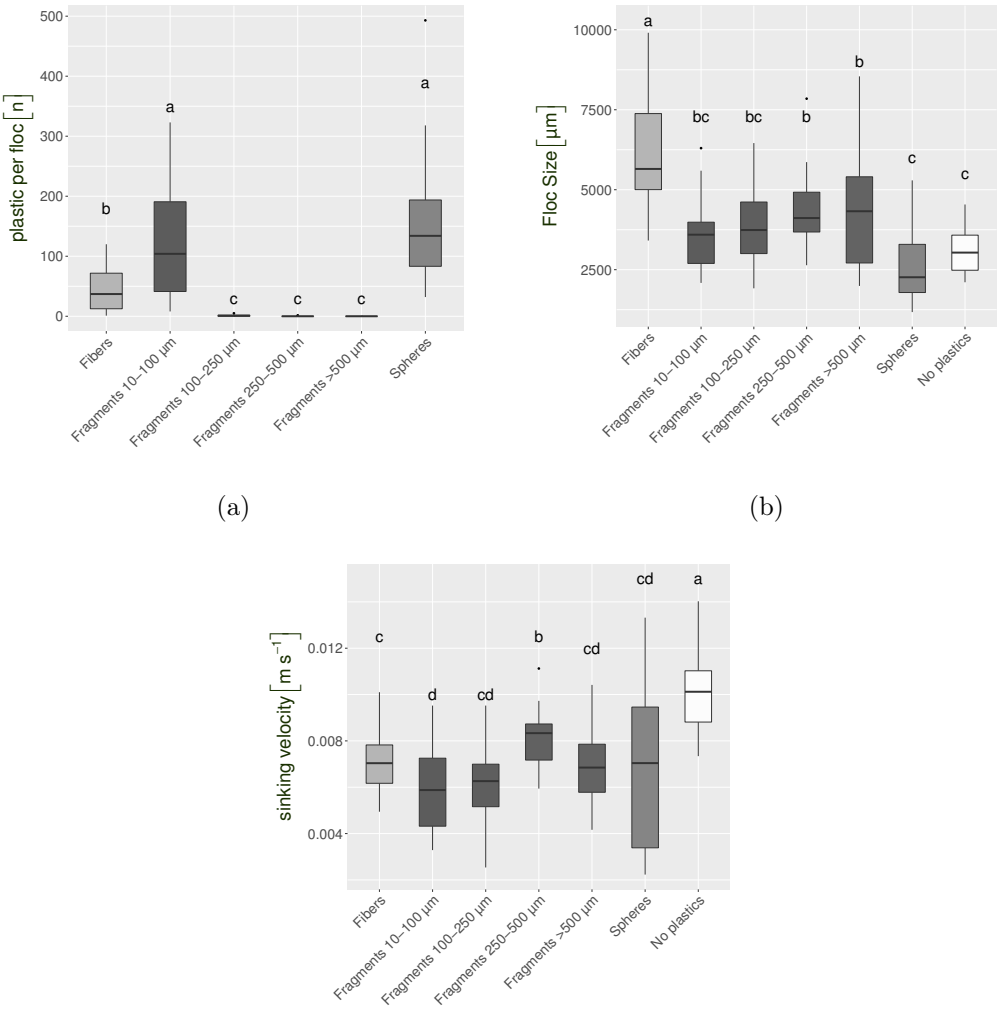

Figure 2: Plastic content, size and sinking velocity of flocs formed by addition of 300 µM Fe to Bautzen water containing different types of MP. Thirty individual flocs of each MP type were characterized. Letters indicate significant differences tested by using ANOVA (floc size, $p < 0.05$) or non-parametric bootstrapping (plastic content and sinking velocity, 95 % CI).

Floc mediated MP transport into sediments

The sediment appeared soft and unconsolidated (Table S4) with grain sizes referring to clay (~3 %), sand (~11 %) and silt (~86 %) (Table S5). The sediment had a homogeneous appearance showing no visible layering. The water content decreased from 92.97 ± 0.36 % (mean ± SD, n: 10) in the top 2 cm to 86.431 ± 0.52 %

(mean ± SD, n: 10), while density increased from 1.079 ± 0.018 g cm^{-3} (mean ± SD, n: 10) to 1.132 ± 0.024 g cm^{-3} (mean ± SD, n: 10) (Table S5) from the top (0 – 2 cm) to bottom layer (8 – 11 cm). To distinguish MP released or retained from small flocs generated at 100 µM Fe from that of large flocs formed at 300 µM Fe, initially buoyant spheres with different fluorescence labels were used (yellow: small flocs, red: large flocs). Experiments were started by adding iron flocs with PE to the overlying water of the sediment cores. Approximately 11775 red spheres inside of 300 µM Fe flocs and 3231 yellow spheres inside of 100 µM Fe flocs were added to each core (Table S3). The flocs settled through the water column and accumulated shortly at the sediment surface (Figure S5). Then they continued sinking through the sediment surface. Flocs were completely buried into the sediments and no longer visible at the surface after 24 h in the anoxic and 6 days in the oxic treatments (Figure S5). The anoxic cores showed extensive gas formation, which resulted in bubble release from the sediment. No obvious gas formation took place in the oxic cores, but bioturbation by burrowing chironomid larvae down to a depth of ~24 cm was observed.

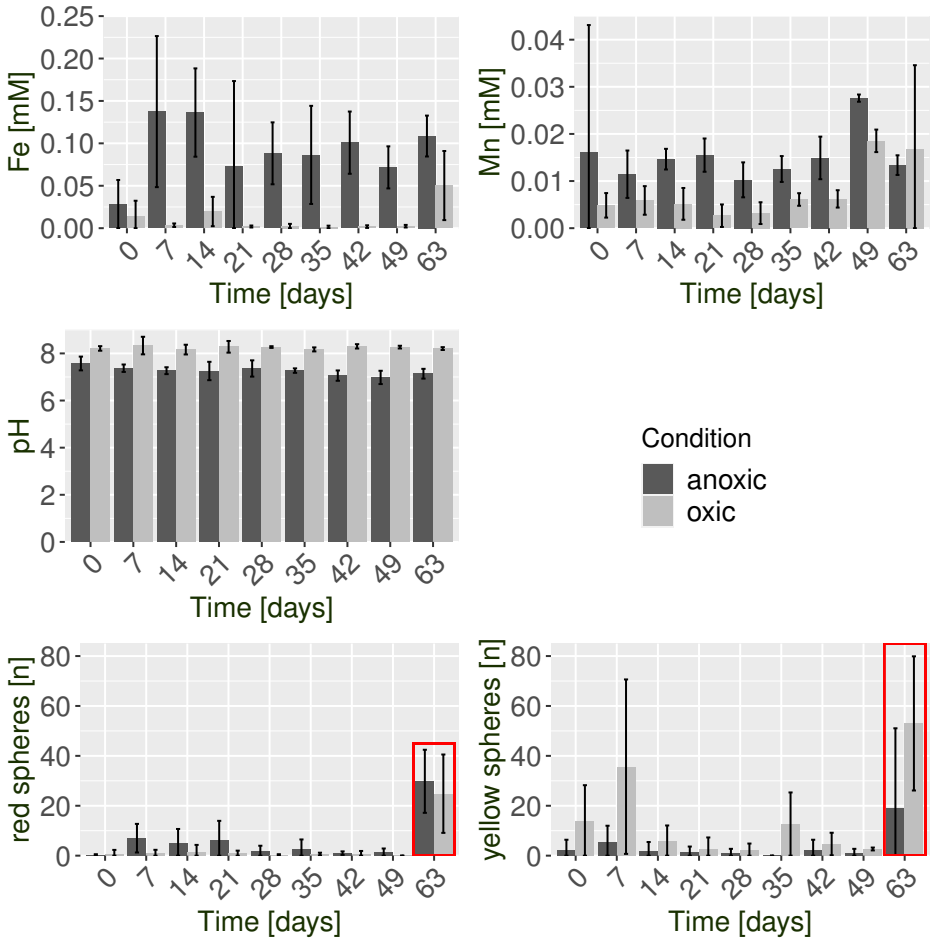

Figure 3: : Bar plots showing the results of weekly water phase samplings. Means and standard deviations are reported with 5 (anoxic) or 6 (oxic) replicates (July and October joined) for Fe and Mn concentrations, pH and release of red spheres from large 300 µM Fe flocs. 3 replicates (October) are reported for the yellow spheres released from small 100 µM Fe flocs. The red framing indicates the last sampling date, where the values for spheres are obtained by sampling the whole water phase above the sediment.

Iron reduction took place in the anoxic cores, while it was less pronounced in the oxic cores (Figure 3). MP release from the sediment was low throughout the whole experiment and not linked (Spearman's rank correlation, red spheres rho: 0.45, yellow spheres rho: -0.28) to the iron release (Figure 3). By the end of the experiment, a total of 63 ± 27 (mean ± SD, n: 5) red spheres initially added within 300 µM Fe flocs and 35 ± 20 (mean ± SD, n: 3) yellow spheres initially added within 100 µM Fe flocs were released from the anoxic cores, while 34 ± 56 (mean ± SD, n:

6) red spheres and 117 ± 42 (mean ± SD, n: 3) yellow spheres were released from the oxic cores. The number of spheres retained within the sediments of the core exceeded the number of spheres released into the water phase by far. In the anoxic cores 3234 ± 487 (mean ± SD, n: 5) red spheres and yellow spheres 298 ± 404 (mean ± SD, n: 3) and in the oxic cores 6108 ± 721 (mean ± SD, n: 6) red spheres and 1641 ± 1063 (mean ± SD, n: 3) yellow spheres were found in the sediments at the end of the experiment (Table S6). Approximately 85 % of the recovered yellow spheres and > 95 % of the red spheres were found within the sediment (Figure 4a). Hence the majority of MP were retained within the sediments (Figure 4a). Significantly more spheres (yellow and red; non-parametric bootstrapping, 95 % confidence) were recovered from the oxic compared to anoxic cores, indicating a sampling bias (Table S6). Most spheres were found within the uppermost 2 cm of the sediments (Figure 4b). However, spheres were also detected in deeper layers. In the anoxic cores low numbers of spheres were present in the 2 – 5 cm layer. Their abundance decreased sharply with depth with only very few spheres recovered from 5 – 8 cm depth and no spheres recovered from the 8 – 11 cm layer of the anoxic cores. In the oxic cores, spheres were found even in the deepest layer of 8 -11 cm depth, indicating a deeper burial compared to the anoxic cores. Comparatively high numbers of spheres were recovered from the 2 -5 cm and 5 -8 cm layer of the oxic cores. Similar patterns were also observed for the cores from July (Figure 4). Chironomid burrows were found throughout all layers of the oxic cores, averaging on 2 - 5 visible burrows per layer.

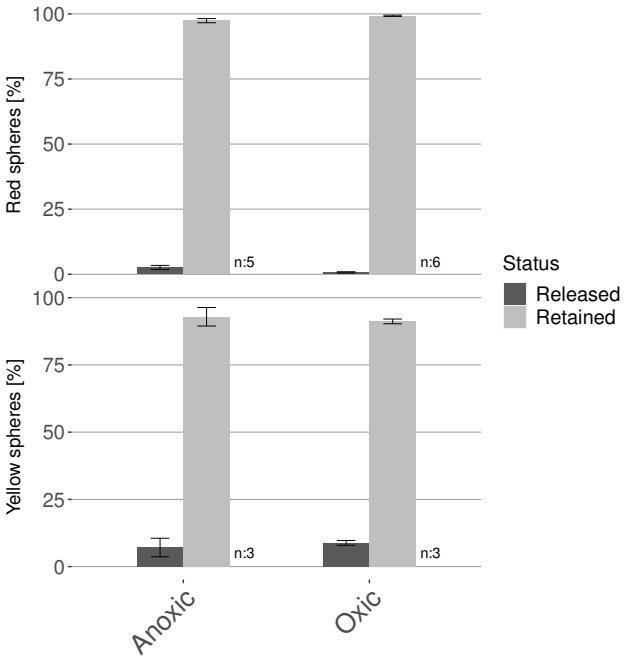

(a)

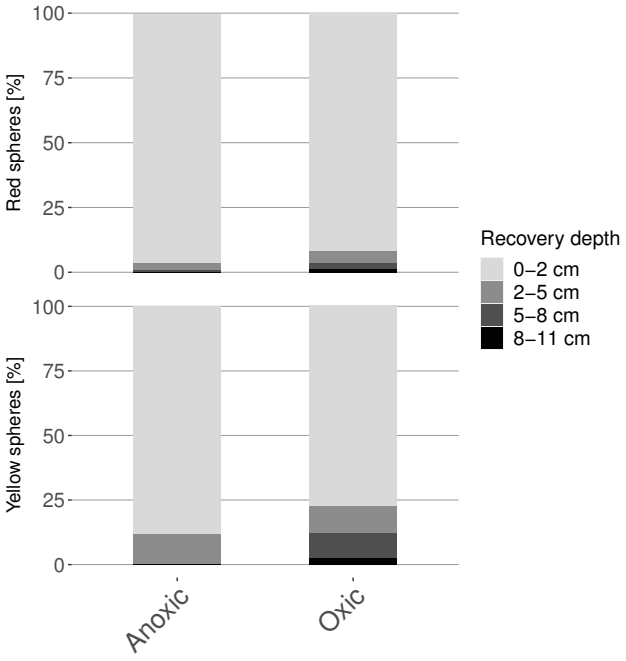

(b)

Figure 4: Recovery of PE spheres from sediment core experiments, with a) ratio of released and retained spheres within the cores (July October) and b) relative depth distribution of spheres (October). Results from the experiments in October and July are combined for the large flocs (red spheres) whereas only results from October are presented for the small flocs (yellow spheres).

Discussion

In this study we presented evidence that PE MP are aggregated into sinking flocs formed by iron precipitates and organic material, irrespective of their shape. These flocs rapidly transported initially buoyant PE micro-spheres deep into freshwater sediments, leading to stable deposition given the long incubation time of 63 days

Iron-mediated aggregation and settling of MP

The addition of ferrous iron sulfate to surface water of Bautzen reservoir induced the formation of sinking flocs. This iron flocculation is a well-known process described in nature (Tipping et al., 1981) or employed in the context of water treatment technologies (Teh et al., 2016). Flocs formed in our study were comparatively large, ranging from approximately 500 to $>$ 3000 µm, whereas iron-organo lake aggregates are typically smaller with sizes from 60 µm (Reiche et al., 2011) to 350 µm (Elliott and Warren, 2014). However, organic and iron contents were comparable to natural flocs (Elliott et al., 2012; Reiche et al., 2011). Iron-floc formation is usually considered being a complex process involving the interaction of different microbial consortia forming complex 3-dimensional structures of EPS (Mori et al., 2017) which enclose biogenic iron mineral grains and bacterial cells (Elliott and Warren, 2014). However, floc formation might also occur rapidly during seasonal lake mixing events without the involvement of complex microbial consortia (Oliver et al., 1985). This mode of formation might be more similar to the technically used iron coagulation processes (Ma et al., 2019) and to the experimental procedure used in the presented study. Even though we attempted to mimic natural conditions by using reservoir water, natural pH and partly natural iron concentrations (Elliott and Warren, 2014), the formed flocs will differ from natural ones. This should be considered when discussing the potential impact of iron flocculation in lakes on the fate of MP.

Further we could show that the iron-organo flocs readily incorporated buoyant MP. The incorporation was depended on the size of the plastics. This is in line with other studies showing an increasing aggregation potential with decreasing MP particle size (Shams et al., 2020), which might be explained by the higher collision frequency of smaller particles (Quik et al., 2014). The overall removal efficiency of 300 µM Fe

was higher for spheres compared to fragments or fibers, which might be explained by differences in size or polymer density. In another study iron concentrations of 370 µM were found to remove up to 90 % of small polystyrene MP from waster-effluents (Rajala et al., 2020), emphasizing the high potential of iron-organo flocs to remove MP.

The iron-organo flocs investigated in our study can be considered as a relevant type of aggregate capable to incorporate and sink buoyant MP in freshwater. Previous studies showed that iron flocs formed during lake mixing could precipitate buoyant cyanobacteria (Oliver et al., 1985) colonies (size: 63 µm) and large PE (Leiser et al., 2020) MP (size: 4 x 4 x 0.15 mm). Although not proven in field experiments, it is likely that comparable aggregates forming in stratified lakes are capable to precipitate buoyant PE MP (Bravidor et al., 2015). This is in line with many studies showing the removal of MP from the water column via aggregation mechanisms (Kvale et al., 2020). The iron-organic flocs are similar to other MP bearing aggregates such marine (Maggi, 2013) or lake snow (Grossart and Simon, 1993), phytoplankton- (Long et al., 2015), EPS-(Möhlenkamp et al., 2018), and TEP-(Michels et al., 2018) based flocs regarding their sizes, sinking velocities and densities. However the fate of aggregated MP once reaching the sediment surface is largely unknown.

Redox-independent burial of MP

Using long-termed sediment core experiments we could show that iron-organic aggregates containing initially buoyant MP rapidly subside into sediments and are not re-mobilized within 63 days. Hence we conclude that the aggregation followed by sedimentation onto muddy sediments might lead to relatively stable deposition of MP in stagnant water bodies.

Contrary to our initial hypothesis, anoxic conditions and iron reduction did not lead to a significant re-mobilization of MP from the sediments. Although more MP was released from anoxic compared to oxic cores, the majority of PE spheres remained in the sediments. This might be explained by the rapid downward transport of the iron flocs from the sediment surface into the sediments, by which MP was most likely trapped within the sediment matrix. Hence unlike iron oxide bound solutes

such as pollutants or nutrients (Mortimer, 1942), MP are not re-mobilized by anoxic conditions.

Sediments from the deepest part of Bautzen reservoir were used for our study. They were fine-grained, organic rich and rather unconsolidated. These are common properties of muddy sediments found in low current zones such as deeper parts of lakes (Håkanson, 1981) and reservoirs (Abraham et al., 1999) or the basin of the Baltic sea (Näkki et al., 2019). Recent studies showed that MP is preferentially deposited in such low flow zones, making muddy sediments a likely depository of these anthropogenic particles (Zobkov et al., 2020). In comparable deep-sea sediments from the Rockall Trough, MP was found in undisturbed layers with an approximate age of $>$ 150 years (Courtene-Jones et al., 2020). This can only be explained by redistribution of MP in the sediments after their deposition. Our results showed that aggregates containing MP can indeed easily penetrate the first cm of sediments. This offers a possible explanation for the unexpected appearance of MP in sediment layers deposited before the industrial production of the detected polymer types.

The penetration of large particles through muddy sediments has been attributed to their gravitational force (Huettel et al., 1996) overcoming the cohesive force of the sediment particles (Wheatcroft, 1992). The cohesiveness and density of sediments increase with depth, which will stop the downward movement of the flocs. It has been reported that large flocs formed by aluminum flocculation will accumulate in a depth of 10 cm in muddy lake sediments (Łopata et al., 2020). However in our study most PE spheres, which can be considered as proxy for the flocs, accumulated within the first 2 cm of the sediment. This is in line with findings indicating that phytoplankton aggregates accumulate and degrade within the upper few cm of lake sediments (Schulz and Conrad, 1995). Still a minor fraction has been transported deeper into the sediment reaching a depth of at least 11 cm. Interestingly the smaller 100 µM Fe flocs reached deeper layers than the larger 300 µM Fe flocs, which is contradictory to the settling model driven by gravitational force. This might be explained by the higher potential of small flocs to migrate through small channels or cavities (Rusch and Huettel, 2000). In conclusion, results from other studies already indicated the subsiding of MP (Courtene-Jones et al., 2020) or of metal-organo flocs (Lewandowski et al., 2003; Łopata et al., 2020) into sediments. We could show that

the rapid transport of buoyant PE into freshwater sediments can be facilitated by low density iron-rich organic aggregates. As the fate of aggregates strongly depends on the properties of the underlying sediment, generality of our results is limited. Still, our findings should be applicable to most reservoirs and lakes because the type of sediment we investigated is typical for them. More studies are needed to determine the response of other sediment types.

Apparently PE spheres were transported deeper into the sediments of oxic cores compared to anoxic cores. This might be caused by the presence of chironomid larvae in the oxic cores building long burrows (Figure S6). It has been previously reported that bioturbation by invertebrates will transport MP in fine-grained muddy sediments rather down-, than upwards (Näkki et al., 2017; Näkki et al., 2019). Therefore the burrowing and biodiffusive (Baranov et al., 2016) activity of the chironomids might explain the deeper distribution of spheres in the oxic cores. Our experimental set-up excluded bioturbation by larger animals such as macroinvertebrates and benthivorous fish which exert complex and diverse modes of re-mobilization (Adámek and Maršálek, 2013). Based on our results the possible effect of bioturbation on MP distribution in Bautzen reservoir cannot be evaluated completely.

Different limitations of the sediment core experiments need to be mentioned. Firstly, lower numbers of spheres were recovered from the anoxic compared to the oxic cores. This is particularly striking for the yellow spheres bound to 100 µM Fe flocs. It cannot be ruled out that the spheres or flocs were transported even deeper than the 11 cm layer used as lowest boundary. Extensive gas bubbles formed within the anoxic cores, which produced large voids in the deeper layers of the sediment. PE spheres might have fallen through these voids which brought them deeper into the cores than the sampled 11 cm layer. Considering that the missing spheres were not liberated from the sediments, but rather incorporated deeper than expected, this does not affect most of our statements. However, the assumption that spheres were transported deeper into the sediments of the oxic cores compared to the anoxic might not be justified.

Freshwater systems could play a substantial role for the retention of MP transported from land to sea, as indicated by the presented results. Once initially buoyant MP

is incorporated into sinking aggregates and reaches the sediment, they will rapidly be deposited inside the sediment matrix. Excluding other processes such as current driven sediment re-suspension or bioturbation by larger organisms, this deposition might be stable even for longer time periods. Deposition of MP during summer stratification could lead to permanent deposition, as no bioturbation takes place under anoxia, while several mm of sediments are settling over the MP during this time. Comparable conditions have been described leading to excellent fossilization of organic tissue or carcasses in stratified lakes(Franzen, 1985), for which undisturbed deposition over geological time-scale is required. This indicates that permanent and undisturbed deposition of MP in freshwater sediments might be possible under certain conditions. The stability of this deposition or possible mechanisms leading to MP release needs to be investigated in further studies. This could contribute to a better understanding of MP fate in freshwaters.Freshwater systems might play a bigger role in the permanent deposition of MP into sediments and prevent transport to the oceans, which are having a lower capacity to immobilize MPs given their low Fe concentration.

Material and methods

Study site and sampling

Study site and sampling Bautzen reservoir, located in the eastern part of Germany, is a rather large (5.3 km^2) and moderately deep (mean depth 7.4 m) water body (Kasprzak et al., 2007). It shows a labile summer stratification (June-September), with an anoxic hypolimnion frequently disrupted by strong winds(Kerimoglu and Rinke, 2013). Sediment cores and surface water samples were taken at the deepest point (~11 m) of the reservoir. Sediment cores were retrieved on 30^{th} of July and 19^{th} of October 2020 using a gravity corer (UWITEC, Austria and PVC liners of 60 x 9 cm). Hence two replicate experiments with sediment cores obtained during different seasons were conducted. Profiles of chlorophyll a, pH, oxygen concentration and temperature (Figure S1) were recorded using a multiparameter probe (Sea Sun Technologies, Germany). Additional water chemistry data was provided by the state

reservoir administration of Saxony / Landestalsperrenverwaltung des Freistaates Sachsen (LTV).

MP specification and preparation

We used PE spheres (d: 118 ± 6 µm, ρ: 0.98 g cm^{-3}) spiked with fluorescent red Rhodamine B (RHBPMS-0.98 106-125 µm) or yellow stain (UVBGPMS-0.98 106-125 µm) from Cospheric, USA. PE fragments (ρ: 0.92 g cm^{-3}, Alfa Aesar 9002-88-4) were passed through a sieving cascade of 500 µm, 250 µm, 100 µm and 10 µm stainless steel sieves (Retsch, Germany), to obtain four defined size ranges of fragments: >500 µm ((ESD)(Kaiser et al., 2019): 727 ± 118 µm, n: 30), 500 - 250 µm (ESD: 466 ± 90 µm, n: 30), 250 - 100 µm (ESD: 234 ± 55 µm, n: 30) and 100 – 10 µm (ESD: 86 ± 26 µm, n: 30). The fragments were stained with fluorescent iDyePolyPink following established methods (Karakolis et al., 2019). PE fibers (4600 x 24 µm, ρ: 0.92 g cm^{-3}) were kindly provided by Baumhueter extrusion GmbH, Germany (PB Eurofiber F-2106).

Floc formation and investigation of MP aggregation potential

Whether the formation of iron-rich lake snow ("iron flocs") might aggregate and sink buoyant MP was tested by mixing surface water from Bautzen reservoir (Table S1) with MP and varying concentrations of $Fe(II)SO_4$. Bautzen water was stored at 20° C in the dark and used for experiments within 2 weeks after sampling. Prior to use, the water was filtered through 10 µm stainless steel sieves and the filtrate was adjusted to pH 9.5 by adding small quantities of NaOH (1 M). This high pH was chosen to reflect the alkaline conditions of the surface water during the time of summer stratification (Figure S1). Experiments were conducted in triplicates per MP type by amending 500 ml filtrate with 300 µl (final concentration: 300 µM) or 100 µl (final concentration: 100 µM) $FeSO_4$ x 7 H_2O stock-solution (500 mM, pH 1.8) inside of airtight 1-liter bottles. Thereafter 10 mg l^{-1} of MP fibres (9.0 x 10^3 particles l^{-1}), spheres (2.4 x 10^4 particles l^{-1}) or fragments (either fragments 10 – 100 µm: 6.6 x 10^4 particles l^{-1}, fragments 100 -250 µm: 3.2 x 10^3 particles l^{-1}, fragments 250 – 500 µm: 2.2 x 10^2 particles l^{-1} or fragments > 500: 1.1 x 10^3 particles l^{-1}) were added

separately to the respective bottles. Additionally, triplicates without added MP were used as control. The bottles were incubated on tumbling roller incubators (3-4 rpm, 20° C, RM5, M. Zipperer GmbH, Germany) in ambient daylight for 24 h. Sinking velocity, size and plastic content of 10 individual flocs out of each bottle (triplicates per plastic type, n: 30) formed by 300 µM Fe were recorded following established methods Leiser et al., 2021. Total amount of precipitated MP was quantified by repeating the bottle incubations, but recovering all flocs formed within the respective bottles. The flocs were gently washed with tap water, centrifuged (3000 rpm), weighted and extracted through incubation (1 h, room temperature) with 10 ml HCl (1 M) followed by vigorous shaking (1 min) on a vortex mixer. The resulting solution was filtered onto stainless-steel filters and examined for their total plastic content employing a light microscope. Sinking velocity of flocs formed by 100 µM Fe could not be assessed due to their small size. Therefore solely total plastic content and average floc size (n: 30) were recorded.

Floc characterization

The properties of iron flocs produced by 100 µM and 300 µM Fe without additional MP were further characterized by different methods. Density of 6 individual flocs was determined by titrating with NaCl solution (20 % m/v) until neutral buoyancy, followed by pycnometer measurement of the resulting solution at 20° C (Leiser et al., 2021). Water content, dry mass, loss on ignition and total mass of flocs were measured by centrifuging (3000 rpm, 20 min) all flocs formed within bottles (n: 6) in pre-weighted conical centrifuge tubes. Subsequently the flocs were transferred into aluminum weighing pans and mass was weighted in wet state, after drying (60° C, 24 h) and after burning (550° C, 24 h). Fe content of the flocs' wet mass was determined by dissolving defined, centrifuged (3000 rpm, 20 min) fractions (n: 6) in hydroxylamine hydrochloride-HCl (0.5 / 1 M) followed by measurement via ferrozine assay (Stookey, 1970). Confocal laser scanning microscopy (CLSM) was used to examine 5 randomly chosen spots each on 10 individual flocs produced with 300 µM Fe. The biovolumes of algae, bacteria, cyanobacteria and EPS were calculated from the resulting CLSM imaging data-sets (n: 50).

Experimental set-up of sediment incubation experiment

Whether MP can be released from iron-organo flocs laying on-top of natural freshwater sediments was tested with sediment cores from Bautzen reservoir. Cores were grouped into two different treatments (oxic and anoxic condition) with 3 replicates each. The anoxic triplicates were bubbled with N2 until depletion of O2 as measured via an internal oxygen optode (Pyroscience, Germany). Afterwards the anoxic cores were closed with custom-made covers preventing intrusion of oxygen and allowing anoxic sampling (Dadi et al., 2017). The oxic triplicates were closed with the same covers and bubbled constantly by air to maintain oxic conditions. The O_2 levels in the cores was permanently recorded and adjusted on daily basis by N_2 or O_2 bubbling if necessary. Flocs formed by 300 µM Fe and containing red-fluorescent Rhodamine B PE spheres were produced as already described. In addition, for the experiment conducted in October, flocs formed by 100 µM Fe aggregating yellow-fluorescent PE spheres were prepared. The flocs were gently washed with tap water (three times) to remove non-aggregated MP spheres. Subsequently, they were carefully added to the cores, allowing them to settle to the sediment surface. The October cores were first supplemented with flocs from 300 µm Fe solutions (red spheres) and afterwards with flocs from 100 µm Fe solutions (yellow spheres). The overlying water was exchanged by bottom to top through-flow of approximately 2 L of Bautzen surface water to remove spheres released by physical breakage of the flocs. Cores were photographed in 24 h intervals in the first week after floc application and in weekly intervals thereafter.

Sampling procedure of sediment incubation experiment

Water samples for Fe(II), Mn, pH and released MP were taken in weekly intervals using syringes. Fe(II) was measured using ferrozine assay (Stookey, 1970), while Mn was measured using formaldoxime method (Burlage et al., 1998). The plastics were sampled by removing 120 ml (corresponding to 2 cm) of the uppermost part of the water-column using a syringe. Sampled water was not replaced. The water was filtered over stainless steel filters (10 µm) and retained spheres were counted under a light microscope. The experiments were run for 63 days at 16° C in the dark, after

which the whole water phase of sediment cores was removed and examined for their plastic content. Afterwards the cores were sliced into sections of 0-2 cm, 2-5 cm, 5-8 cm and 8-11 cm using a sediment core cutter (Uwitec, Austria). The sections were transferred into centrifugation tubes and extracted by sonication followed by addition of NaCl (20 %, ρ: 1.56 g cm^{-3}) for density separation. The resulting suspension was centrifuged (3000 rpm, 15 min) and frozen by the addition of dry ice. The top layer of the frozen solution was transferred into conical centrifuge tubes by flushing with water and filtered onto stainless steel grids. The MP contents of the layers were counted under the light microscope. The recovery rate was assessed by the addition of 1.2 x 10^4 fluorescent PE spheres to sediments sections (0-2 cm, 2-5 cm, 5-8 cm, 8-11 cm) of a control core, followed by the already described extraction method. 1.06 x 10^4 $\pm$ 3100 particles (mean $\pm$ sd, n: 4) were recovered from the sediments leading to recovery rate of 89.51 $\pm$ 2.61 % (mean $\pm$ sd) for this method (data not shown). One anoxic core of the July experiment was lost due to inappropriate handling, resulting in lower sample numbers for the anoxic treatments. The bulk density, porosity, water content, dry mass, organic content and grain size distributions of two control cores were determined by standard methods(Dadi et al., 2017). Furthermore the Fe(II) / Fe(III) and Mn contents of the sediments were determined after extraction with HCl (1 M) and hydroxylamine hydrochloride – HCl (0.5 / 1 M) using ferrozine or formaldoxime assay, respectively.

CLSM imaging

Flocs were visualized using CLSM in combination with different fluorescent dyes as described elsewhere (Leiser et al., 2021). In brief, flocs were mounted in microscope chamber slides (Thermo Fisher Scientific) and stained with Aleuria aurantia lectin (AAL)(Neu et al., 2001) and SybrGreen (Neu et al., 2002). Imaging was done by a TCS SP5X upright microscope equipped with white laser and water-immersible lens () . Aleuria aurantia lectin (Vector Laboratories, USA) labeled with Alexa Fluor 633 (Thermo Fisher Scientific, USA) was used to visualize the extracellular polymeric substances (EPS) of the flocs (Neu et al., 2001). Bacteria were identified via SybrGreen staining, while algae and cyanobacteria were identified by the aut-

ofluorescence of their chlorophyll a or phycobilins, respectively. The different filter configurations used for excitation and emission are listed in Table S2. Imaris (Bitplane) was used to visualize the images, which were printed by Photoshop (Adobe). The biovolumes of algae, bacteria, cyanobacteria and EPS were semi-quantitatively calculated employing an adaption of ImageJ (Staudt et al., 2004).

Statistical analysis

Statistical testing was only conducted for datasets with a minimum sample size of 5 individual replicates. Q-Q plots were used to check for data normality. Bartlett's test was used to test variance homogeneity prior to two-sided ANOVA (Type II) which was used to compare group means. Residual plots were examined to verify the reliability of the ANOVA. Group means were assumed to be significantly different from each other for $p < 0.05$. Samples not meeting assumptions of the ANOVA were tested by non-parametric two-sided bootstrapping (Efron and Tibshirani, 1986). The 95 % confidence intervals (CI) of median differences of 10000 bootstrapped samples were reported. Differences in median CI higher or lower than zero were defined as significantly different from each other by 95 % chance. Spearman's rank correlation was used to calculate correlation coefficients. The statistical method used is noted in the respective result section. Software R (R Core Team, 2018) was used for all statistical analysis and data visualizations.

References for Chapter 4

Abraham, J., Allen, P. M., Dunbar, J. A., & Dworkin, S. I. (1999). Sediment type distribution in reservoirs: Sediment source versus morphometry. *Environmental Geology*, *38*(2), 101–110. https://doi.org/10.1007/s002540050406

Adámek, Z., & Maršálek, B. (2013). Bioturbation of sediments by benthic macroinvertebrates and fish and its implication for pond ecosystems: a review. *Aquaculture International*, *21*(1), 1–17. https://doi.org/doi:10.1007/s10499-012-9527-3

Baranov, V., Lewandowski, J., Romeijn, P., Singer, G., & Krause, S. (2016). Effects of bioirrigation of non-biting midges (Diptera: Chironomidae) on lake sediment respiration. *Scientific Reports*, *6*, 1–10. https://doi.org/10.1038/srep27329

Bravidor, J., Kreling, J., Lorke, A., & Koschorreck, M. (2015). Effect of fluctuating oxygen concentration on iron oxidation at the pelagic ferrocline of a meromictic lake. *Environmental Chemistry*, *12*(6), 723–730. https://doi.org/10.1071/EN14215

Burlage, R., Atlas, R., & Stahl, D. (1998). *Techniques in Microbial Ecology* (1st ed.). Oxford University Press on Demand. https://doi.org/10.1016/s0580-9517(08)x7011-4

Chubarenko, I., Bagaev, A., Zobkov, M., & Esiukova, E. (2016). On some physical and dynamical properties of microplastic particles in marine environment. *Marine Pollution Bulletin*, *108*(1-2), 105–112. https://doi.org/10.1016/j.marpolbul.2016.04.048

Cornell, R., & Schwertmann, U. (2003). *The iron oxides: structure, properties, reaction, occurrences and uses* (1st ed.). John Wiley & Sons. https://doi.org/10.1002/3527602097

Courtene-Jones, W., Quinn, B., Ewins, C., Gary, S. F., & Narayanaswamy, B. E. (2020). Microplastic accumulation in deep-sea sediments from the Rockall

Trough. *Marine Pollution Bulletin*, *154*, 111092. https://doi.org/10.1016/j.marpolbul.2020.111092

Dadi, T., Harir, M., Hertkorn, N., Koschorreck, M., Schmitt-Kopplin, P., & Herzsprung, P. (2017). Redox Conditions Affect Dissolved Organic Carbon Quality in Stratified Freshwaters. *Environmental Science and Technology*, *51*(23), 13705–13713. https://doi.org/10.1021/acs.est.7b04194

Deppe, T., & Benndorf, J. (2002). Phosphorus reduction in a shallow hypereutrophic reservoir by in-lake dosage of ferrous iron. *Water Research*, *36*(18), 4525–4534. https://doi.org/10.1016/S0043-1354(02)00193-8

Di, M., & Wang, J. (2018). Microplastics in surface waters and sediments of the Three Gorges Reservoir, China. *Science of the Total Environment*, *616-617*, 1620–1627. https://doi.org/10.1016/j.scitotenv.2017.10.150

Díez, S., Noonan, G. O., MacFarlane, J. K., & Gschwend, P. M. (2007). Ferrous iron oxidation rates in the pycnocline of a permanently stratified lake. *Chemosphere*, *66*(8), 1561–1570. https://doi.org/10.1016/j.chemosphere.2006.08.017

Efron, B, & Tibshirani, R. (1986). Bootstrap Methods for Standard Errors. *Statistical Science*, *1*(1), 54–75. http://www.jstor.org/stable/2245500

Elliott, A. V., Plach, J. M., Droppo, I. G., & Warren, L. A. (2012). Comparative floc-bed sediment trace element partitioning across variably contaminated aquatic ecosystems. *Environmental Science and Technology*, *46*(1), 209–216. https://doi.org/10.1021/es202221u

Elliott, A. V., & Warren, L. A. (2014). Microbial engineering of floc Fe and trace element geochemistry in a circumneutral, remote lake. *Environmental Science and Technology*, *48*(12), 6578–6587. https://doi.org/10.1021/es403754t

Enders, K., Käppler, A., Biniasch, O., Feldens, P., Stollberg, N., Lange, X., Fischer, D., Eichhorn, K. J., Pollehne, F., Oberbeckmann, S., & Labrenz, M. (2019). Tracing microplastics in aquatic environments based on sediment analogies. *Scientific Reports*, *9*(1), 1–15. https://doi.org/10.1038/s41598-019-50508-2

Franzen, J. L. (1985). Exceptional preservation of Eocene vertebrates in the lake deposit of Grube Messel (West Germany). *Extraordinary fossil biotas: their*

ecological and evolutionary significance, *186*, 181–186. https://doi.org/10.1098/rstb.1985.0150

Grossart, H. P., & Simon, M. (1993). Limnetic macroscopic organic aggregates (lake snow): Occurrence, characteristics, and microbial dynamics in Lake Constance. *Limnology and Oceanography*, *38*(3), 532–546. https://doi.org/10.4319/lo.1993.38.3.0532

Grossart, H. P., Simon, M., & Logan, B. E. (1997). Formation of macroscopic organic aggregates (lake snow) in a large lake: The significance of transparent exopolymer particles, phytoplankton, and zooplankton. *Limnology and Oceanography*, *42*(8), 1651–1659. https://doi.org/10.4319/lo.1997.42.8.1651

Håkanson, L. (1981). Determination of Characteristic Values for Physical and Chemical Lake Sediment Parameters. *Water Resources Research*, *17*(6), 1625–1640.

Huettel, A., Ziebis, W, & Forster, S. (1996). Flow-induced uptake of particulate matter in permeable sediments. *Limnology and Oceanography*, (2), 309–322.

Kaiser, D., Estelmann, A., Kowalski, N., Glockzin, M., & Waniek, J. J. (2019). Sinking velocity of sub-millimeter microplastic. *Marine Pollution Bulletin*, *139*, 214–220. https://doi.org/10.1016/j.marpolbul.2018.12.035

Kaiser, D., Kowalski, N., & Waniek, J. J. (2017). Effects of biofouling on the sinking behavior of microplastics. *Environmental Research Letters*, *12*(12). https://doi.org/10.1088/1748-9326/aa8e8b

Kasprzak, P., Benndorf, J., Gonsiorczyk, T., Koschel, R., Krienitz, L., Mehner, T., Hülsmann, S., Schultz, H., & Wagner, A. (2007). Reduction of nutrient loading and biomanipulation as tools in water quality management: Long-term observations on Bautzen Reservoir and Feldberger Haussee (Germany). *Lake and Reservoir Management*, *23*(4), 410–427. https://doi.org/10.1080/07438140709354027

Kerimoglu, O., & Rinke, K. (2013). Stratification dynamics in a shallow reservoir under different hydro-meteorological scenarios and operational strategies. *Water Resources Research*, *49*(11), 7518–7527. https://doi.org/10.1002/2013WR013520

Kvale, K., Prowe, A. E., Chien, C. T., Landolfi, A., & Oschlies, A. (2020). The global biological microplastic particle sink. *Scientific Reports*, *10*(1), 1–12. https://doi.org/10.1038/s41598-020-72898-4

Lagarde, F., Olivier, O., Zanella, M., Daniel, P., Hiard, S., & Caruso, A. (2016). Microplastic interactions with freshwater microalgae: Hetero-aggregation and changes in plastic density appear strongly dependent on polymer type. *Environmental Pollution*, *215*, 331–339. https://doi.org/10.1016/j.envpol.2016.05.006

Leiser, R., Jongsma, R., Bakenhus, I., Möckel, R., Philipp, B., Neu, T. R., & Wendt-Potthoff, K. (2021). Interaction of cyanobacteria with calcium facilitates the sedimentation of microplastics in a eutrophic reservoir. *Water Research*, *189*, 116582. https://doi.org/10.1016/j.watres.2020.116582

Leiser, R., Wu, G.-M., Neu, T. R., & Wendt-Potthoff, K. (2020). Biofouling, metal sorption and aggregation are related to sinking of microplastics in a stratified reservoir. *Water Research*, 115748. https://doi.org/10.1016/J.WATRES.2020.115748

Lewandowski, J., Schauser, I., & Hupfer, M. (2003). Long term effects of phosphorus precipitations with alum in hypereutrophic Lake Süsser See (Germany). *Water Research*, *37*(13), 3194–3204. https://doi.org/10.1016/S0043-1354(03)00137-4

Long, M., Moriceau, B., Gallinari, M., Lambert, C., Huvet, A., Raffray, J., & Soudant, P. (2015). Interactions between microplastics and phytoplankton aggregates: Impact on their respective fates. *Marine Chemistry*, *175*, 39–46. https://doi.org/10.1016/j.marchem.2015.04.003

Long, M., Paul-Pont, I., Hégaret, H., Moriceau, B., Lambert, C., Huvet, A., & Soudant, P. (2017). Interactions between polystyrene microplastics and marine phytoplankton lead to species-specific hetero-aggregation. *Environmental Pollution*, *228*, 454–463. https://doi.org/10.1016/j.envpol.2017.05.047

Łopata, M., Augustyniak, R., Grochowska, J., Parszuto, K., Tandyrak, R., & Wiśniewski, G. (2020). Behavior of Aluminum Compounds in Soft-Water Lakes Subjected to Experimental Reclamation with Polyaluminum Chloride.

Water, Air, and Soil Pollution, *231*(7). https://doi.org/10.1007/s11270-020-04708-6

Ma, B., Xue, W., Hu, C., Liu, H., Qu, J., & Li, L. (2019). Characteristics of microplastic removal via coagulation and ultrafiltration during drinking water treatment. *Chemical Engineering Journal*, *359*, 159–167. https://doi.org/10.1016/j.cej.2018.11.155

Maggi, F. (2013). The settling velocity of mineral , biomineral , and biological particles and aggregates in water. *Journal of Geophysical Research: Oceans*, *118*(January), 2118–2132. https://doi.org/10.1002/jgrc.20086

Merga, L. B., Redondo-Hasselerharm, P. E., Van den Brink, P. J., & Koelmans, A. A. (2020). Distribution of microplastic and small macroplastic particles across four fish species and sediment in an African lake. *Science of the Total Environment*, *741*, 140527. https://doi.org/10.1016/j.scitotenv.2020.140527

Michels, J., Stippkugel, A., Lenz, M., Wirtz, K., & Engel, A. (2018). Rapid aggregation of biofilm-covered microplastics with marine biogenic particles. *Proceedings. Biological sciences*, *285*(1885), 20181203. https://doi.org/10.1098/rspb.2018.1203

Möhlenkamp, P., Purser, A., & Thomsen, L. (2018). Plastic microbeads from cosmetic products: An experimental study of their hydrodynamic behaviour, vertical transport and resuspension in phytoplankton and sediment aggregates. *Elementa*, *6*. https://doi.org/10.1525/elementa.317

Mori, J. F., Ueberschaar, N., Lu, S., Cooper, R. E., Pohnert, G., & Küsel, K. (2017). Sticking together: Inter-species aggregation of bacteria isolated from iron snow is controlled by chemical signaling. *ISME Journal*, *11*(5), 1075–1086. https://doi.org/10.1038/ismej.2016.186

Mortimer, C. H. (1942). The exchange of dissolved substances between mud and water in lakes. *Journal of Ecology*, *30*(1), 147–201.

Näkki, P., Setälä, O., & Lehtiniemi, M. (2017). Bioturbation transports secondary microplastics to deeper layers in soft marine sediments of the northern Baltic Sea. *Marine Pollution Bulletin*, *119*(1), 255–261. https://doi.org/10.1016/j.marpolbul.2017.03.065

Näkki, P., Setälä, O., & Lehtiniemi, M. (2019). Seafloor sediments as microplastic sinks in the northern Baltic Sea – Negligible upward transport of buried microplastics by bioturbation. *Environmental Pollution*, *249*, 74–81. https://doi.org/10.1016/j.envpol.2019.02.099

Neu, T. R., Swerhone, G. D., & Lawrence, J. R. (2001). Assessment of lectin-binding analysis for in situ detection of glycoconjugates in biofilm systems. *Microbiology*, *147*(2), 299–313. https://doi.org/10.1099/00221287-147-2-299

Neu, T. R., Kuhlicke, U., & Lawrence, J. R. (2002). Assessment of fluorochromes for two-photon laser scanning microscopy of biofilms. *Applied and Environmental Microbiology*, *68*(2), 901–909. https://doi.org/10.1128/AEM.68.2.901-909.2002

Oliver, R., Thomas, R., Reynold, C., & Walsby, A. (1985). The sedimentation of buoyant microcystis colonies caused by precipitation with an iron- containing colloid. *Proceedings of the Royal Society B*, *223*(1233), 511–528. https://doi.org/10.1098/rspb.1985.0016

Pizarro, J, Belzile, N, Filella, M, Leppard, G. G., Negre, J. C., Perret, D, & Buffle, J. (1995). Coagulation Sedimentation of Submicron Iron Particles in a Eutrophic Lake. *Water Research*, *29*(2), 617–632. https://doi.org/10.1016/0043-1354(94)00167-6

Plach, J. M., Elliott, A. V., Droppo, I. G., & Warren, L. A. (2011). Physical and ecological controls on freshwater floc trace metal dynamics. *Environmental Science and Technology*, *45*(6), 2157–2164. https://doi.org/10.1021/es1031745

Quik, J. T., van De Meent, D., & Koelmans, A. A. (2014). Simplifying modeling of nanoparticle aggregation-sedimentation behavior in environmental systems: A theoretical analysis. *Water Research*, *62*, 193–201. https://doi.org/10.1016/j.watres.2014.05.048

R Core Team. (2018). *R: A language and environment for statistical computing*. R Foundation for Statistical Computing, Vienna, Austria. https://www.r-project.org/

Rajala, K., Grönfors, O., Hesampour, M., & Mikola, A. (2020). Removal of microplastics from secondary wastewater treatment plant effluent by coagula-

tion/flocculation with iron, aluminum and polyamine-based chemicals. *Water Research*, 116045. https://doi.org/10.1016/j.watres.2020.116045

Reiche, M., Lu, S., Ciobotă, V., Neu, T. R., Nietzsche, S., Rösch, P., Popp, J., & Küsel, K. (2011). Pelagic boundary conditions affect the biological formation of iron-rich particles (iron snow) and their microbial communities. *Limnology and Oceanography*, *56*(4), 1386–1398. https://doi.org/10.4319/lo.2011.56.4.1386

Rusch, A., & Huettel, M. (2000). Advective particle transport into permeable sediments - Evidence from experiments in an intertidal sandflat. *Limnology and Oceanography*, *45*(3), 525–533. https://doi.org/10.4319/lo.2000.45.3.0525

Schulz, S., & Conrad, R. (1995). Effect of algal deposition on acetate and methane concentrations in the profundal sediment of a deep lake (Lake Constance). *FEMS Microbiology Ecology*, *16*(4), 251–260. https://doi.org/https://doi.org/10.1111/j.1574-6941.1995.tb00289.x

Shams, M., Alam, I., & Chowdhury, I. (2020). Aggregation and Stability of Nanoscale Plastics in Aquatic Environment. *Water Research*, 115401. https://doi.org/10.1016/j.watres.2019.115401

Staudt, C, Horn, H, Hempel, D. C., & Neu, T. R. (2004). Volumetric measurements of bacterial cells and extracellular polymeric substance glycoconjugates in biofilms. *Biotechnology and Bioengineering*, *88*(5), 585–592. https://doi.org/10.1002/bit.20241

Stookey, L. L. (1970). Ferrozine-a new spectrophotometric reagent for iron. *Analytical Chemistry*, *42*(7), 779–781. https://doi.org/10.1021/ac60289a016

Teh, C. Y., Budiman, P. M., Shak, K. P. Y., & Wu, T. Y. (2016). Recent Advancement of Coagulation-Flocculation and Its Application in Wastewater Treatment. *Industrial and Engineering Chemistry Research*, *55*(16), 4363–4389. https://doi.org/10.1021/acs.iecr.5b04703

Tipping, E., Woof, C., & Cooke, D. (1981). Iron oxide from a seasonally anoxic lake. *Geochimica et Cosmochimica Acta*, *45*(9), 1411–1419. https://doi.org/10.1016/0016-7037(81)90275-1

Turner, S., Horton, A. A., Rose, N. L., & Hall, C. (2019). A temporal sediment record of microplastics in an urban lake, London, UK. *Journal of Paleolimnology*, *61*(4), 449–462. https://doi.org/10.1007/s10933-019-00071-7

Venkateswaran, K., Moser, D. P., Dollhopf, M. E., Lies, D. P., Saffarini, D. A., MacGregor, B. J., Ringelberg, D. B., White, D. C., Nishijima, M., Sano, H., Burghardt, J., Stackebrandt, E., & Nealson, K. H. (1999). Polyphasic taxonomy of the genus *Shewanella* and description of *Shewanella oneidensis* sp. nov. *International Journal of Systematic Bacteriology*, *49*(2), 705–724. https://doi.org/10.1099/00207713-49-2-705

Watkins, L., McGrattan, S., Sullivan, P. J., & Walter, M. T. (2019). The effect of dams on river transport of microplastic pollution. *Science of the Total Environment*, *664*, 834–840. https://doi.org/10.1016/j.scitotenv.2019.02.028

Wendt-Potthoff, K., Kloß, C., Schultze, M., & Koschorreck, M. (2014). Anaerobic metabolism of two hydro-morphological similar pre-dams under contrasting nutrient loading (Rappbode Reservoir System, Germany). *International Review of Hydrobiology*, *99*(5), 350–362. https://doi.org/10.1002/iroh.201301673

Wheatcroft, R. A. (1992). Experimental tests for particle size-dependent bioturbation in the deep ocean. *Limnology and Oceanography*, *37*(1), 90–104. https://doi.org/10.4319/lo.1992.37.1.0090

Zobkov, M., Belkina, N., Kovalevski, V., Zobkova, M., Efremova, T., & Galakhina, N. (2020). Microplastic abundance and accumulation behavior in Lake Onego sediments: a journey from the river mouth to pelagic waters of the large boreal lake. *Journal of Environmental Chemical Engineering*, *8*(5), 104367. https://doi.org/10.1016/j.jece.2020.104367

Chapter 5

Manuscript 4

Iron reduction by Shewanella oneidensis does not release microplastics from organo-metallic aggregates

submitted to Limnology and Oceanography Letters on June 11th 2021

Rico Leiser and Katrin Wendt-Potthoff

Abstract

Iron flocculants play a major role in the remediation of water bodies, effectively removing dissolved and particulate pollutants such as microplastics from the water phase through floc formation, followed by gravitational settling. Such flocs are prone to microbial iron reduction while lying on top of anoxic sediments, which possibly leads to floc disintegration and the release of matrix bound microplastics. In this study Shewanella oneidensis was employed to simulate the impact of microbial iron reduction on the release of initially buoyant polyethylene spheres (diameter: 118 m) from sunken iron-organo flocs in long-term (120 days) batch experiments. The flocs iron (oxyhydr)oxides were transformed into sulfides, with most iron (70 – 90 %) being reduced by the end of the experiment. This did not affect the integrity of the flocs, as the organic matrix was not notably degraded or mineralized over time. Only a negligible proportion (0.2 – 2.7 %) of polyethylene spheres was released and subsequently regained buoyancy, while the majority remained bound inside the floc matrix. This study exemplifies that iron-organo flocs are quite stable even when experiencing microbial iron reduction under anoxic conditions. Thereby incorporation into such aggregates may display a potential mode of long term MP storage in freshwater sediments.

Introduction

Iron-based flocculants naturally occurring in freshwaters (Oliver et al., 1985) or employed in water treatment (Deppe and Benndorf, 2002) are known to effectively bind dissolved and particulate pollutants. They form large flocs comprised of precipitated iron (oxyhydr)oxides and organics collected from the surrounding water (henceforth iron-organo flocs), which settle in aqueous media through gravitational force. By this iron-organo flocs may transport initally buoyant particulate matter such as cyanobacterial colonies (Oliver et al., 1985) or the emerging pollutants microplastics (MP, plastic particles < 5 mm) from the water phase into the sediments of water bodies (see Chapter 4).

MP are ubiquitously detected in the sediments of lakes (Su et al., 2016) and freshwater reservoirs (Di and Wang, 2018), with low density polymer types ($\rho < 1.0$ g cm^{-3}) such as polyethylene (PE) usually comprising the highest proportion of detected particles (Li et al., 2020; Lin et al., 2021; Ribeiro et al., 2021). Despite ongoing research efforts, mechanisms governing transport of initially buoyant MP to the profundal zone of standing freshwater bodies and their fate once reaching the sediments are not well understood. Biofilm formation (Chen et al., 2019) with associated mineral entrapment (Leiser et al., 2021) and aggregation with natural particles such as organic (Leiser et al., 2021) or iron-organic flocs (Leiser et al., 2020) have been recognized as important processes leading to sinking of PE MP in freshwater bodies.

Iron-organic flocs are a relevant aggregate type in freshwater bodies, forming during or after summer stratification (Mortimer, 1942). Many freshwater lakes and reservoirs are stratified over summer, with an oxycline separating the oxic epilimnion from the anoxic hypolimnion (Mortimer, 1942). The oxycline is a region with sharp oxygen and density gradients, at which intense iron cycling takes place (Bravidor et al., 2015). Ferrous iron diffuses upwards from the hypolimnion into the epilimnion and precipitates in the form of iron (oxyhydr)oxides right above the oxycline (Bravidor et al., 2015). These minerals aggregate with dissolved and particulate organic material, forming large, (60 to 370 µm) sinking aggregates (Elliott and Warren, 2014; Reiche et al., 2011). These iron-organo flocs sink downwards from the oxycline back

into the hypolimnion and subsequently to the sediments. They have been shown to aggregate cyanobacterial colonies (Oliver et al., 1985) and PE particles (Leiser et al., 2020), by this facilitating their transport into the sediments of standing freshwater bodies. Once reaching the sediments, iron-organo flocs will experience anoxic conditions as long as the overlying water column remains stratified and anoxic. Given their high Fe oxide content (35 – 50 %), iron-organo flocs are prone to iron reduction (Reiche et al., 2011), mediated by specialized sediment-dwelling bacteria such as, freshwater *Shewanella* spp. and *Geobacter* spp. (Kappler et al., 2021). Microbial reduction of iron oxides has been attributed to the release of nutrients (Mortimer, 1942), pollutants (Revesz et al., 2016) and organic matter (Patzner et al., 2020), initially bound to or within the mineral matrix. Whether this also leads to the disintegration of flocs and subsequently to the release of incorporated PE MP, was investigated in laboratory batch experiments employing the model organism *Shewanella oneidensis*. Further the role of iron (oxyhydr)oxides in stabilizing the floc aggregates was studied using acid treatment and microscopic techniques.

Material and methods

Floc preparation and microplastics

PE spheres (d: 118 ± 6 µm, ρ: 0.98 g cm^{-3}) spiked with fluorescent red Rhodamine B (RHBPMS-0.98 106-125 µm) were bought from Cospheric, USA. Surface water from eutrophic Bautzen reservoir (Saxony, Germany) was retrieved on 4th of September 2020, filtered (10 µm) and stored in the dark until use. Iron-organo flocs were formed by addition of 300 µL FeSO4 (500 mM, pH 1.8) and 10 mg PE spheres to 500 mL surface water (pH 9.5) followed by incubation on a tumbling roller incubator (3 – 4 rpm, 24 h, RM5, M. Zipperer GmbH, Germany). To test the effect of iron (oxyhydr)oxides removal on floc stability, several flocs were treated with 1 M HCl (24 h, room temperature) until visible decolorization of the flocs.

Microcosm experiment

The potential to release MP from iron-organo flocs via microbial iron reduction was tested using pure cultures of bacteria *Shewanella oneidensis* LMG19005 (BCCM, Belgium). *S. oneidensis* was grown under oxic conditions for 16 h until late log phase (OD_{600}: 0.8852, cell concentration: $3.54 \times 10^{10} \pm 1 \times 10^{10}$, n: 10) in soy-broth media (Medium 14, BCCM, Belgium) at 28 °C (Xiao et al., 2018). Cells were centrifuged (3x, 1500 rpm, 20 min) and washed with mineral media for iron-reducing *Shewanella spp.* (Burlage et al., 1998) to remove the soy-broth media. Anoxic microcosms (n: 20) containing mineral media (V: 20 mL), 5 iron-organo flocs with PE (3x washed with tap water) and Na-lactate (10 mM), were inoculated with 5 mL of washed *S. oneidensis* cultures (cell concentration in microcosm: 7×10^9 cells L^{-1}). Microcosms were bubbled with nitrogen (1 h) to remove the oxygen, incubated at 28 °C in the dark and sampled right after inoculation, and after 20, 40, 60, and 120 days. On each sampling date the Fe(II) release into the water phase of three microcosms was measured using ferrozine assay. Afterwards the flocs were carefully removed from the microcosms and treated with 1 M HCl. Their Fe(II)/Fe(III) content was analyzed by reduction with hydroxylammonium chloride – HCl (0.5 / 1 M) and ferrozine assay (Stookey, 1970). The solution was then filtered onto stainless steel sieves (10 µm) and the PE spheres formerly bound to the flocs were counted under a light microscope (Zeiss Axioplan). In order to quantify the PE spheres released from the flocs during incubation, the remaining microcosms liquid was filtered and checked for PE spheres as well. On each sampling date two additional microcosms were used to retrieve 6 individual iron-organo flocs, which were examined on 5 randomly chosen spots each using confocal laser scanning microscopy (CLSM). Control microcosms (n: 5) without additional *S. oneidensis* were run in parallel and sampled after 120 days.

Microcopic techniques

Flocs were visualized using confocal laser scanning microscopy as described elsewhere (see Chapter 4, Leiser et al., 2021; Leiser et al., 2020; Neu et al., 2001. Semi-quantitative biovolumes of bacteria, algae, cyanobacteria and extracellular polymeric

substance (EPS) inside the flocs were calculated from CLSM data sets using a customized version of ImageJ (Staudt et al., 2004).

Data analysis

Statistical testing was conducted for datasets with a minimum sample size of 6 individual replicates. Q-Q plots were examined to check for data normality. Variance homogeneity was tested with Bartlett's Test prior to ANOVA (two-sided, Type II) followed by examination of residual plots to verify the reliability of the ANOVA. Null hypothesis of equal group means was discarded for $p < 0.05$. Software R (R Core Team, 2018) was used for all statistical analysis and data visualizations.Mean values with standard deviations or median values with 5 – 95 % confidence intervals (CI) are reported where applicable.

Results and discussion

Iron-organo flocs readily formed in surface water from Bautzen reservoir; incorporating PE spheres (median: 650 particles per 5 flocs, 5 % - 95 % CI: 543 – 1265, n: 12) in their matrix (see Figure 1). The flocs sedimented to the bottom and thereby mediated sinking of the initially buoyant PE.

Treatment with hydrochloric acid lead to the removal of iron from the flocs (Figure 1) but did not destabilize the floc. In addition this treatment did not lead to the release of PE MP from the flocs (data not shown). Hence it can be assumed that iron (oxyhydr)oxides precipitation is a prerequisite for the formation of flocs, but iron is not necessary to assure floc stability after formation. Further PE MP are expected to stick rather within the organic matrix than being covered by iron or iron (oxyhydr)oxides.

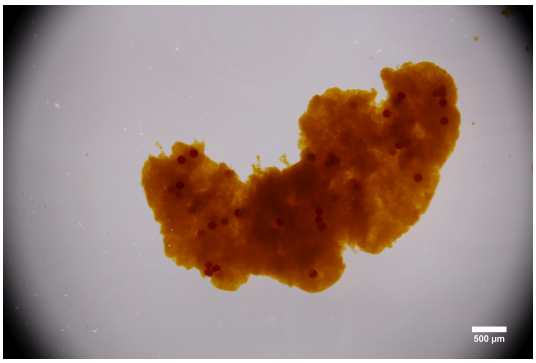

(a) Iron-organo floc with incorporated PE spheres

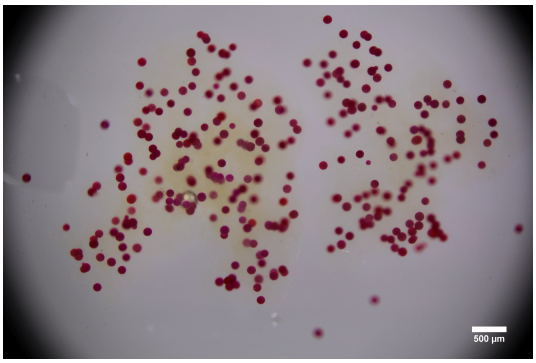

(b) Iron removed by HCl treatment

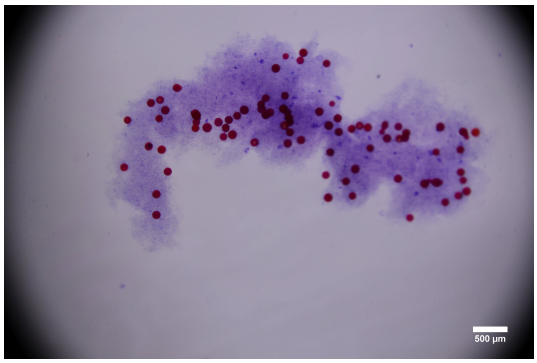

(c) HCl treated floc stained with Crystal violet

Figure 1: Iron-organo floc recorded via light microscope (10x magnification), presented in its natural state (a), after treatment with HCl (1M, 5 hrs.) (b) and after staining the HCl treated floc with crystal violet (0.1 %, 30 min.) (c).

Iron reduction by *S. oneidensis* changed the appearance of the flocs. From day 20 on-wards, flocs were covered by black spots, ultimately turning entirely black until Ddy 60. The color change indicated formation of secondary minerals, which was supported by the increasing number of rounded, reflecting mineral spherules covering the surface of the flocs with extended incubation time (Figure 2b-d).

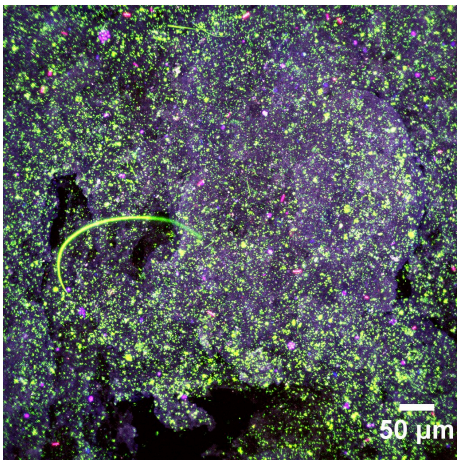

(a) Iron-organo floc at Day 0 without *S. oneidensis*

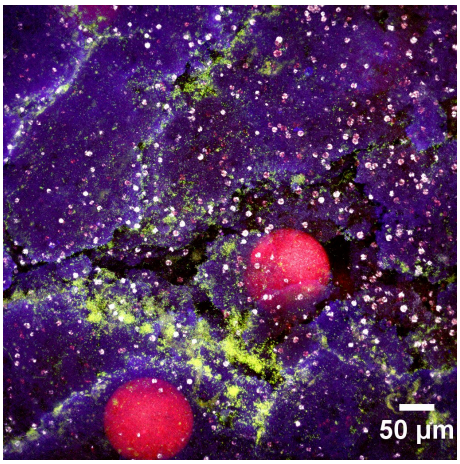

(b) After 20 days of incubation with *S. oneidensis*

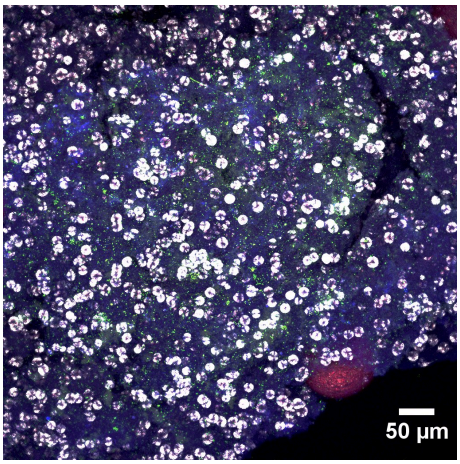

(c) After 40 days

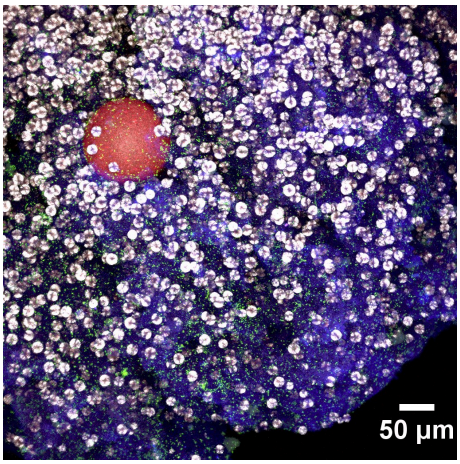

(d) After 60 days

Figure 2: Iron-organo flocs recorded via CLSM right at the beginning (2a), after 20 days (2b), 40 days (2c) and 60 days (2d) of anaerobic incubation with *S. oneidensis*. False color coding refers to Bacteria (green), algae (blue), cyanobacteria (pink), EPS (purple), PE spheres (bright red), reflection by secondary minerals (white)

S. oneidensis is well known for transforming ferrihydrite into magnetite via iron reduction, whose presence was supported by the black color of the flocs (Dippon et al., 2015). However, the rounded spherules (Figure 2) closely resembled pyrite framboids in shape and size (Ohfuji et al., 2005). Further the black flocs exhibited a sulfidic smell when treated with acid, indicating the presence of secondary sulfides. *S. oneidensis* is able to couple sulfite and thiosulfate reduction to lactate oxidation, but cannot reduce sulfate (Dippon et al., 2015). Hence sulfide mineral formation

might have rather been promoted by sulfate-reducing bacteria enclosed inside the non-sterile flocs. Sulfate-reducing bacteria such as *Desulfovibrio* are common in lake water (Berg et al., 2020) and could have been present inside the iron-organo flocs, precipitated from Bautzen reservoir surface water. Consortia of iron and sulfate reducing bacteria are known to precipitate iron sulfides onto the surface of iron (oxyhydr)oxides (Berg et al., 2020). Therefore the observed color change and the formation of spherules could be attributed to the combined activity of *S.oneidenis* and unknown sulfate-reducing bacteria. No floc color change was observed in the control treatment without additionally added *S. oneidensis*.

S. oneidensis was observed to bind to the surface of the iron-organo flocs, accumulating mostly in cracks and on the edges of the flocs (Figure 2b). This is in line with previous findings, reporting that iron reduction of *S. oneidensis* relies on direct contact of the cells with the iron mineral surface or by close range electron shuttling with endogenic flavins or exogenic humic substance (Dippon et al., 2015).

At the end of the experiment most of the iron (up to 90 %, Figure 3) was reduced and either bound to the flocs in form of reduced minerals or released in form of dissolved ferrous iron (Table S1). The transformation of iron minerals did not affect the integrity of the flocs, as indicated by only a minor fraction of the bound PE MP being released during the 120 days incubation (Figure 3, Table S1). Although significantly more plastics (ANOVA, $p < 0.05$) were released on day 60 and day 120 (20 $\pm$ 19 particles, mean $\pm$ sd, n: 6) compared to the previous sampling dates (4 $\pm$ 3, mean $\pm$ sd, n: 9), the proportion of released (median: 8, n: 12) compared to retained MP (median: 650, n: 12) remained negligible (Figure 3).

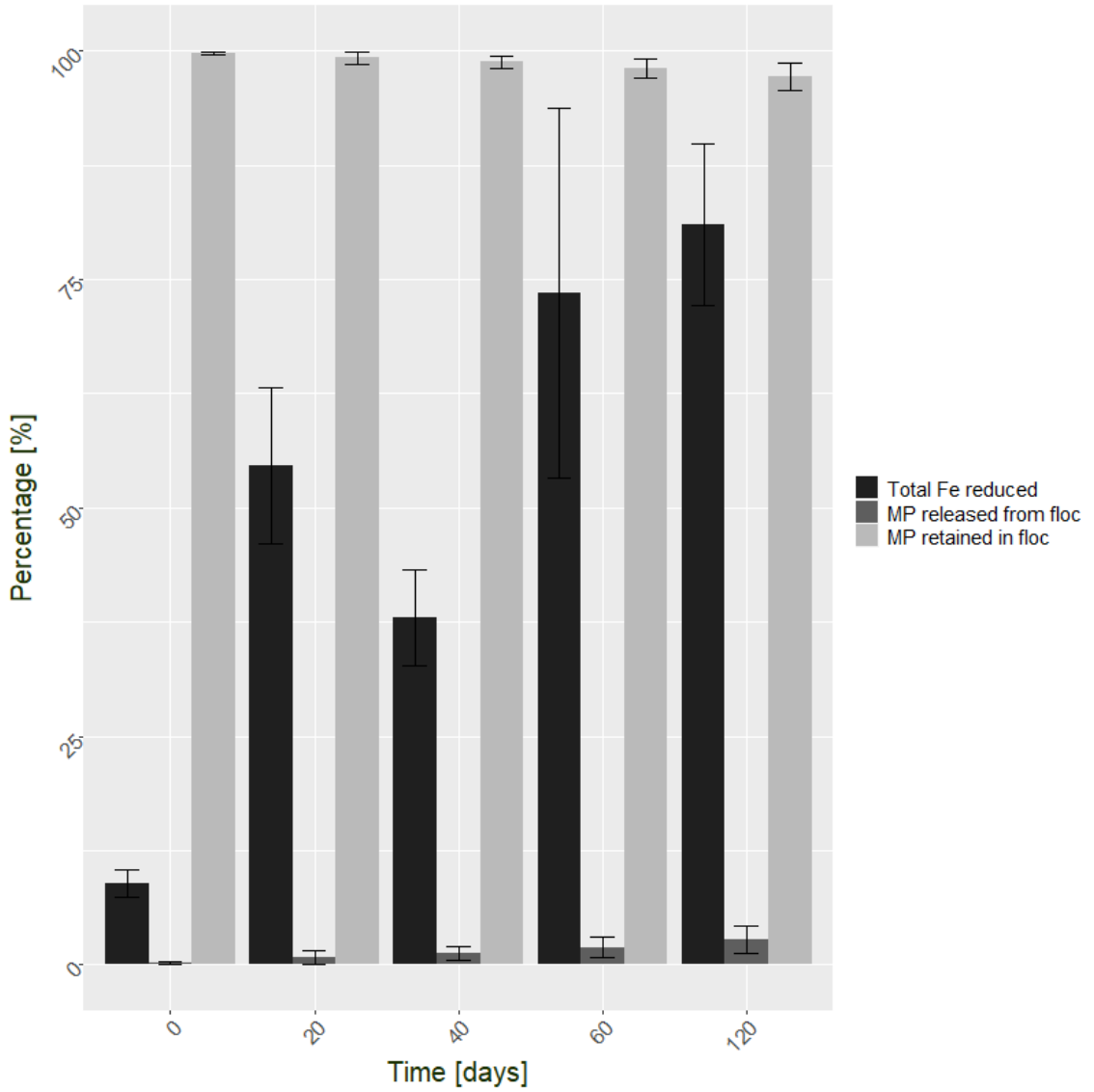

Figure 3: Iron reduction and plastic release from iron-organo flocs incubated with *S. oneidensis* under iron reducing conditions. Bars and arrows display the means and standard deviation of 3 individual replicate microcosms (n: 3).

S. oneidensis is able to use a wide range of different organic compounds for their energy conservation (Venkateswaran et al., 1999), possible enabling them to couple oxidation of the organics bound to the flocs to iron reduction. However, no substantial degradation of the organic floc matrix was observed over time (Figure S1), as indicated by fucosylate glycan binding Aleuria Aurantia lectin (Neu et al., 2001). Association with iron minerals is considered as effective way of carbon preservation in soils and sediments (Lalonde et al., 2012), with organics being protected from microbial degradation by steric hindrance or highly energetic binding to the

mineral surfaces (Arnarson and Keil, 2007). It has been shown that reduction of the preserving iron (oxyhydr)oxides minerals leads to the liberation and subsequent degradation of the associated organic matter (Patzner et al., 2020). However, if the reduction of iron (oxyhydr)oxides is coupled to the simultaneous formation of iron sulfide minerals, these secondary minerals can also effectively bind and preserve organic matter from microbial degradation (Picard et al., 2019). The observed iron sulfide formation in our study supports this phenomenon, and indicates the stability of the iron-organic flocs under anoxic conditions.

An artificial system with lactate as favorable electron donor was used in this study. It cannot be ruled out that *S. oneidensis* preferably utilized the easily degradable lactate instead of the flocs recalcitrant organic matter (Vidal-Melgosa et al., 2021). Although it was entirely consumed by the end of the experiment, lactate might have artificially prevented or retarded the microbial degradation of flocs. Under natural conditions in freshwater sediments, easily degradable substrates are scarce (Wendt-Potthoff et al., 2014) and microbial communities might be specialized to degrade deposited flocs, as it was shown for fresh phytoplankton aggregates mineralized after 12 – 20 weeks in anoxic lake sediments (Schulz and Conrad, 1995). Given their more recalcitrant nature compared to phytoplankton aggregates and following the results of the presented study, it can be expected that iron-organo floc degradation will be considerably slow (several weeks – months) within the cold profundal of lakes or reservoirs. In highly productive Bautzen reservoir, several milimeters of sediments (average deposition rate from June-August 12 g dry weight m^{-2} day^{-1}) are deposited over the approximately three months of summer stratification (unpublished observation). Hence, it is likely that iron-organo flocs lying on the sediment surfaces will become covered by freshly deposited material before being completely mineralized (Schulz and Conrad, 1995). Once MP bearing flocs are covered by fresh sediments, the escape of MP from the sediment matrix becomes unlikely, regardless of the flocs being intact or mineralized.

Conclusions

Iron-organo flocs precipitated from reservoir water effectively sequester PE MP and are stable under anoxic conditions for up to 120 days, even when the flocs experience microbial iron reduction. Hence, it can be assumed that iron-organo flocs lying on-top of anoxic sediments will not readily release incorporated MP into the water phase. Thereby incorporation into such aggregates may display a potential mode of long term MP storage in freshwater reservoirs. Consequently, the use of iron flocculants could contribute to the removal of MP from surface waters and to stable storage in the sediments of freshwater reservoirs. This long term deposition may decrease mobile MP and would mitigate adverse effects of this contaminant for the ecosystems of the downstream rivers, estuaries and subsequently the oceans.

Acknowledgments

We thank Thomas R. Neu for excellent advice and practical help in conducting CLS microscopy. Further we thank Corinna Völkner and Martin Wieprecht for eminent help in field and laboratory work. This research was supported by the BMBF project MikroPlaTaS (02WPL1448A).

References for Chapter 5

Arnarson, T. S., & Keil, R. G. (2007). Changes in organic matter-mineral interactions for marine sediments with varying oxygen exposure times. *Geochimica et Cosmochimica Acta*, *71*(14), 3545–3556. https://doi.org/10.1016/j.gca.2007.04.027

Berg, J. S., Duverger, A., Cordier, L., Laberty-Robert, C., Guyot, F., & Miot, J. (2020). Rapid pyritization in the presence of a sulfur/sulfate-reducing bacterial consortium. *Scientific Reports*, *10*(1), 1–13. https://doi.org/10.1038/s41598-020-64990-6

Bravidor, J., Kreling, J., Lorke, A., & Koschorreck, M. (2015). Effect of fluctuating oxygen concentration on iron oxidation at the pelagic ferrocline of a meromictic lake. *Environmental Chemistry*, *12*(6), 723–730. https://doi.org/10.1071/EN14215

Burlage, R., Atlas, R., & Stahl, D. (1998). *Techniques in Microbial Ecology* (1st ed.). Oxford University Press on Demand. https://doi.org/10.1016/s0580-9517(08)x7011-4

Chen, X., Xiong, X., Jiang, X., Shi, H., & Wu, C. (2019). Sinking of floating plastic debris caused by biofilm development in a freshwater lake. *Chemosphere*, *222*, 856–864. https://doi.org/10.1016/j.chemosphere.2019.02.015

Deppe, T., & Benndorf, J. (2002). Phosphorus reduction in a shallow hypereutrophic reservoir by in-lake dosage of ferrous iron. *Water Research*, *36*(18), 4525–4534. https://doi.org/10.1016/S0043-1354(02)00193-8

Di, M., & Wang, J. (2018). Microplastics in surface waters and sediments of the Three Gorges Reservoir, China. *Science of the Total Environment*, *616-617*, 1620–1627. https://doi.org/10.1016/j.scitotenv.2017.10.150

Dippon, U., Schmidt, C., Behrens, S., & Kappler, A. (2015). Secondary Mineral Formation During Ferrihydrite Reduction by Shewanella oneidensis MR-1 Depends on Incubation Vessel Orientation and Resulting Gradients of Cells,

Fe2+ and Fe Minerals. *Geomicrobiology Journal*, *32*(10), 878–889. https://doi.org/10.1080/01490451.2015.1017623

Elliott, A. V., & Warren, L. A. (2014). Microbial engineering of floc Fe and trace element geochemistry in a circumneutral, remote lake. *Environmental Science and Technology*, *48*(12), 6578–6587. https://doi.org/10.1021/es403754t

Kappler, A., Bryce, C., Mansor, M., Lueder, U., Byrne, J. M., & Swanner, E. D. (2021). An evolving view on biogeochemical cycling of iron. *Nature Reviews Microbiology*, (3). https://doi.org/10.1038/s41579-020-00502-7

Lalonde, K., Mucci, A., Ouellet, A., & Gélinas, Y. (2012). Preservation of organic matter in sediments promoted by iron. *Nature*, *483*(7388), 198–200. https://doi.org/10.1038/nature10855

Leiser, R., Jongsma, R., Bakenhus, I., Möckel, R., Philipp, B., Neu, T. R., & Wendt-Potthoff, K. (2021). Interaction of cyanobacteria with calcium facilitates the sedimentation of microplastics in a eutrophic reservoir. *Water Research*, *189*, 116582. https://doi.org/10.1016/j.watres.2020.116582

Leiser, R., Wu, G.-M., Neu, T. R., & Wendt-Potthoff, K. (2020). Biofouling, metal sorption and aggregation are related to sinking of microplastics in a stratified reservoir. *Water Research*, 115748. https://doi.org/10.1016/J.WATRES.2020.115748

Li, C., Busquets, R., & Campos, L. C. (2020). Assessment of microplastics in freshwater systems: A review. *Science of the Total Environment*, *707*, 135578. https://doi.org/10.1016/j.scitotenv.2019.135578

Lin, L., Pan, X., Zhang, S., Li, D., Zhai, W., Wang, Z., Tao, J., Mi, C., Li, Q., & Crittenden, J. C. (2021). Distribution and source of microplastics in China's second largest reservoir - Danjiangkou Reservoir. *Journal of Environmental Sciences*, *102*, 74–84. https://doi.org/https://doi.org/10.1016/j.jes.2020.09.018

Mortimer, C. H. (1942). The exchange of dissolved substances between mud and water in lakes. *Journal of Ecology*, *30*(1), 147–201.

Neu, T. R., Swerhone, G. D., & Lawrence, J. R. (2001). Assessment of lectin-binding analysis for in situ detection of glycoconjugates in biofilm systems. *Microbiology*, *147*(2), 299–313. https://doi.org/10.1099/00221287-147-2-299

Ohfuji, H., Boyle, A. P., Prior, D. J., & Rickard, D. (2005). Structure of framboidal pyrite: An electron backscatter diffraction study. *American Mineralogist*, *90*(11-12), 1693–1704. https://doi.org/10.2138/am.2005.1829

Oliver, R., Thomas, R., Reynold, C., & Walsby, A. (1985). The sedimentation of buoyant microcystis colonies caused by precipitation with an iron- containing colloid. *Proceedings of the Royal Society B*, *223*(1233), 511–528. https://doi.org/10.1098/rspb.1985.0016

Patzner, M. S., Mueller, C. W., Malusova, M., Baur, M., Nikeleit, V., Scholten, T., Hoeschen, C., Byrne, J. M., Borch, T., Kappler, A., & Bryce, C. (2020). Iron mineral dissolution releases iron and associated organic carbon during permafrost thaw. *Nature Communications*, *11*(1), 1–11. https://doi.org/10.1038/s41467-020-20102-6

Picard, A., Gartman, A., Cosmidis, J., Obst, M., Vidoudez, C., Clarke, D. R., & Girguis, P. R. (2019). Authigenic metastable iron sulfide minerals preserve microbial organic carbon in anoxic environments. *Chemical Geology*, *530*, 119343. https://doi.org/10.1016/j.chemgeo.2019.119343

R Core Team. (2018). *R: A language and environment for statistical computing*. R Foundation for Statistical Computing, Vienna, Austria. https://www.r-project.org/

Reiche, M., Lu, S., Ciobotă, V., Neu, T. R., Nietzsche, S., Rösch, P., Popp, J., & Küsel, K. (2011). Pelagic boundary conditions affect the biological formation of iron-rich particles (iron snow) and their microbial communities. *Limnology and Oceanography*, *56*(4), 1386–1398. https://doi.org/10.4319/lo.2011.56.4.1386

Revesz, E., Fortin, D., & Paktunc, D. (2016). Reductive dissolution of arsenical ferrihydrite by bacteria. *Applied Geochemistry*, *66*, 129–139. https://doi.org/10.1016/j.apgeochem.2015.12.007

Ribeiro, F., Okoffo, E. D., O'Brien, J. W., O'Brien, S., Harris, J. M., Samanipour, S., Kaserzon, S., Mueller, J. F., Galloway, T., & Thomas, K. V. (2021). Out of sight but not out of mind: Size fractionation of plastics bioaccumulated by field deployed oysters. *Journal of Hazardous Materials Letters*, *2*, 100021. https://doi.org/https://doi.org/10.1016/j.hazl.2021.100021

Schulz, S., & Conrad, R. (1995). Effect of algal deposition on acetate and methane concentrations in the profundal sediment of a deep lake (Lake Constance). *FEMS Microbiology Ecology*, *16*(4), 251–260. https://doi.org/https://doi.org/10.1111/j.1574-6941.1995.tb00289.x

Staudt, C, Horn, H, Hempel, D. C., & Neu, T. R. (2004). Volumetric measurements of bacterial cells and extracellular polymeric substance glycoconjugates in biofilms. *Biotechnology and Bioengineering*, *88*(5), 585–592. https://doi.org/10.1002/bit.20241

Stookey, L. L. (1970). Ferrozine-a new spectrophotometric reagent for iron. *Analytical Chemistry*, *42*(7), 779–781. https://doi.org/10.1021/ac60289a016

Su, L., Xue, Y., Li, L., Yang, D., Kolandhasamy, P., Li, D., & Shi, H. (2016). Microplastics in Taihu Lake, China. *Environmental Pollution*, *216*, 711–719. https://doi.org/10.1016/j.envpol.2016.06.036

Venkateswaran, K., Moser, D. P., Dollhopf, M. E., Lies, D. P., Saffarini, D. A., MacGregor, B. J., Ringelberg, D. B., White, D. C., Nishijima, M., Sano, H., Burghardt, J., Stackebrandt, E., & Nealson, K. H. (1999). Polyphasic taxonomy of the genus *Shewanella* and description of *Shewanella oneidensis* sp. nov. *International Journal of Systematic Bacteriology*, *49*(2), 705–724. https://doi.org/10.1099/00207713-49-2-705

Vidal-Melgosa, S., Sichert, A., Francis, T. B., Bartosik, D., Niggemann, J., Wichels, A., Willats, W. G., Fuchs, B. M., Teeling, H., Becher, D., Schweder, T., Amann, R., & Hehemann, J. H. (2021). Diatom fucan polysaccharide precipitates carbon during algal blooms. *Nature Communications*, *12*(1), 1–13. https://doi.org/10.1038/s41467-021-21009-6

Wendt-Potthoff, K., Kloß, C., Schultze, M., & Koschorreck, M. (2014). Anaerobic metabolism of two hydro-morphological similar pre-dams under contrasting nutrient loading (Rappbode Reservoir System, Germany). *International Review of Hydrobiology*, *99*(5), 350–362. https://doi.org/10.1002/iroh.201301673

Xiao, M., Li, M., & Reynolds, C. S. (2018). Colony formation in the cyanobacterium Microcystis. *Biological Reviews*, *93*(3), 1399–1420. https://doi.org/10.1111/brv.12401

Chapter 6

Discussion

Freshwater reservoirs are major sinks for MP along their way from land to sea. The presented dissertation is a combination of field experiments focused on biofilm formation and laboratory experiments elucidating both the potential role of aggregation for MP transport and factors which influence their subsiding into reservoir sediments. Several natural mechanisms leading to the sedimentation of initially buoyant MP and their subsequent long-term storage in sediments have been identified and described for the first time (summarized in Figure 4).

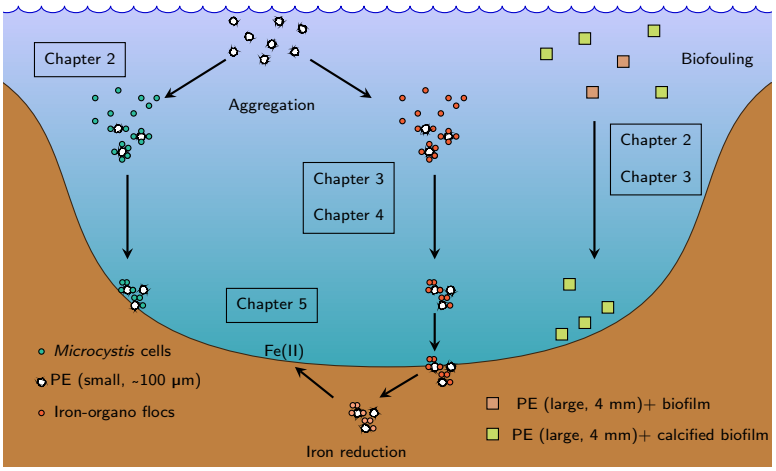

Figure 4: Summarized major findings of the thesis. Mechanism which lead to the sinking of initially buoyant MP are shown next to the Chapter in which they were described in detail.

The study contributes to current knowledge by elucidating how biogeochemical processes influence the fate of MP in standing freshwaters:

- **Chapter 2** demonstrates that cyanobacteria (sessile and planktonic) sink PE

through either calcite precipitation in biofilms or formation of colonies with chelating Ca^{2+}.

- **Chapter 3** indicates that biofouling with microorganisms alone, might not lead to MP sinking, while lake mixing and the formation of iron-organo flocs clearly affects the buoyancy of PE.

- **Chapter 4** further outlines the potential of iron-organo flocs to aggregate different shaped MP and to mediate their transport into reservoir sediments leading to long-term storage of these contaminants.

- **Chapter 5** shows that iron-organo flocs do not disintegrate under iron reducing conditions, which further outlines their potential role to govern the long-term sediment deposition of MP.

Taking these major findings into account, the presence of buoyant MP in sediments can now be more conclusively explained. This further emphasised the important role of reservoirs for MP retention and storage. Consequently, the impact of biofilm formation on the buoyancy of MP in Bautzen and Malter reservoir will be summarized and critically discussed. This is followed by considerations on how aggregation based transport mechanisms might influence MP transport in reservoirs and subsequently how these transport modes govern the deposition of MP into sediments. In an attempt to extrapolate the findings to a larger scale, properties of Malter / Bautzen reservoir are compared and related to conditions found in other standing freshwater bodies. Suggestions for future research directives are provided, which might help to further elucidate the fate of MP in freshwater dams and reservoirs.

6.1 Biofouling affects microplastics fate in reservoirs

Biofilm formation has been identified as major driver for the loss of particle buoyancy in aquatic environments (see Table 4 and references therein). Earlier results from Chinese East Lake (Chen et al., 2019), together with results from this study, indicate that biofouling in standing freshwater bodies differ from what was previously observed in marine settings, regarding community composition and their subsequent impact on the buoyancy of MP (Fazey and Ryan, 2016; Kaiser et al., 2017; Lobelle and Cunliffe, 2011). A major finding was that microbial biomass alone is not sufficient to induce sinking of PE MP (see Chapter 3). Only under presence of minerals (iron (oxyhydr)oxides) (Chapter 3), calcite (Chapter 2)) enough ballasting material accumulated on the particle surfaces to overcome their buoyancy. By comparing mesotrophic Malter with the eutrophic Bautzen reservoir it became evident that the extent of biofouling depended on the bioproductivity of the water body.

In Malter reservoir generally thinner and patchier biofilms (~30 µm thickness), developed compared to the Bautzen reservoir (~100 µm) as analyzed via CLSM (see Figure 5). Precipitation of calcite led to high density biofilms (1.18 g cm^{-3}) in Bautzen reservoir, but was not observed in Malter reservoir. Calcite precipitation could be linked to the presence of sessile cyanobacteria (Zippel and Neu, 2011), which were far more abundant in Bautzen (1.3 x 10^{-2} μm^3 μm^{-2}, median) than in Malter reservoir biofilms (2.1 x 10^{-6} μm^3 μm^{-2}, median). Hence the presence of calcifying cyanobacteria was attributed to the sinking of MP in Bautzen reservoir. This might be generalized to other standing freshwater water bodies such as the East Lake (China), where PP films sunk after the formation of cyanobacteria dominated biofilms during summer (Chen et al., 2019) or the Sanjiadian Reservoir with its highly calcified biofilms (Tianzhi et al., 2014). According to theoretical assumptions (Chubarenko et al., 2016) even sparse coverage (~32 µm) with calcified biofilms would be sufficient to induce sinking of the PE films used in this study.

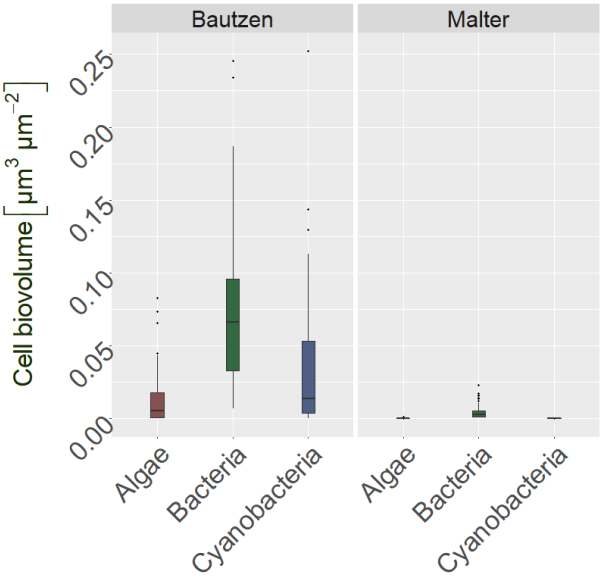

Figure 5: CLSM cell biovolumes of biofilms grown in the epilimnion of Malter reservoir (22 days, n: 50, from Chapter 3) and Bautzen reservoir (29 days, n: 50, from Chapter 2) on PE MP.

Under favorable conditions (light, nutrients available) in the epilimnion such a biofilm thickness can easily be achieved (Rao et al., 1997), which further emphasises the importance of this mechanism for the fate of MP in freshwater reservoirs. However, under light reduced conditions and low temperatures or lacking oxygen as found in the hypolimnion during stratification, biofilms might have lower densities and thickness (Chapter 3, Riese, 2017; Tu et al., 2020) compared to biofilms developed in the epilimnion. Still the formation of biofilms in the hypolimnion is of importance as they facilitate the aggregation with other organic and inorganic particles (e.g. iron-organo flocs, Chapter 3) from the surrounding water (Van Melkebeke et al., 2020).

Some authors stated that biofouled particles sinking from the euphotic into the aphotic zones, will regain their buoyancy due to defouling, once reaching the seafloor (Kooi et al., 2017; Lobelle et al., 2021; Ye and Andrady, 1991). Whether this also true for the shallow Bautzen (mean depth: 8 m) and Malter (mean depth: 16 m) reservoir, cannot be answered by the experimental set-ups used in Chapter 3 & 4. Taking into account that the reservoirs are quite shallow and assuming MP sinking velocities of ~0.0075 m s^{-1} (as recorded for PS particles ρ: 1.05 g cm^{-1}), they would

settle to the sediments in approximately 30 min (Bautzen) - 60 min (Malter) without vertical or lateral mixing currents (Daily and Hoffman, 2020). Hence, oscillating cycles of biofouling followed by defouling and re-emergence of MP, as proposed by popular ocean transport models (Kooi et al., 2017; Lobelle et al., 2021), are rather unlikely to occur and should not be transferred to shallow reservoirs.

It should be considered that the experimental set-up used to study biofouling most likely biased the results. Using cages for the incubation in the reservoirs, larger organisms (> 4 mm) were excluded, which influenced biofilms community composition (Risse-Buhl et al., 2017; Weitere et al., 2018). Further under realistic conditions, MP particles are not fixed at a certain spots, but rather transported to different locations within (epilimnion, hypolimnion) or outside (beach) the water body (Daily and Hoffman, 2020). In reservoirs with intermediate size such as the Malter and Bautzen reservoir, MP particles may rather beach to the shores instead of becoming negatively buoyant due to biofouling. However, the water residence times in Bautzen (199 days, capacity: 44.63 x 10^6 m^3, discharge: 2.6 m^3 s^{-1}) and Malter reservoir (102 days, capacity: 8.78 x 10^6 m^3, discharge: 1 m^3 s^{-1}) might allow the development of sufficient biofilm coverage on MP floating in their surface water (Köngeter, 2013).

Concluding direct ballasting effects by biogenic precipitation of calcite (Chapter 2) and the abiotic formation of iron (oxyhydr)oxides) (Chapter 3) were identified as the most important factors which increase the density of biofilms. For freshwater biofilms rather their sticky nature, which enable them to trap minerals, than the total mass contributed by organisms or organic matrix, shape their physical gravity and effects on MP particle density. Season and trophic status can be considered as important factors influencing both the density and the thickness of biofilms (Chen et al., 2019), hence loss of buoyancy is unlikely to occur in epilimnion of mesotrophic reservoirs during autumn compared to eutrophic reservoirs during summer.

6.2 Microplastics aggregation with cyanobacteria and iron-organo flocs

Aggregation was studied in the laboratory under conditions representative for Bautzen reservoir, regarding Ca^{2+} concentrations (Chapter 2) and by using surface water from the reservoir (Chapter 4 & 5). Although the role of aggregation for MP transport in aquatic systems was addressed by previous studies (see Table 3), this has not been done under the emphasis of conditions prevalent in freshwater reservoirs. Hence this dissertation elucidated the role of different relevant natural aggregation partners (Ca^{2+}, Cyanobacteria, iron-organo flocs) for the transfer of initially buoyant PE MP from the water phase to the sediments of freshwater reservoirs.

Unlike the initial hypothesis, *Microcystis* spp. did not precipitate calcite, but formed rather large and sinking colonies under the chelating effect of Ca^{2+}. This effect was already described (Chen and Lürling, 2020) and it should be mentioned that a range of other factors, such as grazing pressure, toxins, nutrients or cell growth also lead to formation of cyanobacterial colonies (reviewed in Xiao et al., 2018).

It was found that these colonies incorporated small PE MP, which induced their sinking. This is in line with the findings that other microalgae, such as green algae *Chlamydomonas reinhardtii*, flagellate *Tisochrysis lutea*, dinoflagellate *Heterocapsa triquetra* and diatom *Chaetoceros neogracile* (Lagarde et al., 2016; Long et al., 2015; Long et al., 2017) readily formed sinking aggregates with MP. Given the high abundance of *Microcystis* spp. (up to 3 x 10^8 cells l^{-1}, personal communication Alice Rau, Landestalsperrenverwaltung Sachsen), aggregation with cyanobacterial cells governs a high potential for the removal of MP from the surface water of Bautzen reservoir. But also in Malter reservoir phytoplankton cells reach high concentrations during summer (up to 2 x 10^7 cells l^{-1}, personal communication Alice Rau), thereby possibly acting as aggregation partners for floating MP. As many lakes and reservoirs show similar concentrations of cyanobacteria and microalgae compared to Bautzen and Malter reservoir (Feng et al., 2019; Osman-Sigg, 1982) the findings might be transferred to other freshwater systems as well. However, such

high planktonic cell concentrations (blooms) and the tendency to flocculate might be restricted to certain times in the year. Seasonal cyanobacterial blooms usually occur in late summer (Küchler-Krischun and Kleiner, 1990; Thompson et al., 1997), while diatoms are blooming in spring (Kong et al., 2021). Diatoms are widely recognized for forming millimeter - centimeter sized, large fast sinking aggregates during blooms (Alldredge and Gotschalk, 1989). Given by their sticky nature they could also incorporate buoyant PE MP, as already shown in laboratory experiments (Long et al., 2015; Long et al., 2017). Therefore, incorporation of MP into phytoplankton aggregates might not be restricted to late summer cyanobacterial blooms, but could occur throughout the year with different planktonic cells acting as aggregation partners.

In contrary, iron-organo flocs observed in the hypolimnion of Malter reservoir and in laboratory studies using surface water from Bautzen reservoir might be more depending on seasonality. Their appearance will be restricted to the time of summer stratification or shortly after lake mixing (as described in Chapter 3). Iron-organo flocs can reach high concentrations next to the oxycline (10^6 - 10^9 particles l^{-1}) and govern a high potential to aggregate floating particles such as microbial cells or MP (Figure 6, Reiche et al., 2011). Apparently flocs found in the hypolimnion of Malter reservoir did not differ much from flocs formed from Bautzen reservoir surface water (see Figure 6). It can be assumed that the microbial community of the rapidly formed iron-organo flocs was mainly influenced by the organisms present in the surrounding water. The flocs had a high tendency to aggregate planktonic cells from the water phase, which initiated the sedimentation of algae, bacteria and cyanobacteria. As phototrophic algae and cyanobacteria are usually not present in the aphotic hypolimnion, their high abundance in iron-organo flocs from Malter reservoir might indicate a origin from the epilimnion of the water body. This conclusion supports the idea of iron-organo flocs as important collectors of cells (Oliver et al., 1985), nutrients (Mortimer, 1942) and MP (Chapter 3, 4 & 5) in the whole water column of stratified reservoirs.

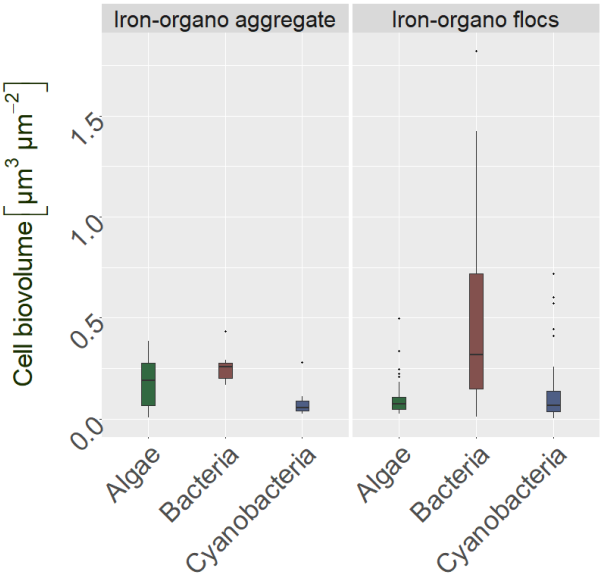

Figure 6: CLSM cell biovolumes of iron-organo aggregates in the hypolimnion of Malter reservoir (n: 7, Chapter 3) and iron-organo flocs formed after addition of 300 µM $FeSO_4$ to Bautzen reservoir water (n: 50, Chapter 4).

Although the data presented in this thesis indicated for the relevance of iron-organo flocs for the transport of particulate matter from the surface to the bottom of freshwater lakes and reservoirs (Oliver et al., 1985), sufficient published data on this process are still scarce (Bravidor et al., 2015; Mori et al., 2017; Reiche et al., 2011). Therefore, formation of iron-organo flocs at the oxycline of stratified freshwaters or during mixing events, remains an interesting but understudied topic of lake research. In the thesis it was shown that iron-organo flocs size dependably aggregated buoyant PE MP, with small MP ($<$ 100 µm) getting more readily incorporated than larger particles ($>$ 100 µm). This size dependence of MP aggregation was already shown in the field (Zhao et al., 2017; Zhao et al., 2018) and can be explained the higher collision frequency of small particles (Quik et al., 2014). Derived from the presented results, it can be assumed that MP particles $<$ 100 µm will be rapidly aggregated (1 - 24 h) with natural aggregation partners such as cyanobacterial cells (Chapter 2) or iron-organo flocs (Chapter 4 & 5), while this might be less relevant for larger MP particles $>$ 100 µm (also hypothesized by Rogers et al., 2020). Therefore, it can be assumed, that biofouling is less important for the transport of small MP, as they will be incorporated into aggregates before developing mature biofilms. However,

colonizing films or early stage biofilms might still be important as they increase particle stickiness and increase aggregation efficiency (Michels et al., 2018; Van Melkebeke et al., 2020). Due to their high concentration in reservoirs, cyanobacteria and iron-organo flocs exhibit a high potential to aggregate and remove small MP from the water phase. They can be considered as carriers collecting buoyant MP at the surface and transporting them downwards to the sediments by gravitational settling.

6.3 Sediment burial of microplastics and microbial iron reduction

Although MP pollution of lake and reservoir sediments is well described, not much is known on about the mechanisms leading to the incorporation of MP into the sediments. Therefore, the role of iron-organo flocs to act as carriers for MP from the surface water into the sediments was studied in Chapter 4. Sediments were often considered as stable surfaces on which MP are deposited and buried over time by materials settling over them, resulting in temporal layered sediments (Dong et al., 2020). This might be true for certain settings, such as deep sea floors (Woodall et al., 2014) or sandy sediments (Waldschläger and Schüttrumpf, 2020) with low bioturbation activity (Gebhardt and Forster, 2018; Näkki et al., 2017; Näkki et al., 2019), but not necessarily for reservoir sediments, especially not at their deepest points (such as the sediments investigated in the presented thesis). Results from Chapter 4 showed that unconsolidated sediments, which are very common for reservoirs, lakes (Franzen, 1985) and certain marine settings (e.g. baltic sea, Näkki et al., 2017), allowed iron-organo flocs to carry MP trough their uppermost layer, reaching depths of more than eight centimeter. This indicates that MP, especially when incorporated into aggregates, might infiltrated quite easily into the upper centimeter of sediments. The downward movements is most likely stopped by the increased bulk density of the sediments in a certain depth. This may partly explain the finding of MP inside of sediment layers older than the start of industrial production of the respective polymer type (Brandon et al., 2019; Courtene-Jones et al., 2020; Turner et al., 2019).

The iron-organo flocs were surprisingly robust, with iron reduction by *S. oneidensis* and even treatment with acid showing little effect on the release of MP (Chapter 5). Flocs formed from POM or DOC under the influence of metal ions (Chin et al., 1998) have been described as quite resistant against microbial degradation. This recalcitrant nature is often attributed to accumulation of complex compounds such as fucose containing sulphated polysaccharides, excreted by planktonic algae cells (Vidal-Melgosa et al., 2021) or steric hindrance through minerals and compaction

(Chin et al., 1998; Lalonde et al., 2012). However, such flocs are not completely inert and might be degraded by enzymatic digestion (Vidal-Melgosa et al., 2021) within the upper centimeters of freshwater sediments (Schulz and Conrad, 1995). The relative stability of flocs still explains the stable deposition of the PE spheres in the sediment cores, as they were degraded after the MP was transported and incorporated into the sediment matrix. The sediments were fine grained (mean grain size ~35 µm) and sticky. Hence, the escape of the MP (diameter: 118 ± 6 µm) can be expected as unlikely, even if the enclosing flocs are degraded over time.

The results presented in Chapter 4 & 5 are an initial step towards the better understanding of MP interaction with sediments. It shows that aggregation might not only lead to sinking of MP but also to the stable deposition of this contaminant in the sediments (Lagarde et al., 2016; Michels et al., 2018; Porter et al., 2018) . Due to similarities in size, shape and density, conclusion drawn for the iron-organo flocs might also be transferred to the cyanobacterial aggregates (Chapter 2) or other organic aggregates (lake snow, diatom aggregates, faecal pellets, pseudofeces) found in reservoirs. Given the widespread distribution of sediments with comparable properties, swift deposition of aggregated MP into the uppermost centimeters of unconsolidated sediments might be common process in many aquatic environments.

Chapter 7

Conclusions and outlook

Two major transport mechanisms, aggregation and biofouling can be considered as important for the MP fate in freshwater reservoirs. Aggregation with cyanobacteria and iron-organo flocs mainly affects small particles, with sizes ~100 µm. In direct comparison the aggregation of small PE fragments with iron-organo flocs (27 % of particles aggregated) was more efficiently than the aggregation with cyanobacteria (0.4 % aggregated). However, under natural conditions cyanobacteria and other phytoplankton are often more abundant or available than iron-organo flocs. Hence, the lower removal efficiency might be outweighted by the higher abundance of sinking phytoplankton aggregates. For large films (> 1 mm), aggregation might be less important, as only four PE particles (0.3 %) were found to be sunken due to aggregation within the Malter reservoir. In contrary, biofouling with calcified biofilms impacted the buoyancy of 10 % of the particles incubated in Bautzen reservoir. However, this might be only valid for PE films and not necessarily for other MP shapes (e.g. fragments, spheres, fibers). Due to their flexibility and small surfaces, fibers might be less prone to biofouling compared to the films (Chubarenko et al., 2016). Fibers were sunken by aggregation with iron-organo flocs (37 % of deployed fibers) in the laboratory. This is an important finding, as fibers are the most common MP shape in surface waters and sediments of freshwater reservoirs (see Table 1). Hence, aggregation based transport mechanisms might be more crucial for the fate of MP in freshwater reservoirs than direct ballasting effects from biofouling. Both aggregated plastics and biofouled squares can be expected to subside easily into the soft sediments of the reservoirs, which possibly leads to stable deposition over longer timescales.

Although some mechanisms governing the fate of MP in freshwater reservoir surface water and sediments have been elucidated in this thesis, several issues remained not

adequately addressed:

- Biofilm formation and biofouling has been extensively studied, still it remains uncertain which factors shape the physical gravity of the fouling films. Entrapment of minerals from the water and formation of stable gas bubbles by photosynthetic activity have been observed occasionally. Such factors need to be quantified in order to determine the contribution of biofilms to MP sinking or floating under various environmental conditions.

- There is evidence that MP accumulate within the layers of the thermocline/halocline of the baltic sea (Minna and Uurasj, 2021). Whether the thermocline of stratified freshwater reservoirs also displays an accumulation zone for MP might be an interesting topic for future research.

- The infiltration of MP into sediments is up to now understudied. Laboratory studies with glass spheres indicate that infiltration of MP might only be possible for MP smaller than the pore size of the sediment (Waldschläger and Schüttrumpf, 2020). However, in the presented study infiltration of mm sized aggregates into µm sized pore spaces was observed. This indicates that mechanistic understanding of MP infiltration into realistic sediments, especially when bound to aggregates, is still lacking and should be addressed by suitable studies.

- Association with diatom aggregates has been proven to effectively remove initially buoyant MP from the water phase in laboratory experiments (Long et al., 2017). As many lakes and reservoirs show extensive winter and spring blooms of diatoms, followed by flocculation and sinking to the sediments in form of sticky phytoaggregates (Kong et al., 2021), this topic might be also relevant under environmental conditions. Suitable incubation experiments during or at the end of diatom blooms might lead to further insight, whether aggregation might take place in lakes and could possibly transfer MP into sediments.

- Taking into account that freshwater reservoir are rather small (compared to the oceans), MP particles will be deposited on the beaches or cycled between

shore and water phase as proposed by a modelling study (Daily and Hoffman, 2020). This leads to the assumption that a significant proportion of MP will be deposited at the beaches of the reservoirs instead of within the sediments. For a better understanding of reservoirs role to store MP, the beach deposition should be investigated in more detail.

Acknowledgements

First of all I would like to thank my supervisor Katrin Wendt-Potthoff, for her support and excellent advises. Many thanks for all the time and night-shifts spent on reading my drafts, listening to my ideas and helping for realizing my experiments.

Thanks to my co-authors, Insa Bakenhus, Bodo Philipp and Robert Möckel for providing me novel techniques, methods and substantial improvements of the manuscripts. Special thanks go to Gi-Mick Wu, who was not only my Co-Author, but also taught me the proper use of R and statistics.

Many thanks to my co-Author and office-mate Tallent Dadi for the kind words and good advises throughout the years.

To my co-Author and intern Maja Schumann, thanks for the efforts and enthusiasm while working in lab with me. Also many thanks to Franziska Reggelin for helping me in many occasion and experiments.

Dear Mibi working group, dear Philipp Keller, Matthias Koschorreck, Peifang Leng, Antje Nieber, Carolin Waldemer and Patrick Aurich, thanks for the supportive and pleasant working conditions. In addition the Department of Lake Research, my co-supervisor Bertram Boehrer and Karsten Rinke are acknowledged for the scientific discussions, input and access to the laboratories.

Many thanks to Thomas R. Neu for the outstanding help and expertise in microscopy. Your knowledge and skills were eye-opening for me.

Also I would like to thank the members of the MikroPlaTas-Project for the nice time together. Especially I thank my fellow PhD. students Claudia Drago, Lukas Kruckenfellner, Diana Michler-Kozma, and Marie Rauchschwalbe, for the discussions and supportive atmosphere during our meetings. Particular thanks go to Rense Jongsma, for the help with the manuscript and your idea to conduct an experiment in Bautzen reservoir. Also I appreciate Guntram Weithoff very much

for giving me the practical chance to supervise students in Potsdam University and for leading the council in the disputation.

Credits are given to the Landestalsperrenverwaltung Sachsen, for kindly providing accesses and infrastructure for the sampling campaigns and experiments in the reservoirs. In particular I thank Alice Rau for her fast, kind and professional responses to any question related to water chemistry in Bautzen and Malter.

Zuletzt noch einen ganz besonderen Dank an die TechnikerInnen, welche mit ihrer Zeit, Einsatz und Ratschlägen wesentlich zum Gelingen der Arbeit beigetragen haben. Vielen Dank an Ute Kuhlicke für die viele Hilfe und Arbeit am Mikroskop. Danke an Corinna Völkner und Martin Wieprecht für die Hilfe im Labor, bei den Probenahmen, der allgemeinen Organisation und nicht zuletzt Danke für die Gespräche, Tipps und Grillabende.

References

Alimi, O. S., Farner Budarz, J., Hernandez, L. M., & Tufenkji, N. (2018). Microplastics and nanoplastics in aquatic environments: aggregation, deposition, and enhanced contaminant transport. *Environmental Science and Technology*, *52*(4), 1704–1724. https://doi.org/10.1021/acs.est.7b05559

Amaral-Zettler, L. A., Zettler, E. R., & Mincer, T. J. (2020). Ecology of the plastisphere. *Nature Reviews Microbiology*, *18*(3), 139–151. https://doi.org/10.1038/s41579-019-0308-0

Andersen, T. J., Rominikan, S., Olsen, I. S., Skinnebach, K. H., & Fruergaard, M. (2021). Flocculation of PVC microplastic and fine-grained cohesive sediment at environmentally realistic concentrations. *Biological Bulletin*, *240*(1), 42–51. https://doi.org/10.1086/712929

Andrady, A. L. (2017). The plastic in microplastics: A review. *Marine Pollution Bulletin*, *119*(1), 12–22. https://doi.org/10.1016/j.marpolbul.2017.01.082

Artham, T., Sudhakar, M., Venkatesan, R., Madhavan Nair, C., Murty, K. V., & Doble, M. (2009). Biofouling and stability of synthetic polymers in sea water. *International Biodeterioration and Biodegradation*, *63*(7), 884–890. https://doi.org/10.1016/j.ibiod.2009.03.003

Ateia, M., Zheng, T., Calace, S., Tharayil, N., Pilla, S., & Karanfil, T. (2020). Sorption behavior of real microplastics (MPs): Insights for organic micropollutants adsorption on a large set of well-characterized MPs. *Science of the Total Environment*, *720*. https://doi.org/10.1016/j.scitotenv.2020.137634

Badger, M. R., & Price, G. D. (2003). CO_2 concentrating mechanisms in cyanobacteria: Molecular components, their diversity and evolution. *Journal of Experimental Botany*, *54*(383), 609–622. https://doi.org/10.1093/jxb/erg076

Barry, R. C., Schnoor, J. L., Sulzberger, B., Sigg, L., & Stumm, W. (1994). Iron oxidation kinetics in an acidic alpine lake. *Water Research*, *28*(2), 323–333. https://doi.org/10.1016/0043-1354(94)90270-4

Battin, T. J., Besemer, K., Bengtsson, M. M., Romani, A. M., & Packmann, A. I. (2016). The ecology and biogeochemistry of stream biofilms. *Nature Reviews Microbiology*, *14*(4), 251–263. https://doi.org/10.1038/nrmicro.2016.15

Battin, T. J., Kaplan, L. A., Newbold, J. D., Cheng, X., & Hansen, C. (2003). Effects of current velocity on the nascent architecture of stream microbial biofilms. *Applied and Environmental Microbiology*, *69*(9), 5443–5452. https://doi.org/10.1128/AEM.69.9.5443-5452.2003

Besseling, E., Quik, J. T., Sun, M., & Koelmans, A. A. (2017). Fate of nano- and microplastic in freshwater systems: A modeling study. *Environmental Pollution*, *220*, 540–548. https://doi.org/10.1016/j.envpol.2016.10.001

Bravidor, J., Kreling, J., Lorke, A., & Koschorreck, M. (2015). Effect of fluctuating oxygen concentration on iron oxidation at the pelagic ferrocline of a meromictic lake. *Environmental Chemistry*, *12*(6), 723–730. https://doi.org/10.1071/EN14215

Bulleri, F., Ravaglioli, C., Anselmi, S., & Renzi, M. (2021). The sea cucumber holothuria tubulosa does not reduce the size of microplastics but enhances their resuspension in the water column. *Science of The Total Environment*, *781*, 146650. https://doi.org/https://doi.org/10.1016/j.scitotenv.2021.146650

Cai, L., Hu, L., Shi, H., Ye, J., Zhang, Y., & Kim, H. (2018). Effects of inorganic ions and natural organic matter on the aggregation of nanoplastics. *Chemosphere*, *197*, 142–151. https://doi.org/10.1016/j.chemosphere.2018.01.052

Chen, H., & Lürling, M. (2020). Calcium promotes formation of large colonies of the cyanobacterium Microcystis by enhancing cell-adhesion. *Harmful Algae*, *92*(1), 101768. https://doi.org/10.1016/j.hal.2020.101768

Chen, X., Xiong, X., Jiang, X., Shi, H., & Wu, C. (2019). Sinking of floating plastic debris caused by biofilm development in a freshwater lake. *Chemosphere*, *222*, 856–864. https://doi.org/10.1016/j.chemosphere.2019.02.015

Chubarenko, I., Bagaev, A., Zobkov, M., & Esiukova, E. (2016). On some physical and dynamical properties of microplastic particles in marine environment. *Marine Pollution Bulletin*, *108*(1-2), 105–112. https://doi.org/10.1016/j.marpolbul.2016.04.048

Cole, M., Lindeque, P. K., Fileman, E., Clark, J., Lewis, C., Halsband, C., & Galloway, T. S. (2016). Microplastics alter the properties and sinking rates of zooplankton faecal pellets. *Environmental Science and Technology*, *50*(6), 3239–3246. https://doi.org/10.1021/acs.est.5b05905

Cornell, R., & Schwertmann, U. (2003). *The iron oxides: structure, properties, reaction, occurrences and uses* (1st ed.). John Wiley & Sons. https://doi.org/10.1002/3527602097

Cunha, C., Faria, M., Nogueira, N., Ferreira, A., & Cordeiro, N. (2019). Marine vs freshwater microalgae exopolymers as biosolutions to microplastics pollution. *Environmental Pollution*, *249*, 372–380. https://doi.org/10.1016/j.envpol.2019.03.046

Daily, J., & Hoffman, M. J. (2020). Modeling the three-dimensional transport and distribution of multiple microplastic polymer types in Lake Erie. *Marine Pollution Bulletin*, *154*. https://doi.org/10.1016/j.marpolbul.2020.111024

de Haan, W. P., Sanchez-Vidal, A., & Canals, M. (2019). Floating microplastics and aggregate formation in the Western Mediterranean Sea. *Marine Pollution Bulletin*, *140*(January), 523–535. https://doi.org/10.1016/j.marpolbul.2019.01.053

De Oliveira, T. T. S., Andreu, I., Machado, M. C., Vimbela, G., Tripathi, A., & Bose, A. (2020). Interaction of Cyanobacteria with Nanometer and Micron Sized Polystyrene Particles in Marine and Fresh Water. *Langmuir*, *36*(14), 3963–3969. https://doi.org/10.1021/acs.langmuir.9b03644

Deppe, T., & Benndorf, J. (2002). Phosphorus reduction in a shallow hypereutrophic reservoir by in-lake dosage of ferrous iron. *Water Research*, *36*(18), 4525–4534. https://doi.org/10.1016/S0043-1354(02)00193-8

Di, M., Liu, X., Wang, W., & Wang, J. (2019). Manuscript prepared for submission to environmental toxicology and pharmacology pollution in drinking water source areas : Microplastics in the Danjiangkou Reservoir , China. *Environmental Toxicology and Pharmacology*, *65*, 82–89. https://doi.org/10.1016/j.etap.2018.12.009

Di, M., & Wang, J. (2018). Microplastics in surface waters and sediments of the Three Gorges Reservoir, China. *Science of the Total Environment*, *616-617*, 1620–1627. https://doi.org/10.1016/j.scitotenv.2017.10.150

Dietrich, W. E. (1982). Settling Velocity of Natural Particles. *Water Resources*, *18*(6), 1615–1626.

Dioses-Salinas, D. C., Pizarro-Ortega, C. I., & De-la Torre, G. E. (2020). A methodological approach of the current literature on microplastic contamination in terrestrial environments: Current knowledge and baseline considerations. *Science of The Total Environment*, *730*, 139164. https://doi.org/https://doi.org/10.1016/j.scitotenv.2020.139164

Dittrich, M., & Koschel, R. (2002). Interactions between calcite precipitation (natural and artificial) and phosphorus cycle in the hardwater lake. *Hydrobiologia*, *469*, 49–57. https://doi.org/10.1023/A:1015571410442

Drago, C., Pawlak, J., & Weithoff, G. (2020). Biogenic aggregation of small microplastics alters their ingestion by a common freshwater micro-invertebrate. *Frontiers in Environmental Science*, *8*, 1–11. https://doi.org/10.3389/fenvs.2020.574274

Dris, R., Gasperi, J., Mirande, C., Mandin, C., Guerrouache, M., Langlois, V., & Tassin, B. (2017). A first overview of textile fibers, including microplastics, in indoor and outdoor environments. *Environmental Pollution*, *221*, 453–458. https://doi.org/https://doi.org/10.1016/j.envpol.2016.12.013

Duis, K., & Coors, A. (2016). Microplastics in the aquatic and terrestrial environment: sources (with a specific focus on personal care products), fate and effects. *Environmental Sciences Europe*, *28*(1), 1–25. https://doi.org/10.1186/s12302-015-0069-y

Edlin, G., Lin, L., & Kudrna, R. (1975). Plastic films on the bottom of the Skagerack. *Nature*, *255*, 735–737. https://doi.org/10.1038/253600a0

Evans, S., & Todd, J. A. (1997). Late jurassic soft-bodied wood epibionts preserved by bioimmuration. *Lethaia*, *30*(3), 185–189. https://doi.org/https://doi.org/10.1111/j.1502-3931.1997.tb00459.x

Fazey, F. M., & Ryan, P. G. (2016). Biofouling on buoyant marine plastics: An experimental study into the effect of size on surface longevity. *Environmental Pollution*, *210*, 354–360. https://doi.org/10.1016/j.envpol.2016.01.026

Flemming, H. C., Neu, T. R., & Wozniak, D. J. (2007). The EPS matrix: The "House of Biofilm Cells". *Journal of Bacteriology*, *189*(22), 7945–7947. https://doi.org/10.1128/JB.00858-07

Flemming, H. C., & Wingender, J. (2010). The biofilm matrix. *Nature Reviews Microbiology*, *8*(9), 623–633. https://doi.org/10.1038/nrmicro2415

González-Pleiter, M., Velázquez, D., Edo, C., Carretero, O., Gago, J., Barón-Sola, Á., Hernández, L. E., Yousef, I., Quesada, A., Leganés, F., Rosal, R., & Fernández-Piñas, F. (2020). Fibers spreading worldwide: Microplastics and other anthropogenic litter in an Arctic freshwater lake. *Science of the Total Environment*, *722*, 137904. https://doi.org/10.1016/j.scitotenv.2020.137904

Grossart, H. P., & Simon, M. (1993). Limnetic macroscopic organic aggregates (lake snow): Occurrence, characteristics, and microbial dynamics in Lake Constance. *Limnology and Oceanography*, *38*(3), 532–546. https://doi.org/10.4319/lo.1993.38.3.0532

Grossart, H. P., Simon, M., & Logan, B. E. (1997). Formation of macroscopic organic aggregates (lake snow) in a large lake: The significance of transparent exopolymer particles, phytoplankton, and zooplankton. *Limnology and Oceanography*, *42*(8), 1651–1659. https://doi.org/10.4319/lo.1997.42.8.1651

Guerrero, R, Pedrós-Alió, C, Schmidt, T. M., & Mas, J. (1985). A survey of buoyant density of microorganisms in pure cultures and natural samples. *Microbiologia (Madrid, Spain)*, *1*(1-2), 53–65.

Ha, T., Id, N., Tang, F. H. M., & Maggi, F. (2020). Sinking of microbial-associated microplastics in natural waters, 1–20. https://doi.org/10.1371/journal.pone.0228209

Hartmann, N. B., Hüffer, T., Thompson, R. C., Hassellöv, M., Verschoor, A., Daugaard, A. E., Rist, S., Karlsson, T., Brennholt, N., Cole, M., Herrling, M. P., Hess, M. C., Ivleva, N. P., Lusher, A. L., & Wagner, M. (2019). Are we speaking the same language? Recommendations for a definition and categorization

framework for plastic debris. *Environmental Science and Technology*, *53*(3), 1039–1047. https://doi.org/10.1021/acs.est.8b05297

Hermsen, E., Mintenig, S. M., Besseling, E., & Koelmans, A. A. (2018). Quality criteria for the analysis of microplastic in biota samples: A critical review. *Environmental Science & Technology*, *52*(18), 10230–10240. https://doi.org/10.1021/acs.est.8b01611
doi: 10.1021/acs.est.8b01611

Hess, H., Ausich, W. I., Brett, C. E., & Simms, M. J. (1999). Lower jurassic posidonia shale of southern germany. *Fossil crinoids* (183–196). Cambridge University Press. https://doi.org/10.1017/CBO9780511626159.025

Hoellein, T., Rojas, M., Pink, A., Gasior, J., & Kelly, J. (2014). Anthropogenic litter in urban freshwater ecosystems: Distribution and microbial interactions. *PLoS ONE*, *9*(6). https://doi.org/10.1371/journal.pone.0098485

Hossain, M. R., Jiang, M., Wei, Q. H., & Leff, L. G. (2019). Microplastic surface properties affect bacterial colonization in freshwater. *Journal of Basic Microbiology*, *59*(1), 54–61. https://doi.org/10.1002/jobm.201800174

Huang, Y., Tian, M., Jin, F., Chen, M., Liu, Z., & He, S. (2020). Coupled effects of urbanization level and dam on microplastics in surface waters in a coastal watershed of Southeast China. *Marine Pollution Bulletin*, *154*, 111089. https://doi.org/10.1016/j.marpolbul.2020.111089

Hübner, M. K., Michler-Kozma, D. N., & Gabel, F. (2020). Microplastic concentrations at the water surface are reduced by decreasing flow velocities caused by a reservoir. *Fundamental and Applied Limnology / Archiv für Hydrobiologie*. https://doi.org/10.1127/fal/2020/1307

Jambeck, J. R., Geyer, R., Wilcox, C., Siegler, T. R., Perryman, M., Andrady, A., Narayan, R., & Law, K. L. (2015). Plastic waste inputs from land into the oceans. *Science*, *347*(6223), 768–771. https://doi.org/10.1126/science.1260352

Kaiser, D., Estelmann, A., Kowalski, N., Glockzin, M., & Waniek, J. J. (2019). Sinking velocity of sub-millimeter microplastic. *Marine Pollution Bulletin*, *139*, 214–220. https://doi.org/10.1016/j.marpolbul.2018.12.035

Kaiser, D., Kowalski, N., & Waniek, J. J. (2017). Effects of biofouling on the sinking behavior of microplastics. *Environmental Research Letters*, *12*(12). https://doi.org/10.1088/1748-9326/aa8e8b

Kanhai, L. D. K., Gardfeldt, K., Krumpen, T., Thompson, R. C., & O'Connor, I. (2020). Microplastics in sea ice and seawater beneath ice floes from the Arctic Ocean. *Scientific Reports*, *10*(1), 5004. https://doi.org/10.1038/s41598-020-61948-6

Kappler, A., Bryce, C., Mansor, M., Lueder, U., Byrne, J. M., & Swanner, E. D. (2021). An evolving view on biogeochemical cycling of iron. *Nature Reviews Microbiology*, (3). https://doi.org/10.1038/s41579-020-00502-7

Kesy, K., Labrenz, M., Scales, B. S., & Kreikemeyer, B. (2021). Vibrio colonization is highly dynamic in early microplastic-associated biofilms as well as on field-collected microplastics.

Kesy, K., Oberbeckmann, S., Kreikemeyer, B., & Labrenz, M. (2019). Spatial environmental heterogeneity determines young biofilm assemblages on microplastics in baltic sea mesocosms. *10*, 1–18. https://doi.org/10.3389/fmicb.2019.01665

Khatmullina, L., & Chubarenko, I. (2019). Transport of marine microplastic particles: why is it so difficult to predict? *Anthropocene Coasts*, *2*(1), 293–305. https://doi.org/10.1139/anc-2018-0024

Khatmullina, L., & Isachenko, I. (2017). Settling velocity of microplastic particles of regular shapes. *Marine Pollution Bulletin*, *114*(2), 871–880. https://doi.org/10.1016/j.marpolbul.2016.11.024

Koelmans, A. A., Kooi, M., Law, K. L., & van Sebille, E. (2017). All is not lost: Deriving a top-down mass budget of plastic at sea. *Environmental Research Letters*, *12*(11), 114028. https://doi.org/10.1088/1748-9326/aa9500

Köngeter, J. (2013). Der talsperrenbau in deutschland. *Talsperren in deutschland* (pp. 1–33). Springer.

Kooi, M., & Koelmans, A. A. (2019). Simplifying microplastic via continuous probability distributions for size, shape, and density. *Environmental Science & Technology Letters*, *6*(9), 551–557. https://doi.org/10.1021/acs.estlett.9b00379

Kooi, M., Van Nes, E. H., Scheffer, M., & Koelmans, A. A. (2017). Ups and Downs in the ocean: Effects of biofouling on vertical transport of microplastics. *Environmental Science and Technology*, *51*(14), 7963–7971. https://doi.org/10.1021/acs.est.6b04702

Kowalski, N., Reichardt, A., & Waniek, J. J. (2016). Sinking rates of microplastics and potential implications of their alteration by physical, biological, and chemical factors. *Marine Pollution Bulletin*, *109*(1), 310–319. https://doi.org/10.1016/j.marpolbul.2016.05.064

General overview, Metal adsorption section!!

Küchler-Krischun, J., & Kleiner, J. (1990). Heterogeneously nucleated calcite precipitation in Lake Constance. A short time resolution study. *Aquatic Sciences*, *52*(2), 176–197. https://doi.org/10.1007/BF00902379

Ladwig, R., Hanson, P. C., Dugan, H. A., Carey, C. C., Zhang, Y., Shu, L., Duffy, C. J., & Cobourn, K. M. (2021). Lake thermal structure drives interannual variability in summer anoxia dynamics in a eutrophic lake over 37 years. *Hydrology and Earth System Sciences*, *25*(2), 1009–1032. https://doi.org/10.5194/hess-25-1009-2021

Lagarde, F., Olivier, O., Zanella, M., Daniel, P., Hiard, S., & Caruso, A. (2016). Microplastic interactions with freshwater microalgae: Hetero-aggregation and changes in plastic density appear strongly dependent on polymer type. *Environmental Pollution*, *215*, 331–339. https://doi.org/10.1016/j.envpol.2016.05.006

Lee, B. D., Apel, W. A., & Walton, M. R. (2004). Screening of cyanobacterial species for calcification. *Biotechnology Progress*, *20*(5), 1345–1351. https://doi.org/10.1021/bp0343561

Li, C., Gan, Y., Dong, J., Fang, J., Chen, H., Quan, Q., & Liu, J. (2020). Impact of microplastics on microbial community in sediments of the Huangjinxia Reservoir—water source of a water diversion project in western China. *Chemosphere*, *253*, 126740. https://doi.org/https://doi.org/10.1016/j.chemosphere.2020.126740

Li, L., Geng, S., Wu, C., Song, K., Sun, F., Visvanathan, C., Xie, F., & Wang, Q. (2019a). Microplastics contamination in different trophic state lakes along the

middle and lower reaches of Yangtze River Basin. *Environmental Pollution*, *254*, 112951. https://doi.org/10.1016/j.envpol.2019.07.119

Li, S., Liu, H., Gao, R., Abdurahman, A., Dai, J., & Zeng, F. (2018). Aggregation kinetics of microplastics in aquatic environment: Complex roles of electrolytes, pH, and natural organic matter. *Environmental Pollution*, *237*, 126–132. https://doi.org/10.1016/j.envpol.2018.02.042

Li, Y., Wang, X., Fu, W., Xia, X., Liu, C., Min, J., Zhang, W., & Crittenden, J. C. (2019b). Interactions between nano/micro plastics and suspended sediment in water: Implications on aggregation and settling. *Water Research*, *161*, 486–495. https://doi.org/10.1016/j.watres.2019.06.018

Lin, L., Pan, X., Zhang, S., Li, D., Zhai, W., Wang, Z., Tao, J., Mi, C., Li, Q., & Crittenden, J. C. (2021). Distribution and source of microplastics in China's second largest reservoir - Danjiangkou Reservoir. *Journal of Environmental Sciences*, *102*, 74–84. https://doi.org/https://doi.org/10.1016/j.jes.2020.09.018

Linders, T., Infantes, E., Joyce, A., Karlsson, T., Ploug, H., Hassellöv, M., Sköld, M., & Zetsche, E.-M. (2018). Particle sources and transport in stratified Nordic coastal seas in the Anthropocene. *Elem Sci Anth*, *6*(1), 29. https://doi.org/10.1525/elementa.149

Liu, C., Qiu, J., Tang, Z., Hu, H., Meng, F., & Li, A. (2021). Effects of polystyrene microplastics on growth and toxin production of *Alexandrium pacificum*. *Toxins*, *13*(4). https://doi.org/10.3390/toxins13040293

Lobelle, D., & Cunliffe, M. (2011). Early microbial biofilm formation on marine plastic debris. *Marine Pollution Bulletin*, *62*(1), 197–200. https://doi.org/10.1016/j.marpolbul.2010.10.013

Lobelle, K. M. K. A. A., Delphine, Laufkötter, C., Jongedijk, C. E., Kehl, C., & van Sebille, E. (2021). Global modeled sinking characteristics of biofouled microplastic. *Journal of Geophysical Research: Oceans*.

Long, M., Moriceau, B., Gallinari, M., Lambert, C., Huvet, A., Raffray, J., & Soudant, P. (2015). Interactions between microplastics and phytoplankton aggregates: Impact on their respective fates. *Marine Chemistry*, *175*, 39–46. https://doi.org/10.1016/j.marchem.2015.04.003

Long, M., Paul-Pont, I., Hégaret, H., Moriceau, B., Lambert, C., Huvet, A., & Soudant, P. (2017). Interactions between polystyrene microplastics and marine phytoplankton lead to species-specific hetero-aggregation. *Environmental Pollution*, *228*, 454–463. https://doi.org/10.1016/j.envpol.2017.05.047

Mao, Y., Ai, H., Chen, Y., Zhang, Z., Zeng, P., Kang, L., Li, W., Gu, W., He, Q., & Li, H. (2018). Phytoplankton response to polystyrene microplastics: Perspective from an entire growth period. *Chemosphere*, *208*, 59–68. https://doi.org/10.1016/j.chemosphere.2018.05.170

Martinez, R. E., Gardés, E., Pokrovsky, O. S., Schott, J., & Oelkers, E. H. (2010). Do photosynthetic bacteria have a protective mechanism against carbonate precipitation at their surfaces? *Geochimica et Cosmochimica Acta*, *74*(4), 1329–1337. https://doi.org/10.1016/j.gca.2009.11.025

Mbedzi, R., Cuthbert, R. N., Wasserman, R. J., Murungweni, F. M., & Dalu, T. (2020). Spatiotemporal variation in microplastic contamination along a subtropical reservoir shoreline, 23880–23887.

McCave, I. N. (1984). Size spectra and aggregation of suspended particles in the deep ocean. *Deep Sea Research Part A, Oceanographic Research Papers*, *31*(4), 329–352. https://doi.org/10.1016/0198-0149(84)90088-8

McCormick, A., Hoellein, T. J., Mason, S. A., Schluep, J., & Kelly, J. J. (2014). Microplastic is an abundant and distinct microbial habitat in an urban river. *Environmental Science and Technology*, *48*(20), 11863–11871. https://doi.org/10.1021/es503610r

Meijer, L. J., van Emmerik, T., van der Ent, R., Schmidt, C., & Lebreton, L. (2021). More than 1000 rivers account for 80% of global riverine plastic emissions into the ocean. *Science Advances*, *7*(18).

Melton, E. D., Swanner, E. D., Behrens, S., Schmidt, C., & Kappler, A. (2014). The interplay of microbially mediated and abiotic reactions in the biogeochemical Fe cycle. *Nature Reviews Microbiology*, *12*(12), 797–808. https://doi.org/10.1038/nrmicro3347

Merz-Preiß, M., & Riding, R. (1999). Cyanobacterial tufa calcification in two freshwater streams: Ambient environment, chemical thresholds and biological pro-

cesses. *Sedimentary Geology*, *126*(1-4), 103–124. https://doi.org/10.1016/S0037-0738(99)00035-4

Miao, L., Yu, Y., Adyel, T. M., Wang, C., Liu, Z., Liu, S., Huang, L., You, G., Meng, M., Qu, H., & Hou, J. (2021). Distinct microbial metabolic activities of biofilms colonizing microplastics in three freshwater ecosystems. *Journal of Hazardous Materials*, *403*, 123577. https://doi.org/10.1016/j.jhazmat.2020.123577

Michels, J., Stippkugel, A., Lenz, M., Wirtz, K., & Engel, A. (2018). Rapid aggregation of biofilm-covered microplastics with marine biogenic particles. *Proceedings. Biological sciences*, *285*(1885), 20181203. https://doi.org/10.1098/rspb.2018.1203

Moreschi, A. C., Callil, C. T., Christo, S. W., Ferreira Junior, A. L., Nardes, C., de Faria, É., & Girard, P. (2020). Filtration, assimilation and elimination of microplastics by freshwater bivalves. *Case Studies in Chemical and Environmental Engineering*, *2*, 100053. https://doi.org/10.1016/j.cscee.2020.100053

Mortimer, C. H. (1942). The exchange of dissolved substances between mud and water in lakes. *Journal of Ecology*, *30*(1), 147–201.

Nakano, D., & Strayer, D. L. (2014). Biofouling animals in fresh water: Biology, impacts, and ecosystem engineering. *Frontiers in Ecology and the Environment*, *12*(3), 167–175. https://doi.org/10.1890/130071

Neu, T. R., Swerhone, G. D., & Lawrence, J. R. (2001). Assessment of lectin-binding analysis for in situ detection of glycoconjugates in biofilm systems. *Microbiology*, *147*(2), 299–313. https://doi.org/10.1099/00221287-147-2-299

Oberbeckmann, S., & Labrenz, M. (2020). Marine microbial assemblages on microplastics: Diversity, adaptation, and role in degradation. *Annual Review of Marine Science*, *12*, 209–232. https://doi.org/10.1146/annurev-marine-010419-010633

Oberbeckmann, S., Osborn, A. M., & Dunhaime, M. (2016). Microbes on a bottle: Substrate, season and geography influence community composition of microbes colonizing marine plastic debris. *PLoS ONE*, *11*(8), 1–24. https://doi.org/10.1371/journal.pone.0159289

Ogonowski, M., Motiei, A., Ininbergs, K., Hell, E., Gerdes, Z., Udekwu, K. I., Bacsik, Z., & Gorokhova, E. (2018). Evidence for selective bacterial community structuring on microplastics. *Environmental Microbiology*, *00*. https://doi.org/10.1111/1462-2920.14120

Oliver, R., Thomas, R., Reynold, C., & Walsby, A. (1985). The sedimentation of buoyant microcystis colonies caused by precipitation with an iron- containing colloid. *Proceedings of the Royal Society B*, *223*(1233), 511–528. https://doi.org/10.1098/rspb.1985.0016

Ortíz-Caballero, Z. K., Rentería-Villalobos, M., Montero-Cabrera, M. E., Manjón-Collado, G., Santellano-Estrada, E., & Rentería-Monterrubio, A. (2019). Fractionation of chemical species in surface water from El Granero reservoir, Chihuahua, Mexico. *Environmental Earth Sciences*, *78*(24), 1–13. https://doi.org/10.1007/s12665-019-8756-4

Osman-Sigg, G. K. (1982). *Kolloidale und suspendierte Teilchen in natürlichen Gewässern Partikelgrössenverteilung und natürliche Koagulation im Zürichsee* (Doctoral dissertation). https://doi.org/https://doi.org/10.3929/ethz-a-000250473Rights

Patzner, M. S., Mueller, C. W., Malusova, M., Baur, M., Nikeleit, V., Scholten, T., Hoeschen, C., Byrne, J. M., Borch, T., Kappler, A., & Bryce, C. (2020). Iron mineral dissolution releases iron and associated organic carbon during permafrost thaw. *Nature Communications*, *11*(1), 1–11. https://doi.org/10.1038/s41467-020-20102-6

PlasticsEurope. (2020). *Plastic-the Facts 2020* (tech. rep.).

Pojar, I., Stănică, A., Stock, F., Kochleus, C., Schultz, M., & Bradley, C. (2021). Sedimentary microplastic concentrations from the Romanian Danube River to the Black Sea. *Scientific Reports*, 1–9. https://doi.org/10.1038/s41598-021-81724-4

Porter, A., Lyons, B. P., Galloway, T. S., & Lewis, C. (2018). Role of marine snows in microplastic fate and bioavailability. *Environmental Science and Technology*, *52*(12), 7111–7119. https://doi.org/10.1021/acs.est.8b01000

Primpke, S., Christiansen, S. H., Cowger, W., Frond, H. D., Deshpande, A., Fischer, M., Holland, E. B., Meyns, M., O'Donnell, B. A., Ossmann, B. E., Pittroff,

M., Sarau, G., Scholz-Böttcher, B. M., & Wiggin, K. J. (2020). Critical assessment of analytical methods for the harmonized and cost-efficient analysis of microplastics. *Appl. Spectrosc.*, *74*(9), 1012–1047. http://as.osa.org/abstract.cfm?URI=as-74-9-1012

Quik, J. T., van De Meent, D., & Koelmans, A. A. (2014). Simplifying modeling of nanoparticle aggregation-sedimentation behavior in environmental systems: A theoretical analysis. *Water Research*, *62*, 193–201. https://doi.org/10.1016/j.watres.2014.05.048

Reiche, M., Lu, S., Ciobotă, V., Neu, T. R., Nietzsche, S., Rösch, P., Popp, J., & Küsel, K. (2011). Pelagic boundary conditions affect the biological formation of iron-rich particles (iron snow) and their microbial communities. *Limnology and Oceanography*, *56*(4), 1386–1398. https://doi.org/10.4319/lo.2011.56.4.1386

Riding, R. (2006). Cyanobacterial calcification, carbon dioxide concentrating mechanisms, and Proterozoic-Cambrian changes in atmospheric composition. *Geobiology*, *4*(4), 299–316. https://doi.org/10.1111/j.1472-4669.2006.00087.x

Risse-Buhl, U., Anlanger, C., Kalla, K., Neu, T. R., Noss, C., Lorke, A., & Weitere, M. (2017). The role of hydrodynamics in shaping the composition and architecture of epilithic biofilms in fluvial ecosystems. *Water Research*, *127*, 211–222. https://doi.org/10.1016/j.watres.2017.09.054

Romaní, A. M. (2010). Freshwater Biofilms. *Biofouling*, 137–153. https://doi.org/10.1002/9781444315462.ch10

Rosenhahn, A., Schilp, S., Kreuzer, H., & Grunze, M. (2010). The role of "inter" surface chemistry in marine biofouling prevention. *Physical Chemistry Chemical Physics*, *12*, 4275–4286. https://doi.org/10.1039/c004746p

Salta, M., Wharton, J. A., Blache, Y., Stokes, K. R., & Briand, J. F. (2013). Marine biofilms on artificial surfaces: Structure and dynamics. *Environmental Microbiology*, *15*(11), 2879–2893. https://doi.org/10.1111/1462-2920.12186

Schmidt, C., Kumar, R., Yang, S., & Büttner, O. (2020). Microplastic particle emission from wastewater treatment plant effluents into river networks in Germany: Loads, spatial patterns of concentrations and potential toxicity.

Science of The Total Environment, *737*, 139544. https://doi.org/https://doi.org/10.1016/j.scitotenv.2020.139544

Shams, M., Alam, I., & Chowdhury, I. (2020). Aggregation and Stability of Nanoscale Plastics in Aquatic Environment. *Water Research*, 115401. https://doi.org/10.1016/j.watres.2019.115401

Shang, Q. Q., Fang, H. W., Zhao, H. M., He, G. J., & Cui, Z. H. (2014). Biofilm effects on size gradation, drag coefficient and settling velocity of sediment particles. *International Journal of Sediment Research*, *29*(4), 471–480. https://doi.org/10.1016/S1001-6279(14)60060-3

Sigg, L., & Stumm, W. (2016). *Aquatische Chemie: Einführung in die Chemie natürlicher Gewässer*. vdf Hochschulverlag AG.

Stabel, H. (1986). Calcite precipitation in Lake Constance: Chemical equilibrium, sedimentation, and nucleation by algae. *Limnology and Oceanography*, *31*(5), 1081–1094. https://doi.org/10.4319/lo.1986.31.5.1081

Summers, S., Henry, T., & Gutierrez, T. (2018). Agglomeration of nano- and microplastic particles in seawater by autochthonous and de novo-produced sources of exopolymeric substances. *Marine Pollution Bulletin*, *130*, 258–267. https://doi.org/10.1016/j.marpolbul.2018.03.039

Sun, H., Jiao, R., & Wang, D. (2021). The difference of aggregation mechanism between microplastics and nanoplastics: Role of Brownian motion and structural layer force. *Environmental Pollution*, *268*, 115942. https://doi.org/10.1016/j.envpol.2020.115942

Tavşanoğlu, Ü. N., Başaran Kankılıç, G., Akca, G., Çırak, T., & Erdoğan, (2020). Microplastics in a dam lake in Turkey: type, mesh size effect, and bacterial biofilm communities. *Environmental Science and Pollution Research*, *27*(36), 45688–45698. https://doi.org/10.1007/s11356-020-10424-9

Teranes, J. L., McKenzie, J. A., Bernasconi, S. M., Lotter, A. F., & Sturm, M. (1999). A study of oxygen isotopic fractionation during bio-induced calcite precipitation in eutrophic Baldeggersee, Switzerland. *Geochimica et Cosmochimica Acta*, *63*(13-14), 1981–1989. https://doi.org/10.1016/S0016-7037(99)00049-6

Thompson, J. B., Schultze-Lam, S., Beveridge, T. J., & Des Marais, D. J. (1997). Whiting events: Biogenic origin due to the photosynthetic activity of cyanobacterial picoplankton. *Limnology and Oceanography*, *42*(1), 133–141.

Tianzhi, W., Yunkai, L., Mingchao, L., Peiling, Y., & Zhihui, B. (2014). Biofilms on the surface of gravels and aquatic plants in rivers and lakes with reusing reclaimed water. *Environmental Earth Sciences*, *72*(3), 743–755. https://doi.org/10.1007/s12665-013-2998-3

Tipping, E., Woof, C., & Cooke, D. (1981). Iron oxide from a seasonally anoxic lake. *Geochimica et Cosmochimica Acta*, *45*(9), 1411–1419. https://doi.org/10.1016/0016-7037(81)90275-1

Tu, C., Chen, T., Zhou, Q., Liu, Y., Wei, J., Waniek, J. J., & Luo, Y. (2020). Biofilm formation and its influences on the properties of microplastics as affected by exposure time and depth in the seawater. *Science of the Total Environment*, *734*. https://doi.org/10.1016/j.scitotenv.2020.139237

Turner, S., Horton, A. A., Rose, N. L., & Hall, C. (2019). A temporal sediment record of microplastics in an urban lake, London, UK. *Journal of Paleolimnology*, *61*(4), 449–462. https://doi.org/10.1007/s10933-019-00071-7

Van Sebille, E., Aliani, S., Law, K. L., Maximenko, N., Alsina, J. M., Bagaev, A., Bergmann, M., Chapron, B., Chubarenko, I., Cózar, A., Delandmeter, P., Egger, M., Fox-Kemper, B., Garaba, S. P., Goddijn-Murphy, L., Hardesty, B. D., Hoffman, M. J., Isobe, A., Jongedijk, C. E., … Wichmann, D. (2020). The physical oceanography of the transport of floating marine debris. *Environmental Research Letters*, *15*(2). https://doi.org/10.1088/1748-9326/ab6d7d

Vanderploeg, H. A., Eadie, B. J., Liebig, J. R., Tarapchak, S. J., & Glover, R. M. (1987). Contribution of calcite to the particle-size spectrum of Lake Michigan seston and its interactions with the plankton. *Canadian Journal of Fisheries and Aquatic Sciences*, *44*(11), 1898–1914. https://doi.org/10.1139/f87-234

Waldschläger, K., Lechthaler, S., Stauch, G., & Schüttrumpf, H. (2020). The way of microplastic through the environment – Application of the source-pathway-receptor model (review). *Science of the Total Environment*, *713*, 136584. https://doi.org/10.1016/j.scitotenv.2020.136584

Waldschläger, K., & Schüttrumpf, H. (2019a). Effects of particle properties on the settling and rise velocities of microplastics in freshwater under laboratory conditions. *Environmental Science and Technology*, *53*(4), 1958–1966. https://doi.org/10.1021/acs.est.8b06794

Waldschläger, K., & Schüttrumpf, H. (2019b). Erosion behavior of different microplastic particles in comparison to natural sediments. *Environmental Science & Technology*, *53*(22), 13219–13227. https://doi.org/10.1021/acs.est.9b05394

Wang, C., Xing, R., Sun, M., Ling, W., Shi, W., Cui, S., & An, L. (2020). Microplastics profile in a typical urban river in Beijing. *Science of The Total Environment*, *743*, 140708. https://doi.org/https://doi.org/10.1016/j.scitotenv.2020.140708

Wang, X., Bolan, N., Tsang, D. C. W., Sarkar, B., Bradney, L., & Li, Y. (2021). A review of microplastics aggregation in aquatic environment : Influence factors , analytical methods , and environmental implications. *Journal of Hazardous Materials*, *402*, 123496. https://doi.org/10.1016/j.jhazmat.2020.123496

Watkins, L., McGrattan, S., Sullivan, P. J., & Walter, M. T. (2019). The effect of dams on river transport of microplastic pollution. *Science of the Total Environment*, *664*, 834–840. https://doi.org/10.1016/j.scitotenv.2019.02.028

Watts, A. J., Lewis, C., Goodhead, R. M., Beckett, S. J., Moger, J., Tyler, C. R., & Galloway, T. S. (2014). Uptake and retention of microplastics by the shore crab carcinus maenas. *Environmental Science and Technology*, *48*(15), 8823–8830. https://doi.org/10.1021/es501090e

Weitere, M., Erken, M., Majdi, N., Arndt, H., Norf, H., Reinshagen, M., Traunspurger, W., Walterscheid, A., & Wey, J. K. (2018). The food web perspective on aquatic biofilms. *Ecological Monographs*, *88*(4), 543–559.

Woodall, L. C., Sanchez-Vidal, A., Canals, M., Paterson, G. L., Coppock, R., Sleight, V., Calafat, A., Rogers, A. D., Narayanaswamy, B. E., & Thompson, R. C. (2014). The deep sea is a major sink for microplastic debris. *Royal Society Open Science*, *1*(4). https://doi.org/10.1098/rsos.140317

Microplastic in deep sea sediments

Wu, X., Pan, J., Li, M., Li, Y., Bartlam, M., & Wang, Y. (2019). Selective enrichment of bacterial pathogens by microplastic biofilm. *Water Research*, *165*, 114979. https://doi.org/10.1016/j.watres.2019.114979

Yan, M., Wang, L., Dai, Y., Sun, H., & Liu, C. (2021). Behavior of microplastics in inland waters: Aggregation, settlement, and transport. *Bulletin of Environmental Contamination and Toxicology*, (0123456789). https://doi.org/10.1007/s00128-020-03087-2

Ye, S., & Andrady, A. L. (1991). Fouling of floating plastic debris under Biscayne Bay exposure conditions. *Marine Pollution Bulletin*, *22*(12), 608–613. https://doi.org/10.1016/0025-326X(91)90249-R

Záray, G., Kröpfl, K., Szabó, K., Taba, G., Ács, É., Berlinger, B., Dogan, M., Salih, B., & Akbulut, A. (2005). Comparison of freshwater biofilms grown on polycarbonate substrata in Lake Velence (Hungary) and Lake Mogan (Turkey). *Microchemical Journal*, *79*(1-2), 145–148. https://doi.org/10.1016/j.microc.2004.08.012

Zettler, E. R., Mincer, T. J., & Amaral-Zettler, L. A. (2013). Life in the "plastisphere": Microbial communities on plastic marine debris. *Environmental Science and Technology*, *47*(13), 7137–7146. https://doi.org/10.1021/es401288x

Zhang, F., Wang, Z., Wang, S., Fang, H., & Wang, D. (2019). Aquatic behavior and toxicity of polystyrene nanoplastic particles with different functional groups: Complex roles of pH, dissolved organic carbon and divalent cations. *Chemosphere*, *228*, 195–203. https://doi.org/10.1016/j.chemosphere.2019.04.115

Zhao, S., Danley, M., Ward, J. E., Li, D., & Mincer, T. J. (2017). An approach for extraction, characterization and quantitation of microplastic in natural marine snow using Raman microscopy. *Analytical Methods*, *9*(9), 1470–1478. https://doi.org/10.1039/c6ay02302a

Zhao, S., Ward, J. E., Danley, M., & Mincer, T. J. (2018). Field-Based evidence for microplastic in marine aggregates and mussels: Implications for trophic transfer. *Environmental Science and Technology*, *52*(19), 11038–11048. https://doi.org/10.1021/acs.est.8b03467

Zhiyao, S., Tingting, W., Fumin, X., & Ruijie, L. (2008). A simple formula for predicting settling velocity of sediment particles. *Water Science and Engineering*, *1*(1), 37–43. https://doi.org/10.1016/s1674-2370(15)30017-x

Zippel, B., & Neu, T. R. (2011). Characterization of glycoconjugates of extracellular polymeric substances in tufa-associated biofilms by using fluorescence lectin-binding analysis. *Applied and Environmental Microbiology*, *77*(2), 505–516. https://doi.org/10.1128/AEM.01660-10

Appendices

Appendix A

Supplementary Information for Chapter 2

Interaction of cyanobacteria with calcium facilitates the sedimentation of microplastics in a eutrophic reservoir

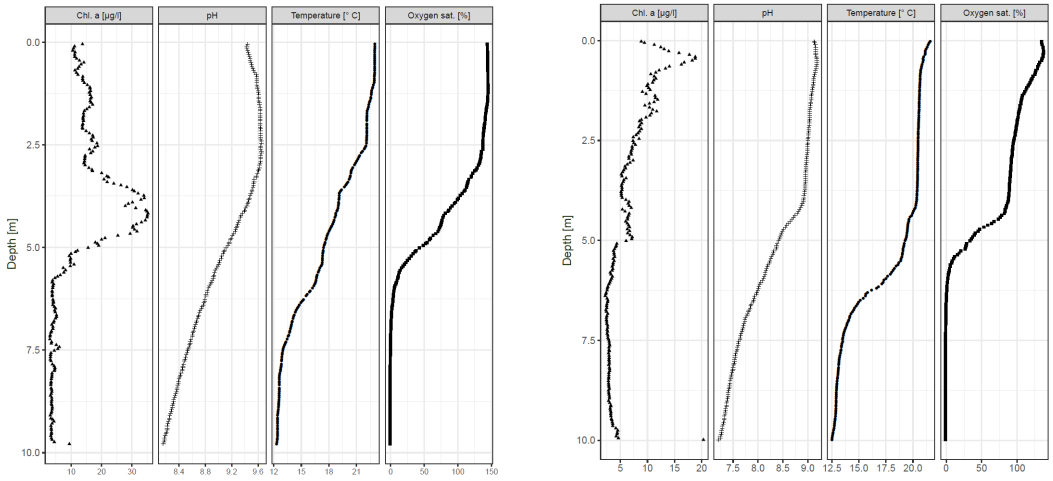

(a) (b)

Figure S 1: Water data of Bautzen reservoir at the beginning in July (a) and the end of the experiment in August (b). Data were acquired employing a multi-parameter probe right beneath the incubation cage. Note the different scales.

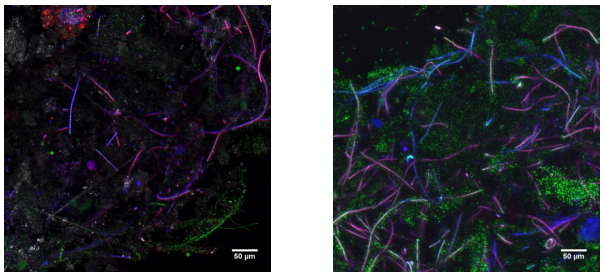

(a) (b)

Figure S 2: CLSM images of (a) biofilms grown on the inner walls of the incubation cage; (b) biofilms grown on PE particle. The colors indicate for, green: bacteria; blue: algae; pink: cyanobacteria. Scale bar has a length of 50 µm.

Table S 1: Excitation and emission wavelengths used for visualization of biofilm components or specific fluorescent molecules via CLSM.

Compound/Component	Excitation	Emission
SybrGreen	561 nm	510 - 580 nm
Phycobilins (autofluorescence)	633 nm	575 - 650
Chlorophyll *a*	633 nm	650 - 720 nm
Calcein	490 nm	505 - 560 nm
iDye PolyPink	560 nm	650 - 720 nm
Reflection	490 nm	480 -500 nm

Bioinformatics procedure

Produced paired-end reads which passed Illumina's chastity filter were subject to de-multiplexing and trimming of Illumina adaptor residuals using Illumina's real time analysis software included in the MiSeq reporter software v2.6. Quality of the reads was checked with FastQC version 0.11.8 (http://www.bioinformatics.babraham.ac.uk/projects/fastqc/). Locus specific primers were trimmed from the sequencing reads with cutadapt v2.3 (Martin, 2011). Paired-end reads were discarded if the primer could not be trimmed. Remaining sequences were merged, quality-filtered and further processed with USEARCH version 11.0.667 (Edgar, 2010). Low-quality reads (expected error >1) and reads with ambiguous

bases or outliers regarding the amplicon size distribution were discarded. Remaining reads were denoised using the UNOISE algorithm (Edgar, 2016b) implemented in USEARCH to form operational taxonomic units (OTUs, >97 % similarity) discarding singletons and chimeras in the process. The resulting OTU abundance table was filtered for possible bleed-in contaminations using the UNCROSS algorithm (Edgar, 2018) and abundances were adjusted for 16S copy numbers using the UNBIAS algorithm (Edgar, 2017). OTUs were compared against the reference sequences of the RDP 16S database (Cole et al., 2014) and taxonomies were predicted considering a minimum confidence threshold of 0.5 using the SINTAX algorithm (Edgar, 2016a) implemented in USEARCH. Libraries, sequencing and data analysis described in this section were performed by Microsynth AG (Balgach, Switzerland).

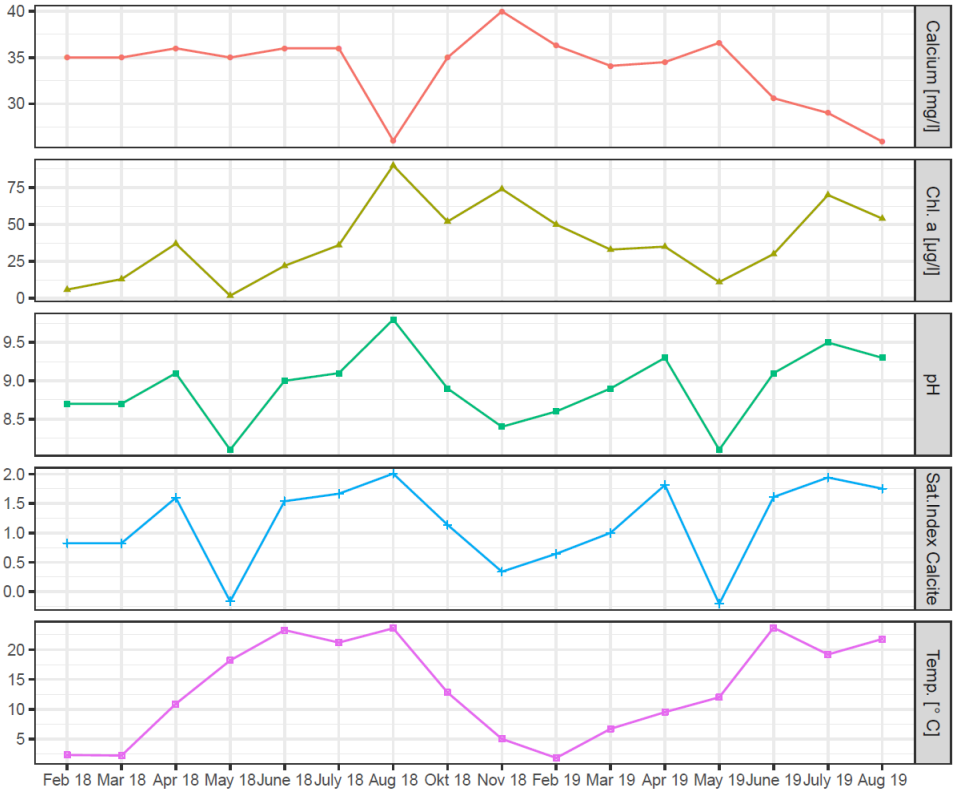

Figure S 3: Water parameters in Bautzen reservoir during the years 2018 and 2019. Chl.a: Chlorophyll a, Temp.: Temperature. Most data were provided by Landestalsperrenverwaltung Saxony which conducts sampling of Bautzen reservoir in monthly intervals. Calcite saturation indices were calculated using Visual MINTEQ using the provided water data.

Table S 2: Sediment traps data from Bautzen reservoir during the ice-free season in 2018. Data from end of August to September were lost due to sampling error. n.d.: not determined. For each measurement mean and standard deviation of three pseudo replicates are given.

Incubation time	Sedimentation rate [g m^{-2} a^{-1}]	Particulate organic carbon content [mg l^{-1}]	Particulate nitrogen content [mg l^{-1}]	Ca content of dry material [mg g^{-1}]
05/12/18-06/13/18	4403 ± 118.9	74 ± 4.2	11 ± 0.3	n.d.
06/13/18-07/11/18	3609 ± 79.5	78 ± 3.5	11 ± 0.3	8.6
07/11/18-08/14/18	4873 ± 17.3	126 ± 3.1	14 ± 0.4	63.1
09/19/18-11/01/18	25907 ± 635.9	676 ± 10.6	104 ± 1.0	n.d.

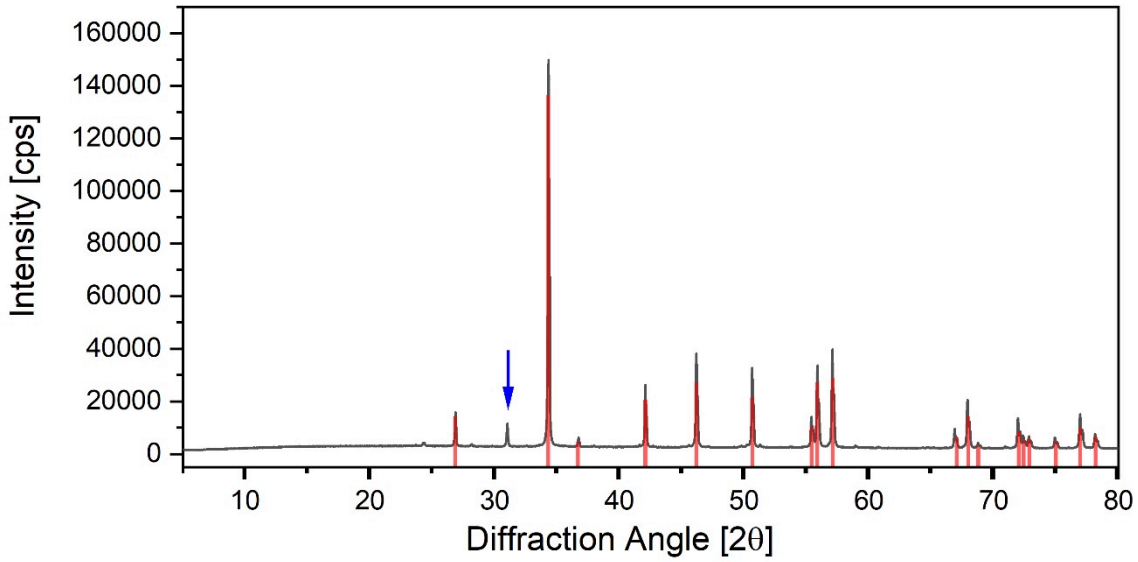

Figure S 4: X-ray diffractogram of the biofilms from Bautzen reservoir, identifying calcite (red: theoretical peak positions and intensities) and very low amount of quartz (indicated by blue arrow).

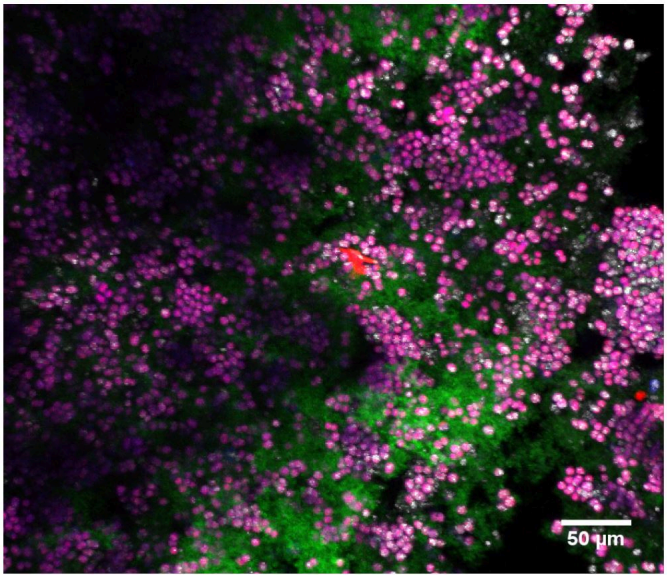

Figure S 5: Cyanobacterial aggregate formed in 60 mg l^{-1} Ca^{2+} approach containing PE microplastic. Colors indicate for, green: calcein; red: PE; pink: cyanobacteria. Scale bar has a length of 50 µm.

Figure S 6: Surface water of Bautzen reservoir on August 21 in 2019 showing elevated concentrations of planktonic cyanobacteria.

Appendix B

Supplementary Information for Chapter 3

Biofouling, metal sorption and aggregation are related to sinking of microplastics in a stratified reservoir

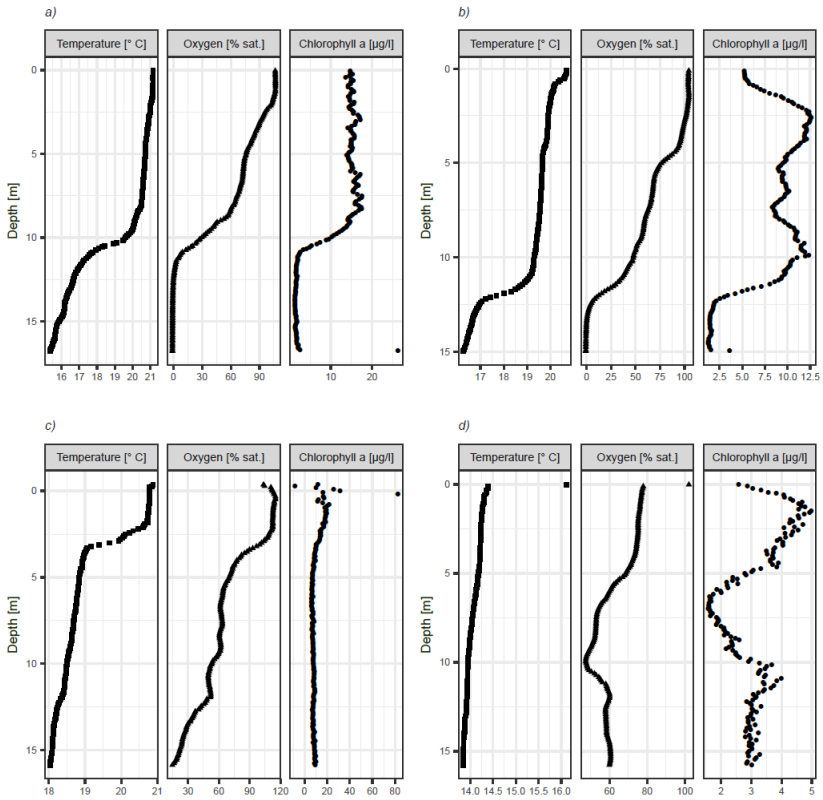

Figure S 1: Probe data displaying the conditions for temperature, chlorophyll a and oxygen within the water column of Malter reservoir. Four different dates are displayed ranging from begin of exposure at August 30 (a), first sampling date at September 5 (b), second sampling date at September 21 (c) and the last sampling date at October 16 (d) 2018.

Table S 1: Water parameters of Malter reservoir measured in monthly intervals by the Landestalsperrenverwaltung des Freistaates Sachsen. Abbreviations are Temp: Temperature; sat.: Saturation; Turb: Turbidity; Chl.a: Chlorophyll a; n.d.: No data. Depths of 1 m, 8 m and 16 m are displayed.

Date	Depth [m]	Temp. [%]	O_2 sat.	pH [860 nm]	Turb. [mg l^{-1}]	P_{total} [mg l^{-1}]	Nitrate [mg l^{-1}]	Iron [µg l^{-1}]	Chl.a [10^6 cells l^{-1}]	Cyanobacteria
10.04.2018	1	10.8	108	7.6	2.1	0.048	4.7	0.032	7.1	0
13.05.2018	1	12.4	106	7.6	2.9	0.052	4.3	0.022	11	0.025
19.06.2018	1	25	142	9	2.5	0.061	3	0.019	28	0
08.07.2018	1	22.2	110	8.6	3.1	0.054	2.5	0.023	25	0143
21.08.2018	1	20.8	104	8.4	2.8	0.092	1.7	0.019	18	2.28
11.09.2018	1	19.2	72	7.5	9.3	n.d.	n.d.	0.018	20	15.4
09.10.2018	1	13.8	83	7.4	9.1	0.095	1.3	0.038	20	12.1
12.11.2018	1	9.4	74	7.5	4.6	0.066	1.1	0.013	12	1
Date	Depth [m]	Temp. [%]	O_2 sat.	pH [860 nm]	Turb. [mg l^{-1}]	P_{total} [mg l^{-1}]	Nitrate [mg l^{-1}]	Iron [µg l^{-1}]	Chl.a [10^6 cells l^{-1}]	Cyanobacteria
10.04.2018	8	8.2	95	7.1	2.5	n.d.	n.d.	n.d.	n.d.	n.d.
13.05.20188	10.9	84	7.3	3.6	n.d.	n.d.	n.d.	n.d.	n.d.	n.d.
19.06.2018	8	15.5	72	7.1	1.2	n.d.	n.d.	n.d.	n.d.	n.d.
08.07.2018	8	17.1	41	7.6	1.7	n.d.	n.d.	n.d.	n.d.	n.d.
21.08.2018	8	19.8	23	6.8	1.3	n.d.	n.d.	n.d.	n.d.	n.d.
11.09.2018	8	19.2	72	7.5	8.9	n.d.	n.d.	n.d.	n.d.	n.d.
09.10.2018	8	13.8	82	7.4	9	n.d.	n.d.	n.d.	n.d.	n.d.
12.11.2018	8	9.4	73	7.4	4.9	n.d.	n.d.	n.d.	n.d.	n.d.
Date	Depth [m]	Temp. [%]	O_2 sat.	pH [860 nm]	Turb. [mg l^{-1}]	P_{total} [mg l^{-1}]	Nitrate [mg l^{-1}]	Iron [µg l^{-1}]	Chl.a [10^6 cells l^{-1}]	Cyanobacteria
10.04.2018	16	7.7	90	7	4.5	0.051	4.9	0.042	4	n.d.
13.05.20188	16	9.6	69	6.8	5.1	0.047	4.3	0.037	1.5	n.d.
19.06.2018	16	12.5	47	6.7	5.1	0.051	3.4	0.022	1.3	n.d.
08.07.2018	16	13.1	21	6.7	3.3	0.051	2.7	0.027	1.4	n.d.
21.08.2018	16	14.7	7	6.7	1.3	0.051	2.3	0.097	1.4	n.d.
11.09.2018	16	18.1	6	6.9	15	n.d.	n.d.	0.19	5	n.d.
09.10.2018	16	13.3	71	7.3	14	0.13	1.2	0.13	12	n.d.
12.11.2018	16	9	71	7.4	12	0.082	1.1	0.034	13	n.d.

Table S 2: Densities used for the calculation of fouling film thickness and mass needed to sink a PE particle (4 x 4 x 0.5 mm, mass: 2.2 mg) calculated using equations 1 & 2. a: Cornell and Schwertmann, 2003, b: Heidorn et al., 1996,c:Chubarenko et al., 2016, d: Besseling et al., 2017, e: Kooi et al., 2017

Fouling material	Specific density of fouling film material [kg m^{-3}]	Fouling film thickness to reach ρ_{water} [m]	Fouling film mass per mg particle weight to reach ρ_{water} [µg mg^{-1}]
Ferrihydrite	3960[a]	$2.03*10^{-6}$	58
Magnetite	5180[a]	$1.44*10^{-6}$	54
Mn Oxide	5030[b]	$1.49*10^{-6}$	55
Bacteria	1500[c]	$1.2*10^{-5}$	131
	1388[d]	$1.5*10^{-5}$	156
	1250[e]	$2.4*10^{-5}$	218

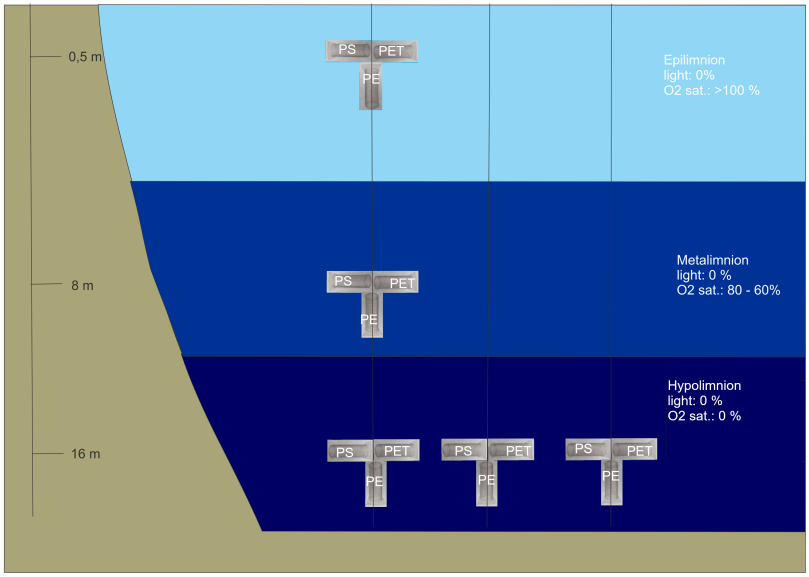

Figure S 2: Experimental set-up in Malter reservoir. Three different cages either containing PE or PET or PS tethered to ropes in different depths. In hypolimnion 3 x 3 cages were used in order to avoid disturbance of the microbial community by oxygen.

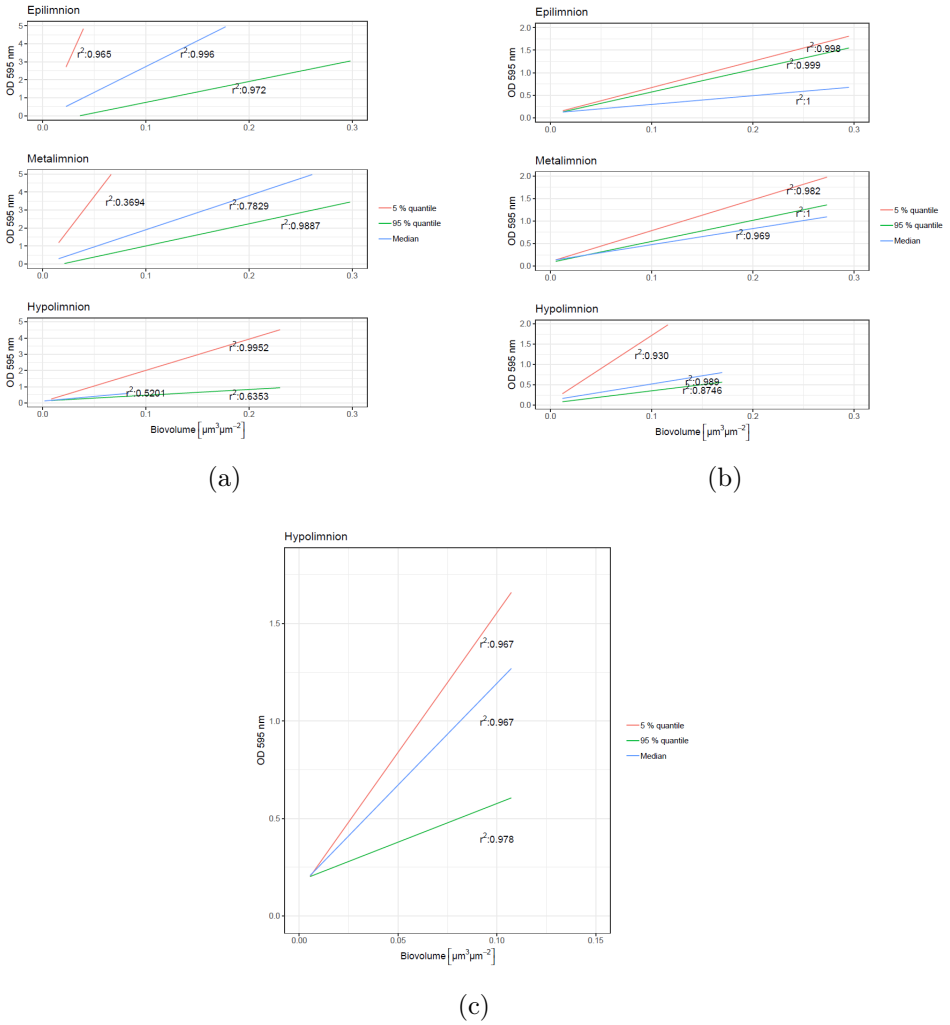

Figure S 3: Linear relationship between total biovolume (sum of algae, bacteria and cyanobacteria biovolume) of cells measured via CLSM and their corresponding biomass measured via crystal violet staining ($OD_{595\ nm}$) on a) PE; b) PET and c) PS. In every incubation depth three different regression lines were obtained for the 5 % quantile; 50 % quantile (Median) and the 95 % quantile for the respective polymers. The regression formulas were calculated using the values from different sampling days. In the case of PET the total biovolume did not increase much for the 95 % quantiles during day 6 and day 22 but strongly increased from day 22 to day 47. This resulted in a formular with higher steepness than the formula calculated for the median. Therefore, the 95 % quantiles graph is laying atop of the median graph in epilimnion and metalimnion.

Table S 3: Linear regression of $OD_{595\ nm}$ and the total biovolume. The r^2 and the plotted regression lines are shown in figure 2. E: Eplimnion; M: Metalimnion; H: Hypolimnion.

PE Depth	Median	Lower CI. [5 %]	Upper CI. [95 %]
E	OD_{595nm}=28.61*Total Biovolume-0.1301	OD_{595nm}=126.18*Total Biovolume-0.1482	OD_{595nm}=11.59*Total Biovolume-0.4144
M	OD_{595nm}=19.00*Total Biovolume+0.0280	OD_{595nm}=12.32*Total Biovolume-0.2287	OD_{595nm}=12.32*Total Biovolume-0.2287
H	OD_{595nm}=5.77*Total Biolvolume+0.0861	OD_{595nm}=3.54*Total Biovolume+12.41	OD_{595nm}=3.54*Total Biovolume+0.1241
PET Depth	Median	Lower CI. [5 %]	Upper CI. [95 %]
E	OD_{595nm}=1.94*Total Biovolume+0.1019	OD_{595nm}=5.85*Total Biovolume+0.0846	OD_{595nm}=5.01*Total Biovolume+0.0700
M	OD_{595nm}=3.56*Total Biovolume+0.1191	OD_{595nm}=6.85*Total Biovolume+0-1014	OD_{595nm}=4.68*Total Biovolume+0.0780
H	OD_{595nm}=4.04*Total Biovolume+0.1163	OD_{595nm}=16.27*Total Biovolume + 0.0884	OD_{595nm}=3.05*Total biovolume + 0.0470
PS Depth	Median	Lower CI. [5 %]	Upper CI. [95 %]
H	OD_{595nm}=10.44*Total Biovolume+0.1496	OD_{595nm}=14.32*Total Biovolume+0.1233	OD_{595nm}=3.96*Total Biovolume+0.1801

Table S 4: Bootstrapped median sinking velocity of PS and PET measured for each sampling date and depth. The median was rounded up to the fourth digit; the lower and upper border of the 95 % confidence interval is given within the brackets. The sample size is given in Figure 4 (of Chapter 4). The sinking velocity for the controls (pristine particles) were PS 0.0076 [0.0075, 0.0076] m s^{-1} and PET 0.0283 [0.0281, 0.0284] m s^{-1}.

Sinking velocity [m s^{-1}]			
Epilimnion Polymer	Day 6	Day 22	Day 47
PS	0.0079 [0.0078,0.0081]	0.0082[0.0079,0.0087]	0.074[0.0073,0.0076]
PET	0.0281[0.0280,0.0282]	0.0281[0.0280,0.0282]	0.0278[0.0271,0.0282]
Metalimnion Polymer	Day 6	Day 22	Day 47
PS	0.0078[0.0077,0.0078]	0.0079[0.0075,0.0085]	0.0073[0.0071,0.0076]
PET	0.0284[0.0282,0.0286]	0.0281[0.0280,0.0282]	0.0273[0.0265,0.0281]
Hypolimnion Polymer	Day 6	Day 22	Day 47
PS	0.0076[0.0076,0.0076]	0.007[0.0076,0.0077]	0.0076[0.0075,0.0078]
PET	0.0284[0.0283,0.0286]	0.0281[0.0279,0.0283]	0.0277[0.0.0270,0.0285]

Appendix C

Supplementary Information for Chapter 4

Burial of microplastics in freshwater sediments facilitated by iron-organo flocs

Table S 1: Water parameters of Bautzen reservoir surface water before and after the addition of various concentrations of $FeSO_4$ x 9 H_2O.

Parameter	Bautzen reservoir water before Fe precipitation	after 100 µM Fe addition	after 300 µM Fe addition	Unit
pH	9.5	7.7	7.7	-
total inorganic carbon	16.7	16.6	12.0	mg l^{-1}
dissolved organic carbon	7.24	4.96	4.45	mg l^{-1}
$Mn_{diss.}$	<0.007	0.027	0.125	mg l^{-1}
$Fe_{diss.}$	0.015	0.084	0.024	mg l^{-1}
total phosphorous	0.13	0.027	0.029	mg l^{-1}
TNb	1.69	1.21	1.09	mg l^{-1}
$NO_{3\text{-}N}$	0.740	0.542	0.564	mg l^{-1}
$NH_{4\text{-}N}$	0.238	<0.010	<0.013	mg l^{-1}
SRP	0.083	<0.003	<0.003	mg l^{-1}
SI	3.77	3.48	3.40	mg l^{-1}

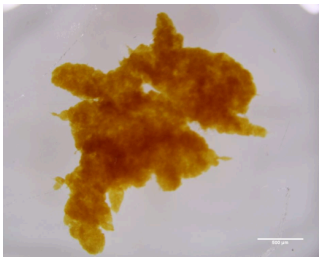

(a) Scale bar: 1000 µm

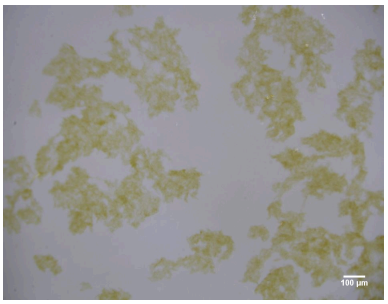

(b) Scale bar: 100 µm

Figure S 1: Flocs formed after the addition of 300 µM (a) and 100 µM $FeSO_4$ (b) in water from Bautzen reservoir

Table S 2: Microplastic content of iron flocs formed after the addition 300 µM or 100 µM $FeSO_4$. Displayed are the means ± standard deviations of 3 individual replicates.

Microplastics	Fe concentration in bottle [µM]	Plastic particles incorporated	Wet weight of precipitated flocs [mg]
Fibers	300	1948±148 (37%)	1057±197
Spheres	300	11775±1010 (99%)	1604±23
Fragments 10 – 100 µm	300	8810±1763 (27%)	727±62
Fragments 100 -250 µm	300	255±142 (16%)	1065±155
Fragments 250 - 500 µm	300	8±1 (4%)	997±104
Fragments > 500 µm	300	1±1 (1%)	978±117
Spheres	100	3275±1735 (28%)	442±88

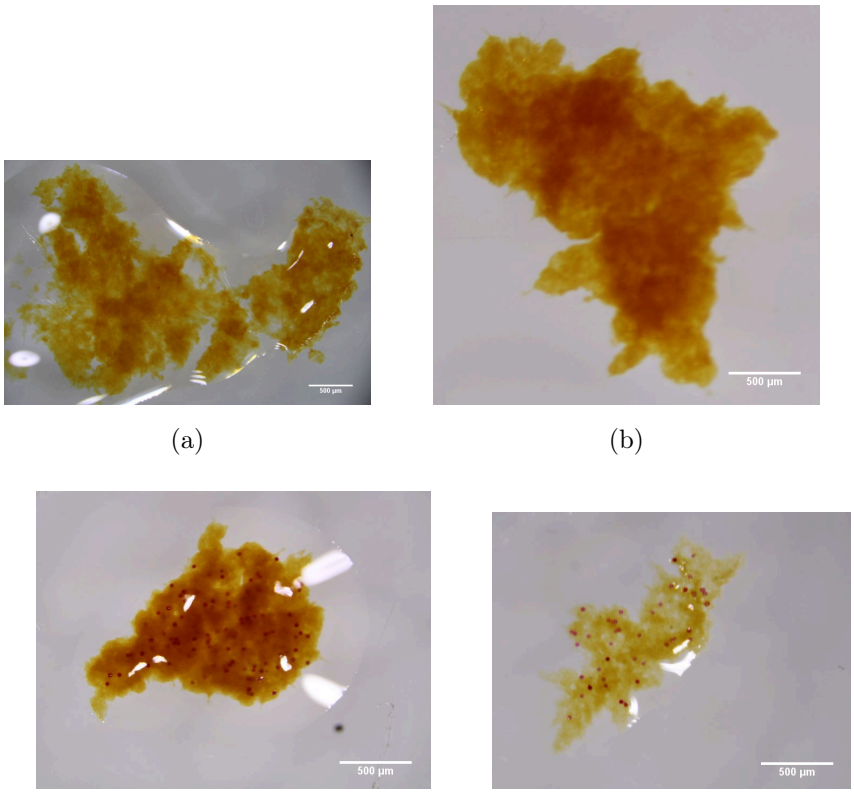

(a) (b)

(c) (d)

Figure S 2: Representative images of flocs formed by addition of different MP shapes and Fe concentrations, with a) showing 300 µM Fe and fibers, b) 300 µM Fe and small Fragments (10-100 µm), c) 300 µM Fe and spheres and d) 100 µM Fe and spheres.

Table S 3: Grain size distribution of 2 sediment cores from Bautzen reservoir. Sediments were classified according to [1] with grain sizes < 6 µm defined as clay, 6 – 63 µm defined as silt and 63 - 2000 µm defined as sand.

Depth	Clay [%]	Silt [%]	Sand [%]
0 - 2 cm	2.72 ± 0.28	82.56 ± 2.67	13.96 ± 2.79
2 – 5cm	2.40 ± 0.75	78.58 ± 1.24	19.02 ± 0.64
5 – 8 cm	3.53 ± 0.35	90.035 ± 0.20	6.43 ± 0.52
8 – 11 cm	3.54 ± 0.27	91.13 ± 0.58	5.33 ± 0.46

Table S 4: Physical properties of two sediment cores from Bautzen reservoir. The mean and standard deviation of 5 replicates per core (n: 10) are reported.

Depth	Density [kg m^{-3}]	Water content [%]	Dry mass [%]	Ash mass [%]
0 – 2 cm	1.079 ± 0.018	92.97 ± 0.36	7.03 ± 0.36	5.59 ± 0.31
2 – 5cm	1.089 ± 0.013	92.42 ± 0.09	7.57 ± 0.09	5.91 ± 0.20
5 – 8 cm	1.108 ± 0.025	85.31 ± 0.08	14.69 ± 0.08	12.92 ± 0.31
8 – 11 cm	1.132 ± 0.024	86.431 ± 0.52	13.57 ± 0.52	12.25 ± 0.49

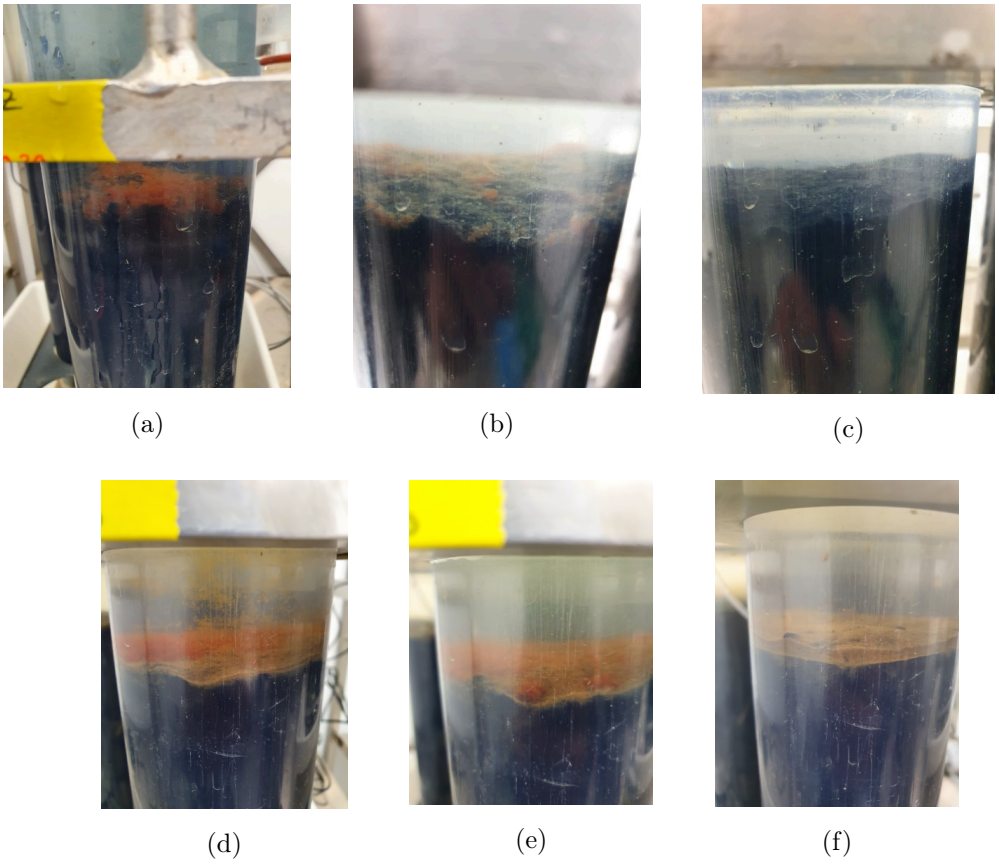

(a) (b) (c) (d) (e) (f)

Figure S 3: Anoxic (a)-(c) and oxic (d)-(f) sediment cores from October experiment with added iron flocs, shortly after addition (a, d), 24h after addition (b, e) and 6 days after addition (c, f).

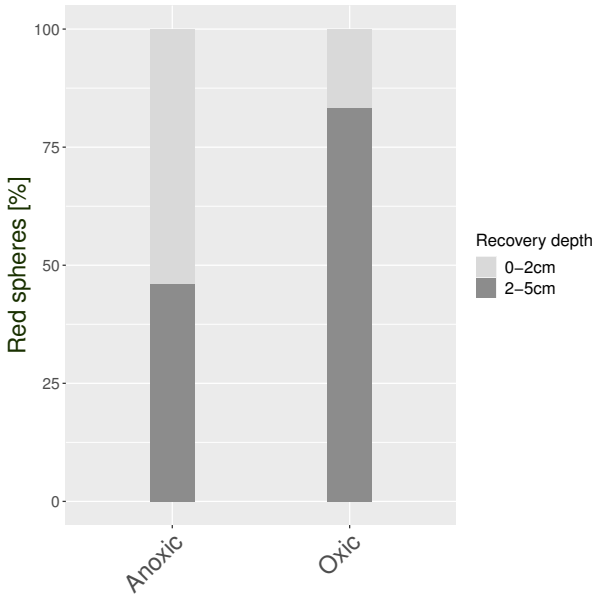

Figure S 4: Relative depth distribution of the red spheres (300 µM flocs) in the July experiment. Displayed are the means of anoxic (n:2) and oxic cores (n:3).

Table S 5: Recovery of MP spheres from sediment cores. N.a.: not available, this term is used for the cores from July 2020, were not yellow spheres were added. The status released refers to spheres found in the water phase, whereas in sediment refers to spheres extracted from the sediments after ending the experiment.

Core	Date	Status	red spheres released	red spheres in sediment	yellow spheres released	yellow spheres in sediment
1	July	anoxic	75	4862	n.a.	n.a.
2	July	anoxic	100	1303	n.a.	n.a.
3	October	anoxic	37	3835	2	18
4	October	anoxic	38	2670	99	869
5	October	anoxic	65	2949	2	7
6	July	oxic	52	5237	n.a.	n.a.
7	July	oxic	25	4477	n.a.	n.a.
8	July	oxic	68	3477	n.a.	n.a.
9	October	oxic	22	9496	146	2522
10	October	oxic	23	6677	166	2256
11	October	oxic	21	3897	87	146

Figure S 5: Oxic core from the October experiment, showing the burrowing of a chironomid larvae close to the walls of the core.

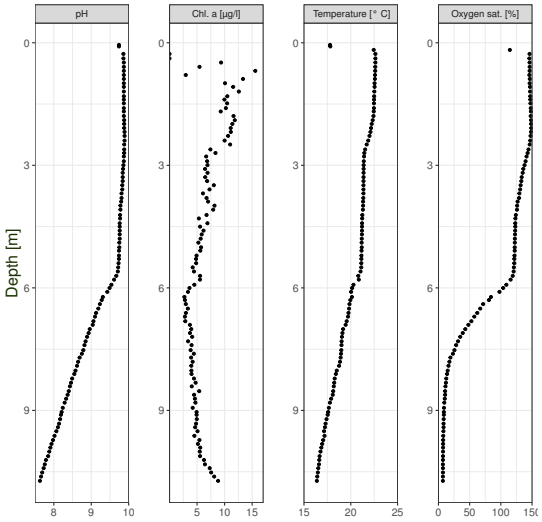

(a)

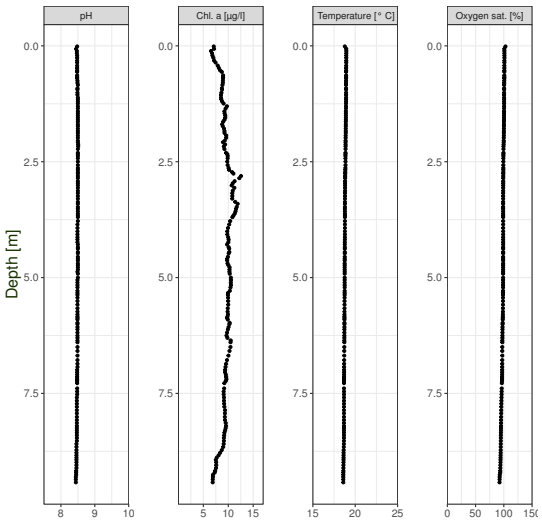

(b)

Figure S 6: Probe profiles showing water parameters in Bautzen reservoir during summer stratification in July 2020 (a) and after lake mixing in September 2020 (b).

Table S 6: Excitation and emission wavelengths used for visualization of biofilm components or specific fluorescent molecules via CLSM.

Compound/Component	Excitation	Emission
SybrGreen	561 nm	510-580 nm
Phycobilins	633 nm	575-650 nm
Chlorophyll a	633 nm	650-720 nm
AAL	633 nm	647 nm
Reflection	490 nm	480-500 nm

Appendix D

Supplementary Information for Chapter 5

Iron reduction by Shewanella oneidensis does not release microplastics from organo-metallic aggregates

Table S 1: Data used to construct Figure 2, presented are numbers PE spheres found either within the flocs or being released to the water phase. Further Fe(II) released to the water phase and Fe(II) or Fe(III) within the flocs normalized to µmol are shown for the individual microcosms of each sampling date.

Time	MP released [n]	MP retained [n]	Fe(II) in water [µmol]	Fe(II) in flocs [µmol]	Fe(III) in flocs [µmol]
Day 0	4	1040	4.06	2.28	3683
	2	1010	4.06	2.22	45.47
	1	1230	4.06	2.17	50.14
Day 20	0	650	5.67	2.98	7.26
	5	590	7.32	1.99	3.89
	8	540	6.80	1.77	3.48
Day 40	8	485	6.04	2.40	7.15
	9	535	6.49	2.20	11.1
	2	540	6.74	3.10	10.74
Day 60	12	707	2.65	16.44	0.72
	5	511	2.89	9.34	8.91
	11	341	2.87	5.74	4.35
Day 120	58	1288	5.23	7.20	1.25
	20	762	5.47	5.32	3.84
	15	1146	5.18	6.16	3.12

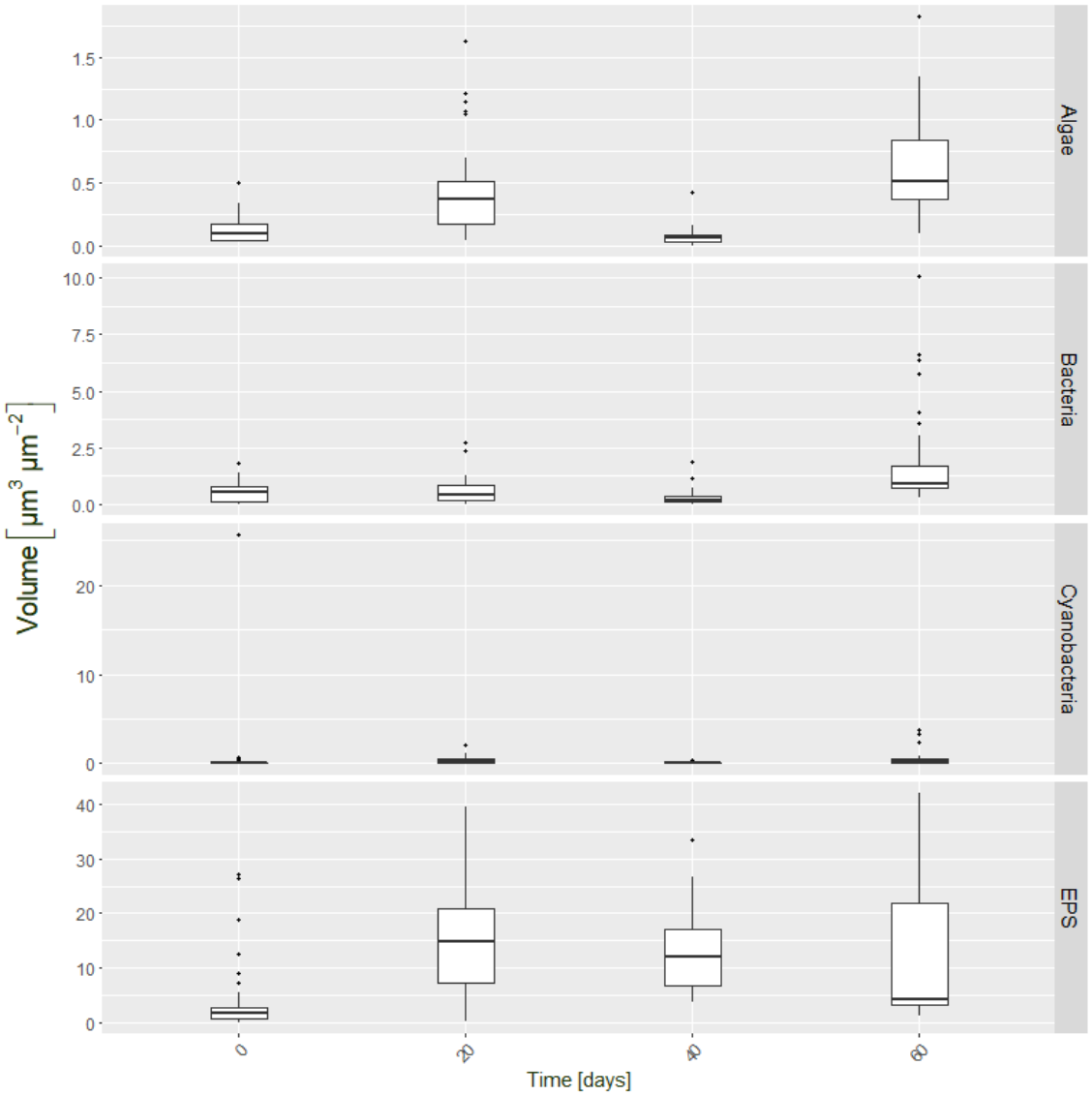

Figure S 1: Change of individual floc components over time, given in their volume per µm^{-2} of floc. The volumes were semi-quantitatively calculated from CLSM datasets obtained from six individual flocs from two different microcosms (3 flocs x 2) examined on 5 sites each (n: 30) for each of the time intervals.

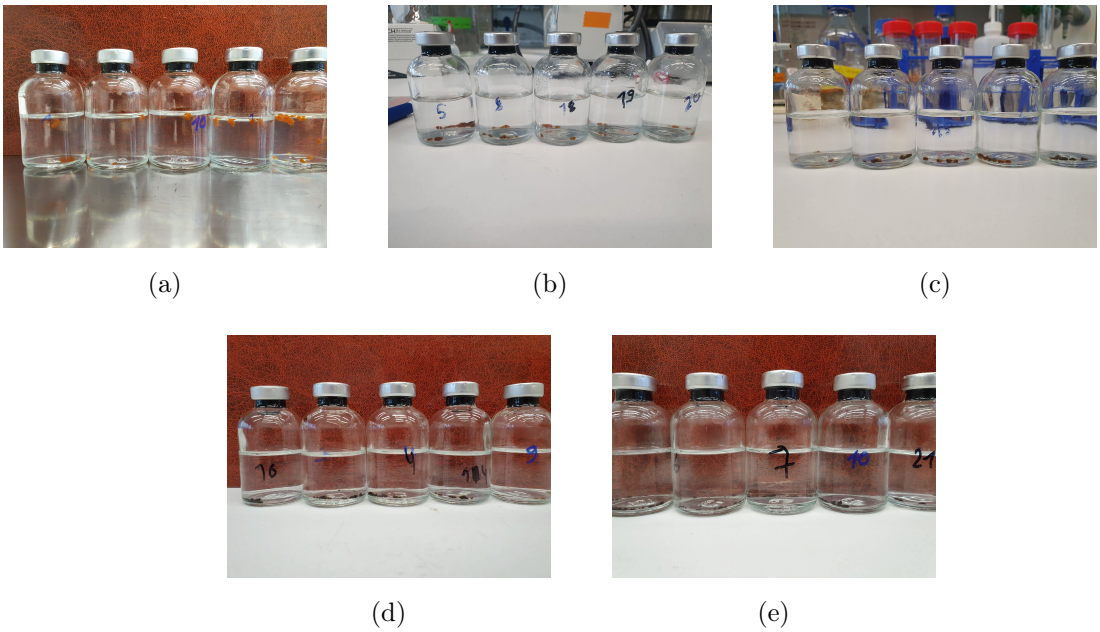

(a) (b) (c)

(d) (e)

Figure S 2: Anoxic microcosms with *S. oneidensis* after (a) 0, (b) 20, (c) 40, (d) 60 and (e) 120 days of incubation. The floating of iron-organo flocs in picture (a) was caused by the nitrogen bubbling.